

*Project Title:* **CLONING SINGLE WALL CARBON NANOTUBES FOR HYDROGEN STORAGE**

Project Period: February 1, 2005 to Dec 31, 2010

Date of Report: August 30, 2012

Recipient: Rice University

Award Number: DE-FC36-05GO15073

Working Partners: [Rice University](#)

Cost-Sharing Partners: [Rice University](#)

Contacts: Prof. James Tour, Principal Investigator  
713-348-6246, [tour@rice.edu](mailto:tour@rice.edu)

Carter Kittrell, Research Scientist  
713-348-5108 [kittrell@rice.edu](mailto:kittrell@rice.edu)

DOE Managers: Jesse Adams

# Executive summary

The purpose of this research is to development the technology required for producing 3-D nano-engineered frameworks for hydrogen storage based on  $sp^2$  carbon media, which will have high gravimetric and especially high volumetric uptake of hydrogen, and in an aligned fibrous array that will take advantage of the exceptionally high thermal conductivity of  $sp^2$  carbon materials to speed up the fueling process while minimizing or eliminating the need for internal cooling systems. A limitation for nearly all storage media using physisorption of the hydrogen molecule is the large amount of surface area (SA) occupied by each  $H_2$  molecule due to its large zero-point vibrational energy. This creates a conundrum that in order to maximize SA, the physisorption media is made more tenuous and the density is decreased, usually well below 1 kg/L, so that there comes a tradeoff between volumetric and gravimetric uptake. Our major goal was to develop a new type of media with high density  $H_2$  uptake, which favors volumetric storage and which, in turn, has the capability to meet the ultimate DoE  $H_2$  goals.

## Uniform pores, well packed

Since  $sp^2$  carbon has unusually high van der Waals interactions, we believed that  $H_2$  could be more densely packed into the pores of dense nanostructured  $sp^2$  carbon materials, and with this new approach, volumetric and gravimetric capacities are no longer a tradeoff, but remain in sync as the density of the media (including  $H_2$ ) is  $\sim 1$  kg/L. In addition, nano-engineered slit pores with identical covalently bonded molecular proppants provides a rigid, crystal-like nano-engineered structure where the slit pores are the same size, with no undersize pores that add mass to the media, or oversized pores with an “empty” middle that is wasted volume.

## Redirect from pure SWCNTs to nano-structured carbon *(added DOE No Go March 29)*

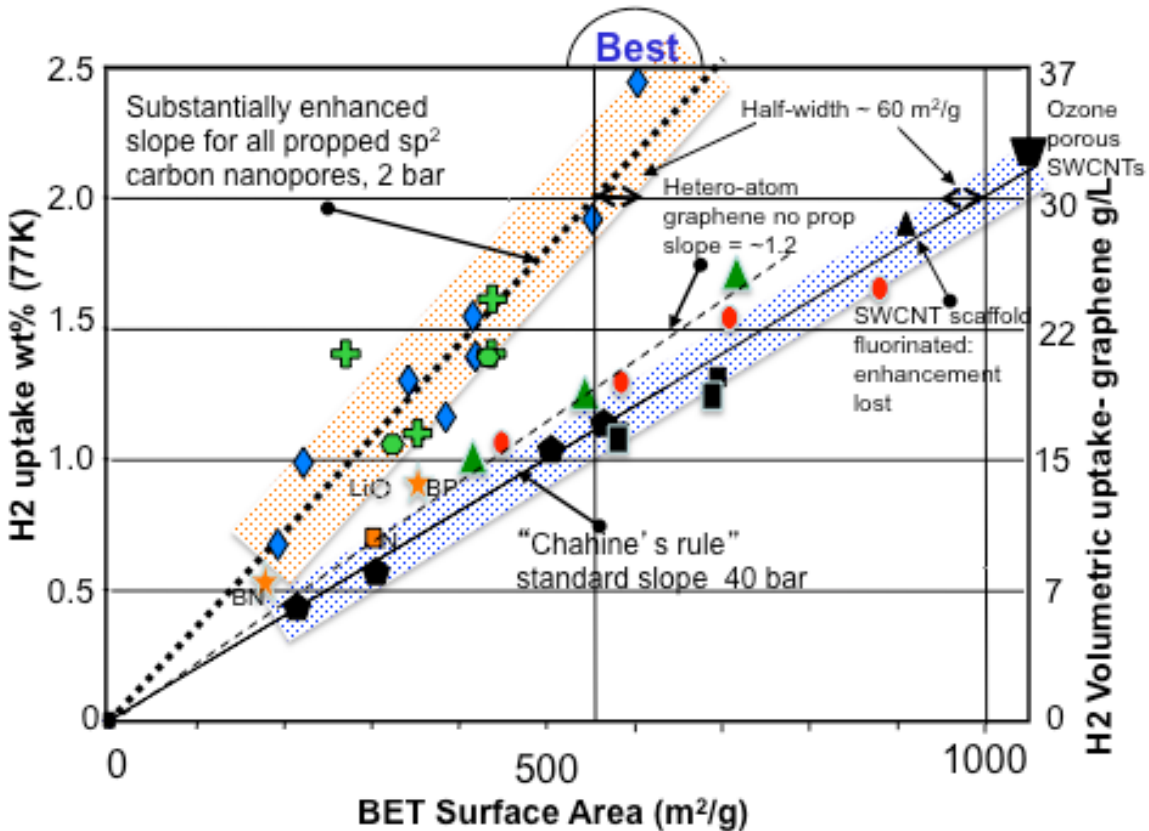
Our original goal was cloning single wall carbon nanotubes (SWCNTs) as a means to provide a source of uniform SWCNTs. We achieved high capacity production of very high quality SWCNTs, proved that cloning was feasible, and learned to spin fibrous SWCNT media. However, the strong van der Waals attractive force between the well-aligned SWCNTs did not have large enough pores to allow the hydrogen to enter. Utilizing substantial input from our research group and very helpful recommendations from the Hydrogen Sorption Center of Excellence (HSCoE) team at the National Renewable Energy Lab (NREL), DOE did a No Go on pure SWCNTs; with a redirect to produce nano-engineered pi-bonded carbon structures for Phase II. We developed solvent-based expansion of the SWCNT structures, followed by reaction with molecular proppants that were covalently bonded to the walls to make a porous  $sp^2$  carbon adsorbent with optimized slit pores. This used both our SWCNT production and fiber spinning capability that had already been developed. Theoretical work by other researchers indicated an ideal pore spacing to be about  $\sim 0.8$  nm, and we experimented with our nano-structured scaffolds with a variety of crosslinks and proppants to test and produce similar size pores.

## Doubly enhanced uptake per unit SA

We were highly successful in proving our main goal as we consistently obtained much higher uptake per unit surface area than common physical  $H_2$  adsorbents. For consistency and exceptional accuracy, all  $H_2$  uptake measurements were performed by HSCoE on the same

instrument at 2 bar of H<sub>2</sub>, as well as surface area (SA); all results are reported as “excess” H<sub>2</sub> uptake due to presence of the adsorbent media, not the total H<sub>2</sub>. “Chahine’s rule” that is used for most H<sub>2</sub> adsorbents is 1wt% per 500 m/g SA at asymptotic pressures (>40 bar) and 77K, whereas we routinely obtained higher (1.85× average) uptake at 2 bar. Allowing a generic 30% increase in uptake by raising the pressure from 2 bar to the asymptotic limit, this puts us at >2wt% per 500 m/g, or at least twice Chahine’s rule. When we fluorinated the sp<sup>2</sup> scaffold, which disrupted the π cloud, the enhancement was lost, and uptake reverted to 1.06 wt% per 500 m/g SA, ~same as Chahine’s rule. We proved that slit pores alone do not provide the enhanced uptake, but they act in concert with the sp<sup>2</sup> pi cloud as a nano-compressor to pack the pores with H<sub>2</sub>. Ozone perforated bulk SWCNT media provided 1.05 wt% per 500 m/g, also obeying Chahine’s rule, showing the randomly induced porosity in SWCNTs also does not cause the 2x enhanced uptake.

### Enhanced Uptake in nanostructured sp<sup>2</sup> slit pores



### Overall accomplishments are summarized on the graph.













All of the propped and/or crosslinked graphene-like carbon samples are clustered around the steeper slope of nearly 2x enhanced uptake per unit SA.

All of the graphene and CNT media without proppants follows the Chahine's rule slope of 1wt% per 500 m<sup>2</sup>/g SA. Fluorination of a scaffold disrupts the pi cloud, drops to lower slope. The Li intercalated is in between due to degradation by moisture.

Heteroatom B, P substituted graphene has higher binding energy 8.5kJ/mol, slightly higher uptake, ~1.2 slope

The Chahine's rule slope of 1 = 1wt% per 500 m<sup>2</sup> /g, and not fitted to the data

The half-width of the shaded areas shows how well the data fits the slope. the deviations tend to be in absolute SA, so that the greater the uptake, the less the deviation from the average slope

-  Blue diamonds: SWNT scaffold expanded and cross-linked (8)
  -  Black triangle: Fluorination kills pi cloud of SWCNT scaffold enhanced uptake is lost
  -  Green hexagon: propped graphene aniline sulfonate & diphenyl crosslink (2)
  -  Green cross: TEG phenyl sulfonate link & proppants (4)
  -  Dotted circle: Li intercalated SWCNT scaffold (sample probably degraded due to moisture)
  -  Black squares: synthetic graphene without proppants (2)
  -  Black pentagons: thermally exfoliated graphene (natural), without proppants (4)
  -  Orange square: Nitrogen substituted graphene without proppants
  -  The ozone perforated bulk SWNTs is from Phase I, before nano-engineered scaffolds
  -  Red dots: Boron hetero-atom doped graphene, enhanced binding energy (4)
  -  Green triangles: Phosphorous hetero-atom doped graphene, enhanced binding energy (3)
  -  Orange Texas star: Double hetero-atom substituted graphene suggests greater enhanced uptake, perhaps due to charge separation which will polarize the H<sub>2</sub> molecules.
- BN = boron + nitrogen; BP = boron + phosphorous

### **Enhanced uptake not explained by increased binding enthalpy**

One might argue that the ~2x enhancement is due to the greater binding enthalpy of H<sub>2</sub> in the slit pore, which has been both calculated and measured by other researchers ca. 8 to 9 kJ/mol. However, our non-scaffold B-substituted and P-substituted graphene has similar increase to ~8.5 kJ/mol, but shows only a d1.2x enhancement rather than a 2x enhancement, a minimally significant increase, which is strong evidence that enhanced binding enthalpy does not a “nano-compressor” make, and does not explain the large enhanced uptake. From a theoretical viewpoint, increased attraction to the surface does not increase H<sub>2</sub>-H<sub>2</sub> attraction, and will not squeeze the H<sub>2</sub> closer to each other on the surface. It is the sp<sup>2</sup> carbon slit pore that is essential in order to make a nano-compressor.

### **High density media achieves DOE volumetric goals (materials only)**

In addition, the density of our SWCNT fibrils was typically 1.3 kg/L, so that volumetric uptake was always higher than gravimetric uptake for our media when comparing the ultimate DOE goals, which correspond to a density of 0.7 kg/L and 7.5wt% for the complete hydrogen storage system when filled, which in turn corresponds to an overall density a little less than 1kg/L. Hence two primary goals for proof of principle for this novel approach to H<sub>2</sub> adsorbents were met, which is high absorption capacity per unit SA, along with a high-density media. Both goals track together and hence there is essentially no volumetric vs. gravimetric tradeoff when the nano-engineered sp<sup>2</sup> carbon media is used. We were not able to achieve high overall SA due to the difficulty in removing the solvent, as the very strong van der Waals attraction that we used to pull the H<sub>2</sub> into the pores also made it difficult to remove all of the solvent, and this is one of the problems that remain for future research. However we were able to achieve DOE 2010 volumetric goals (materials only), and substantially exceed them when including the factor of 1.3× for increasing pressure from our test pressure of 2 bar to 40 bar, or 40 g/L compared to 28 g/L of the DOE 2010 target.

### **Kubas-type binding and alkali metal atoms downselected**

We discontinued work on Kubas-type binding with transition metals, as we discovered that individual transition metal atoms will migrate and form useless clusters on SWCNT in the presence of hydrogen, and reported this at 2008 Annual Merit Review (AMR). We demonstrated that lithium and sodium atoms would spontaneously put charge on the SWCNT, with the idea that this would increase binding energy of the H<sub>2</sub>, and after substantial effort provided a Li functionalized nano-scaffold sample to NREL, but it was degraded and showed the least enhanced uptake of any nano-structured sample. We down-selected this because lithium atoms make the media extremely air and moisture sensitive, with consequent difficulties and potential higher handling costs.

### **Graphene as low cost media (modified March 29)**

The cost of SWCNT is a concern; hence we then switched to graphene, which is also sp<sup>2</sup> carbon, upon recommendation from our HSCoE team leader at the NREL. While it is not yet manufactured in bulk, all the major raw ingredients are among the least expensive industrial chemicals. With graphite ~\$500/tonne, sulfuric acid ~\$100/tonne, etc., and using standard commercial solvent fiber spinning techniques, we estimated \$25 to \$45 media only cost for 1 kg H<sub>2</sub> capacity in our 2010 AMR presentation for large-scale production. Since H<sub>2</sub> has an energy capacity of 33.5 kWh/kg, this can be calculated to be in the range of \$0.75 to \$1.35 per kWh

(materials only). This is less than the DOE 2015 system target is \$2/kWh which provides some leeway for other system costs. We also determined graphene could be spun into a fiber using the same commercial type spinning techniques developed for SWCNT fibers.

### **Transition from SWCNT to Graphene, with the same enhanced uptake**

In the last two years of the 5-year project, we transferred our extensive knowledge of nano-engineered materials from SWCNT to graphene, a monolayer of carbon atom sheet, and the “new kid on the block” at that time. We found that the same enhanced uptake per unit SA applied to graphene that had been propped open. However, unpropped graphene closely follows Chahine’s rule, once again proving that correctly spaced slit nanopores have considerably enhanced uptake. And in lieu of Kubas-type binding or alkali metal surface atoms, we chose atom substitution using boron, phosphorous and nitrogen. Since these are incorporated into the graphene lattice, there are no issues of migration, air sensitivity, or chemical reaction with water vapor; hence no special handling techniques would be needed for the media beyond that of the carbon. With 5.6 atom% B we obtained an increase from 5.5 kJ/mol H<sub>2</sub> binding to 8.6 kJ/mol, and with 7.5 atom% P, the increase was to 8.3 kJ/mol, both showing substantial binding enhancement even though the atom% substitutions were rather low. Nitrogen provided no such enhancement, as other researchers have also reported, and that material was quite disordered. We also experimentally verified the increased H<sub>2</sub> uptake in increasing pressure from 2 bar to 16 bar, with an experimental average of 1.35× increase. For simplicity, we use a more conservative value of 1.3× for uptake at higher pressures. Our highest volumetric uptake was 27 g/L at 2 bar, or 35 g/L at 16 bar (materials only). This substantially exceeds the DOE 2010 system goals of 28 g/L. We did not achieve the gravimetric uptake goal for either SWCNT or graphene. As the program came to a close, we decided that enhanced binding energy was a more important and challenging goal for the remaining time, as this is another proof of principle for the nano-structured material. (We are most grateful to HSCoE partner Channing Ahn of Caltech for the isotherms up to 16 bar and binding energy determinations for N, B, and P substituted graphene; these were the only H<sub>2</sub> uptake measurements not done at NREL.)

### **Why this is important for vehicular hydrogen storage**

Since our research was primarily focused on proof of concept that a nanoengineered sp<sup>2</sup> carbon framework is a new direction for H<sub>2</sub> adsorption media has special and superior H<sub>2</sub> uptake properties, we think the best way to demonstrate the importance of our rather unique approach is to project the outcome of a fully nano-structured graphene media based on extrapolating our quantitative measurements. Can this approach of “packing the pores” conceivably reach the ultimate goals for physisorbed H<sub>2</sub> storage, and in particular, address the difficult problem of high volumetric storage? In addition, the exceptionally high thermal conductivity of sp<sup>2</sup> carbon fibrous media can reduce or eliminate the need for internal coolant tubes saving system weight and volume.

### **A high-density media that is projected to help reach the ultimate DoE goals** *(added section on residual hydrogen, March 29)*

The full SA of graphene is 2650 m<sup>2</sup>/g, hence is inherently less than carbon aerogel or metal organic framework (MOF) - type structures. But this is compensated for by our emphasis on doubling of the uptake per unit SA. Assume 5% SA is consumed by the proppants, with 0.8 nm graphene spacing from both theory and our experiments, then the nano-scaffold density is ~1

kg/L including the H<sub>2</sub>. The average for our six measurements on propped graphene is 1.8 wt% per 500 m<sup>2</sup>/g at 2 bar and 77K. Hence 1.8 wt% becomes 9 wt% at 2 bar and 2500 m<sup>2</sup>/g. Then using the factor of 1.3× increasing pressure to 40 bar, and combining both factors, this can be projected to 11.7 wt% (media + H<sub>2</sub>). Although our spacing of 0.8 nm for the slit pores in graphene provides a density of 1kg/L with H<sub>2</sub>, but allowing a volumetric increase from 0.8 nm to a 1.0 nm pore spacing, with no change of H<sub>2</sub> stored in the slit pore, this still provides a good projection for volumetric capacity of 95 kg/L. With the ultimate DOE system goals of 7.5 wt%, and 70g/L this projection provides leeway for significant additional weight and volume for the rest of the system. Nearly all of the H<sub>2</sub> capacity can be utilized. Much of the H<sub>2</sub> can be drawn off at the initial temperature of 77K to 120K and the “nano-compressor” will equilibrate with the bulk gas, or the temperature can be allowed to increase gradually to maintain ca. 40 bar in the H<sub>2</sub> bulk. If one allows that 10% to 15% of the H<sub>2</sub> is kept as a “reserve” then the temperature cycling need not be more than about 75K while retaining 3 bar delivery pressure. If it is necessary to utilize the “reserve”, then the tank is allowed to warm to ambient temperatures (such as with FC coolant), then the “nano-compressor” effect essentially ceases and the residual H<sub>2</sub> gas at 3 bar will be similar to any common carbon sorbent, 0.05wt% to 0.15wt%. In addition, enhanced binding with atom substitution is projected to increase the storage temperature to 120K and possibly to 150K, reducing insulation requirements. We conclude that our new nano-structured media can pack enough H<sub>2</sub> into the pores to make a media that is projected to help reach the “ultimate” DOE goals for H<sub>2</sub> storage.

# Introduction

The purpose of this research is to development the technology required for producing 3-D nano-engineered frameworks for hydrogen storage based on  $sp^2$  carbon media, which will have high gravimetric and especially high volumetric uptake of hydrogen, and in an aligned fibrous array that will take advantage of the exceptionally high thermal conductivity of  $sp^2$  carbon materials to speed up the fueling process while minimizing or eliminating the need for internal cooling systems. A limitation for nearly all storage media using physisorption of the hydrogen molecule is the large amount of surface area (SA) occupied by each  $H_2$  molecule due to its large zero-point vibrational energy. This creates a conundrum that in order to maximize SA, the physisorption media is made more tenuous and the density is decreased, usually well below 1 kg/L, so that there comes a tradeoff between volumetric and gravimetric uptake. Our major goal was to develop a new type of media with high density  $H_2$  uptake, which favors volumetric storage and which, in turn, has the capability to meet the ultimate DoE  $H_2$  goals.

Work Plan: Tasks to be performed by Rice University, in coordination with other HSCoE members, are as follows:

1. Cutting single wall carbon nanotubes
2. Preparation of SWNT-CAT seed, and growth of supported SWNT-CAT
3. Spin nanotubes into fibers, and expand and cross-link to make 3D scaffold
4. Optimize pore size, test for hydrogen uptake, project uptake, determine binding mechanism
5. Develop extraction methods for residual expansion solvent, and alternative expansion methods which provide less residual solvent
6. Increase pore size to accept metal atoms that use the 3D scaffold as a rigid support for Kubas-type binding
7. Develop methodology to produce samples in sufficient size for measuring binding energy and kinetics by CoE partners.

## Performance of our research based on the tasks of the work plan

The first paragraph is the task, followed by our description of how we executed the task in our research program.

### Task 1. Cutting single wall carbon nanotubes

Reaction of elemental fluorine and ozone with SWNTs occurs at low and room temperature, respectively. In both cases reactions occur in bands along the nanotubes. Studies have shown that with further heating to elevated temperatures or reaction with a strong oxidizing solution such as mixtures of concentrated sulfuric and hydrogen peroxide or nitric acid that cutting occurs in these banded regions. This research will focus on defining the best scalable technology for cutting SWNTs to  $\sim 30$  nm lengths.

-----



The reaction of SWCNTs with fluorine proved useful and was used as an expansion and crosslinking method. It also was most helpful in proof of principle that fluorination of the nano-structured media which destroys the pi cloud so that the structure is no longer  $sp^2$  carbon and the enhanced uptake was also lost. Oxidizing with ozone made the SWCNT media more porous, increasing both SA and total uptake, but no enhanced uptake per unit SA was observed. This shows that random pores, rather than slit pores do not lead to enhanced uptake.

Our research on the spun fibers determined that fibers could be spun as is from the HiPco reactor, and no cutting or other alteration of the SWCNT would be needed to lead to a high-quality expanded nano-structured material. The length of the SWCNT as produced formed an excellent liquid crystal in superacids. Hence the portion of task one involving cutting essentially became moot.

## **Task 2. Preparation of SWCNT-CAT seed, solubilization, and growth of SWCNT-CAT seeds on supports**

The term SWCNT-CAT refers to a nanotube with 30-100 metal atoms added to the end of the nanotube, which includes iron catalyst particles, and iron-nickel catalyst. The SWNT is sidewall functionalized with carboxylic acids, ionic sulfate and quaternary ammonium groups to give solubility in alcohol or water. Oleum is used to solvate the pure nanotubes. These nanotubes are placed on or embedded in high area supports, which insures direct access of hot growth gas to all SWNT-CAT. Different ceramic support surfaces will be investigated for optimum growth of SWNT-CAT. Cloning is done on the pure bundled SWNT-CAT or the SWNT-CAT supported on a ceramic surface. The manner in which nucleation and growth occurs will be investigated and determined.

-----

With guidance from the Hydrogen Storage Center of Excellence (HSCoE) Leadership, we expanded our materials to include nanotubes with an infinite radius of curvature, which is has recently become graphene. (Nobel Laureate award, 2010) Although graphite is a bulk material known to the ancients, graphene is the “new kid on the block” as a one-atom thick layer of  $sp^2$  carbon. Hence it has many chemical similarities to Single wall carbon nanotube (SWCNT), including, as we explained in the Executive Summary, the unusual propensity for greatly enhanced uptake per unit surface area (SA) in nano-engineered structures that are propped open to provide nm-sized slit pores to allow the H<sub>2</sub> to intercalate, without needing to “pry” the individual graphene or SWCNT components apart. There are several reasons for incorporating the “infinite radius” graphene sheet into our molecular toolkit for creating nano-engineered materials. The first is that there is a natural progression to cast a wider net as we increasingly came to understand the chemistry and unique properties of the nanostructured  $sp^2$  carbon slit pore. The second is that the starting material of graphite is a very low cost industrial commodity that can be produced either from the mineral state, or synthesized from carbon sources like wood. A third is that it allows for some heteroatom chemistry that has proved difficult for SWCNTs, hence this is a new route for enhanced binding energy, always a desirable goal for physisorption of H<sub>2</sub> to make storage feasible at less cryogenic temperatures. In the following tasks, progress on both SWCNT and graphene nano-structured materials will be discussed, which shows how similar developments took place for both of these  $sp^2$  carbon molecular tools in our nano-tool kit.

We have developed new synthesis methods using common chemical precursors and sodium metal to remove chloride, and the carbon reacts to form sheets of graphene. This is a very versatile approach, as other atoms may be readily incorporated by using reactive ligands which are pulled off by the sodium, and then are taken up into the sheet. Element selective transmission electron microscopy (TEM) shows that the heteroatoms are uniformly distributed into the graphene sheet (see figure in main report). Additional synthesis is from GO, which expands and separates a natural or synthetic graphite, which is a very low cost precursor. In addition, graphene nanoribbons (GNR) can be made by opening multiwall carbon nanotubes MWCNT using either sulfuric acid and an oxidizer like potassium permanganate, or by alkali metal intercalation. Unlike SWCNT, MWCNT can be made by bulk synthesis processes and are now manufactured by the ton for incorporating into battery electrodes.

### **Task 3. Spin nanotubes into fibers, and expand and cross-link to make 3D scaffold**

The nanotubes are dispersed by high shear mixing in oleum, and then are spun into pure carbon nanotube fibers. The dried fibers are immersed into oleum which intercalates and expands the fiber. This is cross-linked by bifunctional derivatives to make the expanded pore structure into a rigid 3D nanoengineered frame. The remaining solvent is extracted to provide the space for hydrogen uptake.

-----  
This spinning method has been adapted to graphene, using oleum solvents or more recently chlorosulfonic acid or a water-dispersion of graphene oxide. Use of commercial type solvent spinning provides a low cost route to provide fibrous media rather than granular media, which has structural integrity and better thermal conductivity.

A number of different expansion and propping methods were developed. This includes cross-linking with aromatic species like methyl biphenyl groups and tri-phenyl ligands. Aliphatic linkers were also used, such as a bi-functional hexyl linker. Proppants were also used, which do not bind covalently to both surfaces, but rather have functional groups that are strongly attracted by van der Waals and dipole induced dipole attractive interactions. The rigidity of the ligand keeps the SWCNT or the graphene sheets apart. Such ligands are chlorophenyl, phenyl sulfonic, and phthalic acid. In addition, combinations of ligands and linkers were also used. Expansion methods utilized oleum and lithium ammonia and fluorination. We exceeded our goals by discovering several different methodologies were successful. This provides several scalable methodologies so the most efficient and cost effective one can be developed.

### **Beyond task 3: All-in-one processing**

In addition, a fiber was spun after pre-functionalization with phthalic acid ligands attached, so that no post-fiber spinning expansion was needed. The ligand proppants were already in place in this case, hence the slit pores were formed during the spinning process. This is attractive from a production standpoint, as the post-processing steps of expansion, addition of proppants, and solvent extraction is eliminated. Here we exceeded our goals in discovering that multiple steps can be merged into the spinning process, and in doing so, raised the bar on what we consider to be an ideal case: this would be spinning the fibrous media such that upon completion of coagulation, solvent extraction, and drying, the storage media is produced as

continuous fiber ready for macro-assembly, and is not air or moisture sensitive. For task 3, we exceeded our goals and found a better, simpler route to the fibrous media than we proposed.

#### **Task 4. Optimize pore size, project H<sub>2</sub> uptake, determine binding mechanism**

Theoretical predictions indicate that a relative narrow range of pore sizes, ca. 6 to 8 Angstroms, made entirely of sp<sup>2</sup> carbon will show considerably enhanced binding free energy for hydrogen. The range of pore sizes is adjusted by the strength of the expansion solvent and the size of the cross-linker. The correct pore size may increase the uptake per unit surface area, leading to enhanced capacity. The greatly enhanced equilibrium constant packs hydrogen into the pore by what is termed the “nanopump” effect. In addition to routine testing at NREL for hydrogen uptake, samples will be provided to HSCoE partners for testing by NMR and neutron scattering, and the energetics and mechanism for this enhanced binding will be determined.

-----

To our surprise, all of these approaches worked about equally well. The rather narrow range on the Chahine-type plot for propped nano-structured materials shows that it is an intrinsic property of the slit pore that provides the benefit, and not the details. This lends itself to a rather clear picture of the mechanism. Our proppants create slit pores that put us onto the “tail” of the theoretically determined attractive curve for the slit pore. If the pore is narrow, then the H<sub>2</sub> feels attraction from both sides of the pore, with a strongly peaked enhancement in enthalpy -- however, it may also become “stuck” in that confined pore, such as described by Eklund in his empirical binding enthalpy with Raman. However this has a large entropy penalty of a fixed or nearly confined location for the H<sub>2</sub> molecule. But for wider pores, the hydrogen forms a double layer in between the two neighboring pi clouds of the slit pore and is free to move longitudinally, providing a 2-D degree of freedom, and a much reduced entropy penalty for entering the pore. Hence the free energy will not be sharply peaked, but likely to be broad and slowly varying over a range of 7Å to 10Å as the tight pore has higher enthalpy offset by a bigger entropy penalty. The result is that the nano-compressor exhibits about the same degree of compression for this range of proppants and spacings. We believe that we have verified experimentally the theoretically predicted enhanced uptake of H<sub>2</sub> into a pi cloud slit pore, due to the attraction of the H<sub>2</sub> into the pore, rather than binding to a specific surface site.

Using our HSCoE partnership with the National Renewable Energy Lab (NREL) and Channing Ahn at Caltech, we were able to determine the mechanism and energetics of the enhanced binding fit well with theoretical models by Patchkovskii and Seifert [PNAS 2005] as explained above and experimental results by partner Eklund at Penn State, and also determined that the binding enthalpy could be enhanced with addition of boron and phosphorous, whereas nitrogen did not increase binding enthalpy as other partners have predicted. We determined that tests with neutron scattering and NMR were not essential to our fundamental understanding of the storage mechanism; however, such studies could provide useful supplemental information at some future date.

The remarkably reproducible 2x enhanced uptake with a wide variety of conditions made pointed to quite specific projections of maximum H<sub>2</sub> uptake as was provided in the Executive Summary, and demonstrates that the sp<sup>2</sup> slit pore storage media can be projected to substantially

exceed DoE 2015 goals (materials only) which leaves a margin for the rest of the system weight and volume.

We believe that we were fully successful in task 4, and exceeded it by showing that the enhanced uptake does not require a precisely spaced slit-pore but provides enhanced uptake with a variety of proppants and a range of slit pore spacings.

#### **Task 5. Develop extraction methods for residual expansion solvent, and alternative expansion methods (partial merger with task 3)**

The optimum sp<sup>2</sup> pore binds many things well, including the expansion solvent, which is difficult to extract by conventional water extraction methods. Alternate methods using non-protic superacids will be investigated. Also, expansion with highly volatile Lewis acids will be tested. Alternative expansion methods using alkali metals will also be tested to provide an acid-free approach to expansion to make the 3D nanotube scaffold.

-----  
We have tested several methods for expansion, as explained in the previous section. the more volatile chlorosulfonic acid also gave good results. Fluorination is a different expansion method that does not use protic superacids, and the lithium - ammonia expands by the lithium intercalation, which is acting as a Lewis base. Since it is a Lewis base, it is non-protic. Each of these proved to have their own difficulties in solvent extraction, however. No matter what the expansion material, something always likes to remain stuck inside the slit pore - and perhaps this is no surprise, as it is a strongly attractive pore for essentially any species, especially those which can be polarized. We believe that this is a soluble problem but wished to explore as many different options as possible, to lay the groundwork for choosing the best approach later. We were highly successful in our efforts to explore and develop several expansion methods and propping open the slit pores. As explained in Task 3, the discovery of an all-in-one spinning method with built-in proppants becomes a means to bypass the separate task 5 expansion step entirely.

#### **Task 6. Increase pore size to accept metal atoms that use the 3D scaffold as a rigid support for Kubas-type binding**

Generalized Kubas binding occurs for metal atoms on a support which sorbs hydrogen at or near ambient temperatures. The expansion of the nanotube fibers is increased to provide appropriate pore sizes, ca. 9 Angstroms, for intercalation of metals such as lithium. The rigid scaffold prevents flexing or collapse of the pore structure when the hydrogen is added/removed. Such metal intercalated nanotube scaffolds will be made and tested for hydrogen uptake at room temperatures, and in cooperation with several HSCoE partners, the binding energy and mechanisms determined. Work will also be done to examine the intercalated metal morphology under limited cycling to determine the risk of metal agglomeration and/or poisoning.

We explored the addition of alkali metal atoms like lithium, and similarly with calcium. The lithium is extremely hydroscopic, and for this reason gave mediocre results in our uptake. Separate tests with iron and nickel transition metals on SWCNT showed that these became mobile in the presence of H<sub>2</sub>, and the clusters are not conducive to increased binding, but just add weight. These species, which distributed as atoms to achieve the Kubas-type binding, are also very air and moisture sensitive. Hence, we downselected both approaches and discontinued

work on both alkali metals and transition metals for enhanced binding, and shifted our enhanced binding strategy to another approach.

We continued to pursue the same goal of enhanced binding, but by developing scalable synthesis methods incorporating the hetero-atoms into the graphene lattice. These bound atoms cannot move and form useless clusters, and are not air or moisture sensitive; hence moisture can be removed by standard drying oven bake-out methods. And this provided the enhanced binding we sought. Hence we believe that we achieved the goals of enhanced binding, not by subsequent Kubas-type add-ons, but by incorporating the atoms into the carbon skeleton. From the standpoint of materials cost processing, and longevity of the media, this was the better approach. Collaboration with our Caltech partner proved substantial enhanced binding enthalpy increases of over 50% with boron and phosphorous hetero-atom substitution, which would raise the storage temperature from 77K to 120K based on the enhanced free energy to obtain equivalent performance.

**Task 7. Develop methodology to produce samples in sufficient size for measuring binding energy and kinetics by CoE partners.**

The optimum size SWNT material will be determined and the cloning methodology developed earlier will be employed as appropriate to produce the best free energy of binding, and/or best scaffold material for the Kubas-binding metals. Spun fibers will be produced with appropriate sample sizes for NMR and neutron scattering measurements. This will achieve the best nanoengineered  $sp^2$  pore media to reach the project objectives listed below, and the binding energetics, mechanisms, and kinetics for this optimized media will be determined. Collaborative efforts will be done with the Jakobson/Hauge project for theoretical analysis, and to test the use of the vertically aligned nanotube arrays (VANTA), which are subject to the crosslinking methodology and then characterized for hydrogen uptake, and compared to the scaffold produced from the spun fiber.

-----

While we did not scale to large sample size, we chose scalable methods in all our recent graphene work adequate to provide several samples to partner Channing Ahn for isosteric plots to obtain binding energies. In all cases we provided sufficient samples to take the appropriate measurements. In the waning days, the goal was to develop as diverse methods as feasible, to provide proof of principle and a selection of materials. As explained previously, we determined that hetero-atom substitution was preferable to air-sensitive and potentially unstable Kubas-type binding metal atoms, and that NMR and neutron measurements were not necessary at this stage of development, rather emphasizing a systematic study of  $H_2$  uptake measurements and isosteric heats. We engaged in theoretical work with the Jakobson partners at Rice, which helped elucidate the enhanced binding in the slit pore, as well as the size of the space occupied by the  $H_2$  molecule on the surface. We chose not pursue testing the VANTA arrays, as these tended to have irregular spacing which looks kinked under scanning electron microscopy (SEM). Our Rice partners did not find a way to smooth out the kinks, hence the density of the VANTA arrays remained well below that of our spun fibers. We determined that densifying the VANTA array was outside the scope of our project, and downselected this approach for this project. We also determined that since the 2x enhanced uptake per unit SA was relatively insensitive to the type of  $sp^2$  carbon, as long as it was propped slit pores of  $sp^2$  carbon, that cloning of identical SWCNTs

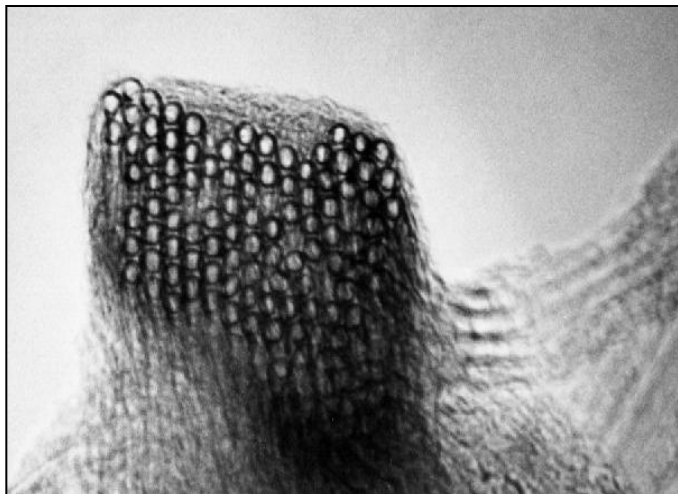
is not necessary to achieve the high density storage of H<sub>2</sub> at 77K or 120K for atom-substituted graphene.

We believe that in demonstrating that essentially all nano-structured sp<sup>2</sup> with permanent slit pores behaved equally well, we were completely successful in achieving our goals of task 7.

-----

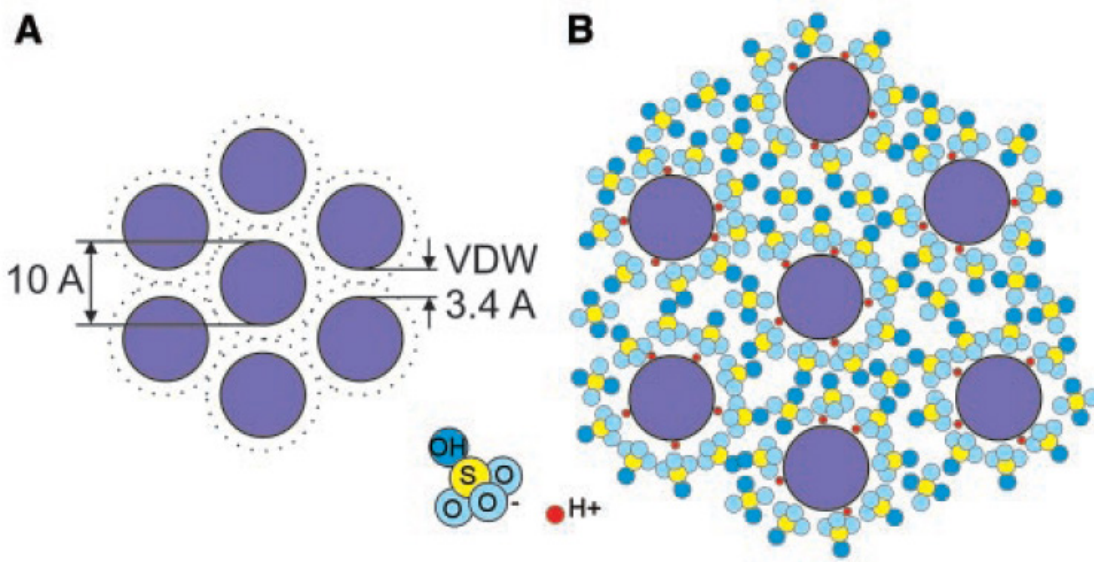
## Why this is important for vehicular hydrogen storage

Since our research was primarily focused on proof of concept that a nanoengineered sp<sup>2</sup> (graphene-like) carbon framework, we believe the best way to explain the importance of our rather unique approach is to project the outcome of a fully nano-structured media of CNT and graphene. CNT was best suited for proof of principle because the molecular geometry and chemistry is well understood, whereas graphene, although it is “the new kid on the block”, is derived from one of the lowest cost bulk industrial materials, whether mineral or synthetic, and hence ultimately would provide a very low cost media.

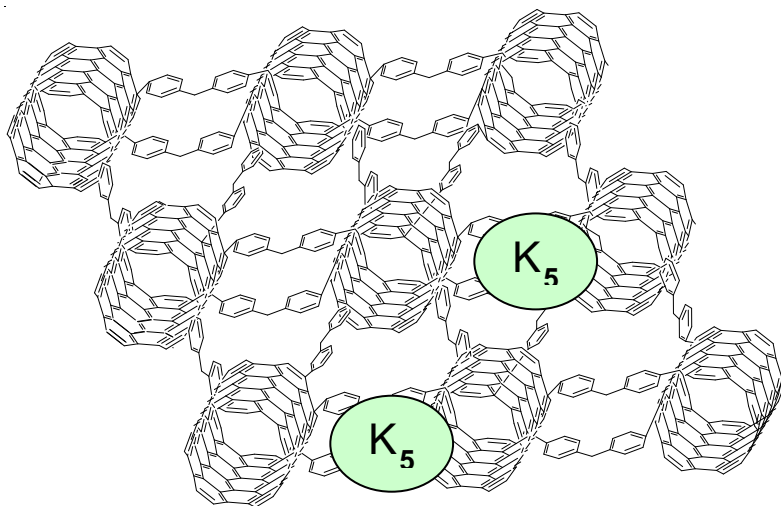


Get citation from Pasha’s TEM paper on SWNT

What can we project the H<sub>2</sub> uptake to be once we overcame the solvent extraction problem and all of the SA and pore volume becomes available for H<sub>2</sub> uptake? Does this approach of “packing the pores” have the feasibility of reaching the DoE 2015 goals, or the ultimate goals for physisorbed H<sub>2</sub> storage, and in particular, addressing the chronically more difficult problem of volumetric storage. And this is likely to be the more critical capacity parameter for public acceptance in private auto use, since a few extra kg is much less of an issue than compromised trunk space, or less back seat legroom, or in the case of the Volt, 2 in the back seat instead of 3.

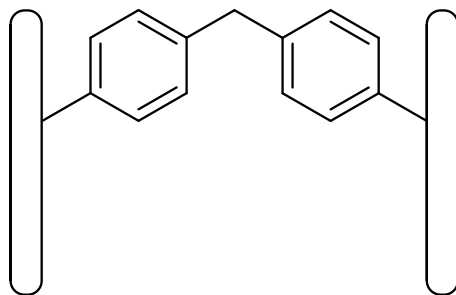


Earlier work, developing spacer methodology  
 Ericson, SCIENCE VOL 305 3 SEPTEMBER 2004, p. 1447



The SA of graphene is inherently limited to 2650 m<sup>2</sup>/g, hence the SA will never be as large as some of the carbon aerogel or MOF - type structures. But this is compensated by our emphasis of doubling of the uptake per unit SA, rather than making ever more tenuous scaffolds. The graphene sheet is quite rigid on the nanoscale, so that even 5% of the SA occupied by proppants is more than enough to make a fully rigid 3D structure. For our CNT work, functionalization of 1 in 50 carbon atoms is common -- it is in the nature of the chemistry for the reactive sites to be well separated. Seifert theory 0.6 to 0.7 nm graphene spacing ideal. Ashley's paper, expansion of CNT by 30% to 40% Fig. 3. This is from 1 nm to 1.4 nm, or added spacing of 0.4 nm. This agrees well with the Seifert work for graphene whereby the 0.33 nm spacing of

packed graphite expands by 0.3 to 0.4 nm to become .6 to .7 nm. Using 0.7 nm, this is an expansion of  $7/3.3 = 2.1x$ , and the density of graphite is 2.2 so the density of the expanded material is  $\sim 1$  g/cc without H<sub>2</sub> uptake. Our nano-scaffold density was typically 1.3 g/cc, but due to retained solvent, it was not feasible to obtain a definitive number, and the calculated number from volumetric expansion is more quantitative. Even if we make a volumetrically conservative choice of greater expansion to 0.8 nm spacing, the expansion is 2.4x and density is 0.91, but when the mass of the H<sub>2</sub> is included, the density is still very close to 1 g/cc.



### **Projection of ultimate uptake for a fully nanoengineered scaffold.**

As we explained in our Ashley 2009 paper, and very much in keeping with the well-established Chahine's rule that uptake is linear in surface area, and that the ultimate SA of fully separated graphene sheets is a precise number, determination of the uptake of our nano-engineered scaffold, once perfected, can be readily calculated. To be conservative, we will use the average of our six graphene measurements with a slope of 1.8wt% per 500m/g at 2 bar rather than our best at 2.1wt% per 500 m/g. Then with the factor of 1.3, this becomes  $1.64 \times 1.3 = 2.13\text{wt\%}$  per 500 m/g.

The average for all six of our propped graphene is 1.8wt% per 500m/g at 2 bar. (Our best uptake for CNT was 2.4wt% and 600 m/g = 2wt% per 500 m/g, so there is excellent consistency for the sp<sup>2</sup> carbon whether it is tubular or flat.) To be conservative in our estimate, we will use the average value for our graphene measurements of 1.8wt%, rather than the best, since we can't be sure the best is reproducible. The projected SA for a fully nano-engineered slit pore graphene scaffold with 5% SA unavailable due to the crosslinking proppants is 2520 m/g. Hence 1.8wt% projects to 9wt% at 2 bar. Then using the factor of 1.3x increasing pressure to 40 bar, this projects to 11.7wt%. Since we are materials scientists and not engineers, we don't attempt to estimate the weight of the rest of the system. But comparing 11.7wt% for materials vs. the ultimate DoE system goals of 7.5wt%, this means that the rest of the system can add up to 56% weight of the media including the hydrogen. Since the pressures are low, and we measured



pressures to be asymptotic under 20 bar, the tank does not need to be heavy. If the “density” of the rest of the system is also 1kg/L like the media, then this also achieves a volumetric capacity of 75 g/L, exceeding the ultimate DoE system goals of 70 g/L.

How can we pack so much hydrogen into the slit nanopores? The special advantage of the slit pore of just the right size is explained in the theoretical Seifert PNAS 2005 paper, which they term a “nanopump”. In effect the higher “pressure” corresponding to higher density inside the slit pore is driven upwards by the difference in the free energy inside the pore vs. the bulk gas, and because the pressure ratio is exponential in the free energy, this can readily become a couple of orders of magnitude higher, hence for 40 bar fill pressure, the density inside the pore can correspond to that of several thousand bar. But this effect only works over a narrow range of slit pore widths, and molar volume of the hydrogen can increase by 50% for only a couple tenths of a nm increase in the pore slit width. This is why the precision nano-engineered scaffold is the key, with identical molecular proppants to provide molecularly precise spacers between the graphene sheets. The cross-linkers are precise, due to molecular dimensions being identical, just as the spacing of the atoms in a sodium chloride crystal are identical.

### **Benefits from atom substitution**

”  $F = RT \ln K_{eq}$

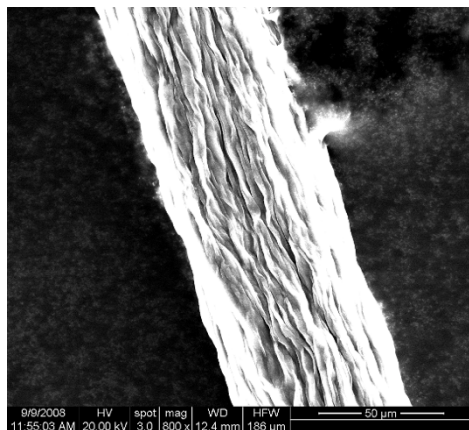
Hence the equilibrium constant inside the pore and hence the compression ratio of the “nanopump” if binding energy can be raised, the temperature also increases linearly. We found that boron atom substitution and phosphorous atom substitution both raised the binding energy from 5.5 to about 8.6 kJ/mol, a ratio of 1.56. Thus T could be increased by the same ratio from 77K x 1.56 = 120K. Our future direction was alternating layers to create charge separation and have dipole induced dipole binding of the hydrogen in the pore. At the least, this is expected to be additive, that is a further increase of 3.1 kJ/mol to 11.7 kJ/mol. This more than doubles the temperature to 164K. This is beneficial because less insulation is needed to preserve the H<sub>2</sub>.

### **Properties of sp<sup>2</sup> carbon nanomaterials**

These aligned arrays have excellent gas flow and kinetic properties, have high energy efficiency, and due to the great rigidity of the nanoscale structure, can endure cycling indefinitely without degradation. Given the many-fold criteria that a successful storage media must meet, as indicated above, there will undoubtedly be a best type, diameter, or small range of diameters of nanotubes that will have the best performance. The cloning technology will then become part and parcel of the nanoengineering of these materials. Our redirect was to graphene due to low cost, which retains the desirable enhanced uptake properties of sp<sup>2</sup> bonded carbon

Since the carbon nanotubes will perform best for hydrogen storage when they are spaced apart in a rigid nanoengineered framework with pores of predetermined and uniform size, the SWNTs from the HiPco reactor are spun into a **high density fiber** of pure, aligned nanotubes. We expand a spun fiber of nanotubes in oleum solvent, and then functionalize them with cross-linkers that hold the nanotubes apart at a fixed distance. The amount of expansion by the oleum and the length of the bifunctional cross-linkers determines the pore size. Theoretical work predicts that this is an optimum pore size that considerably enhances the free energy of binding

for optimum gravimetric uptake. In addition, with no oversize pores, there is no wasted space, and the density of the adsorbing media is optimum, so that volumetric uptake is also optimized.



Our nanoengineering technology allows for adjustment of the spacing to obtain the optimum pore size. This allows the hydrogen molecules to be entirely surrounded in a pore composed of  $sp^2$  carbon, and such  $sp^2$  surroundings providing a unique enclosure of pi-cloud electrons with which the  $H_2$  molecules can bond. Both theory and experiment, including our own work, point to unusually strong binding and high density packing in the  $sp^2$  pore. In addition, carbon nanotubes with unsurpassed thermal conductivity, their superb strength on the nanoscale, and the ability to form adjustable high density structures, will make them excellent candidates for a rigid scaffold for supporting metal atoms with sufficient binding energy for the room temperature uptake of  $H_2$ .

### **Cross-linked SWNT fibers**

The cross-link chemistry for each sample is indicated. We are testing the effect of the quality of the fiber alignment, with “bad fiber” indicating poor macroscale alignment. The BET uptake remains in the normal range. This demonstrates that entanglement of the bundles of nanotubes does not confer any special advantage in gravimetric uptake compared to well aligned fibers, which indicates that the adsorption is within the bundles and not on the exterior surfaces which would be more exposed for the criss-crossed bundles.

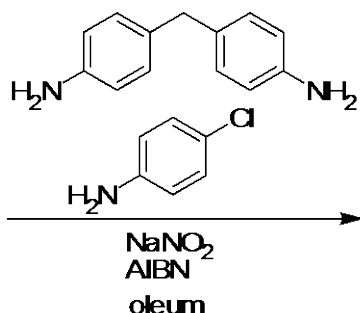
AL-I-148 We heated the fibers in the oleum to see if maybe that would help the functionalization. The results did not increase.

AL-I-157 We functionalized a “bad fiber” in which the SWNTs are not as aligned as the newer samples that we have been using. We then did a series of BET tests as shown below. This shows that the surface area does increase as we heat the fibers higher, suggesting that maybe we are removing some of the sulfuric acid.

ALI-157  
7-10-06

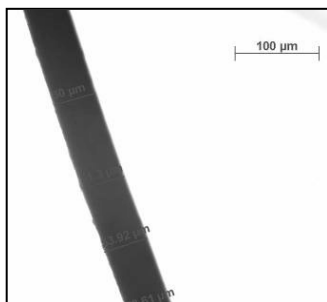


"bad" fiber



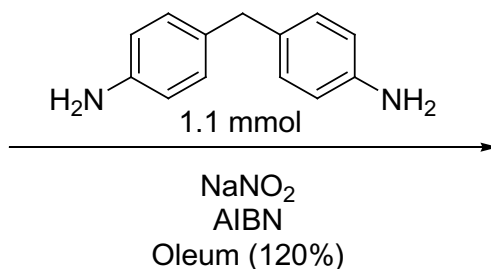
Functionalized Fibers

Heat to 150 °C	Vol of N <sub>2</sub> adsorbed 24.5 cm <sup>3</sup> /g	SA : 90.1 m <sup>2</sup> /g
Heat to 300 °C	Vol of N <sub>2</sub> adsorbed 30.5 cm <sup>3</sup> /g	SA : 110.5 m <sup>2</sup> /g
Heat to 460 °C	Vol of N <sub>2</sub> adsorbed 122.3 cm <sup>3</sup> /g	SA : 412.1 m <sup>2</sup> /g

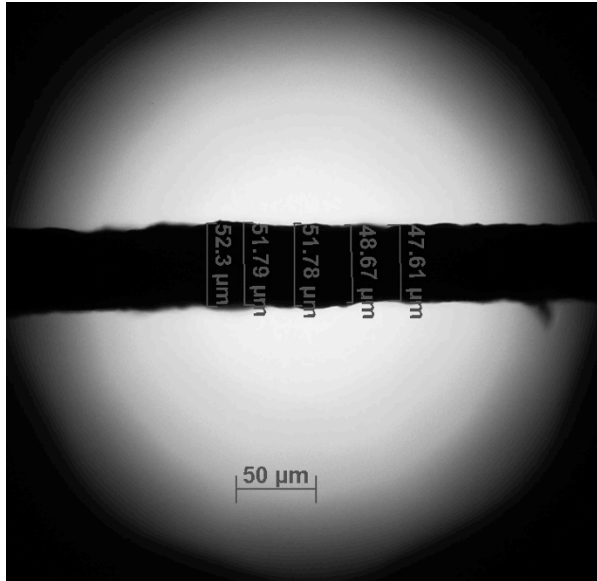


This is 3-D nanoengineering with a selectable pore size, and rigid spacing that does not expand or collapse upon addition or removal of the hydrogen. This media is made by post-processing HiPco reactor material using fiber spinning, subsequent expansion and cross-linked functionalization to create a self-supporting fibrous media. This is suitable for direct storage, or as a 3-D nanostructured scaffold for ambient temperature metal adsorbents.

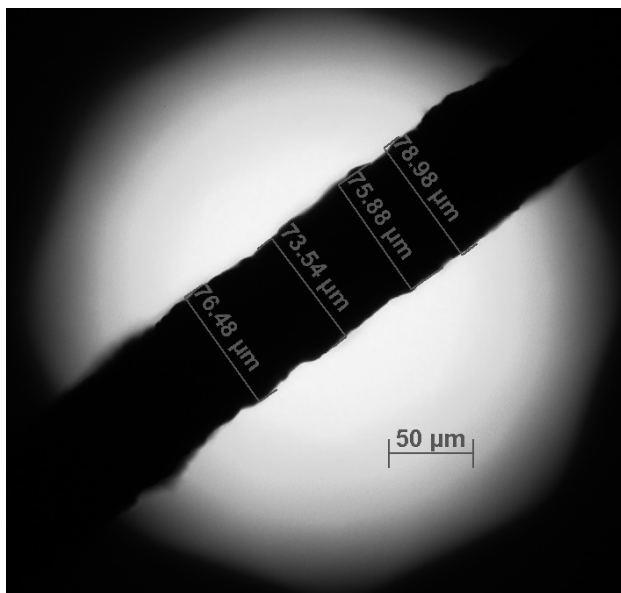
SWNT Fiber  
No mounting



Crosslinked Fiber



Unexpanded, from DoE-1850a average = 51 microns

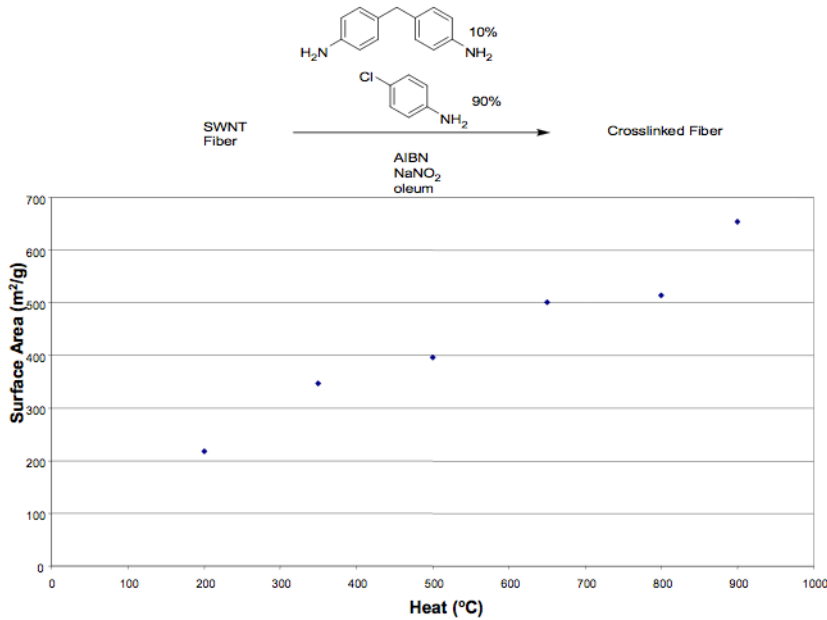


Expanded and Crosslinked fiber, from DoE 1850a  
 average diameter = 76 microns  
 average SWCNT diameter 0.9 nm calculate 9 Å pore size.

**Oleum expanded fiber, heating vs surface area**

expansion in oleum (fuming sulfuric acid) is very good at expanding and crosslinking the nanotubes, but has presented problems with solvent extraction. A study of high temperature processing shows that more acid is removed, and more space is made available for hydrogen uptake. However, the high temperatures also degrade the structure, so that either alternate extraction methods will be needed, or alternate expansion methods such as the lithium ammonia expansion may prove superior.

# Surface Area vs Heating of SWNTs



## 2.0 Characterization of the dibromobiphenyl crosslink

### 2.1 Optical microscopy

Optical microscopy is a valuable tool in measuring swelling of the HiPco fiber. If the crosslinking reaction was successful, we introduced pores in the fibers, which can be seen by an increase in diameter.

Functionalization with 4,4'-dibromobiphenyl via Billup's alkylation method of fiber A in the same reaction setup showed swelling of fiber A. The mean diameter of fiber A estimated by optical microscopy is 97.2  $\mu\text{m}$ . The error (standard deviation) with 18.1  $\mu\text{m}$  indicates that the fiber is not uniform in diameter. The crosslinked fiber has a mean diameter of 158.3  $\mu\text{m}$  with an error of 17.7  $\mu\text{m}$ . This corresponds to an increase in diameter of 62 % (see figure 3)

Figure 1: Diameter of fiber A before (blue) and after (red) the reaction

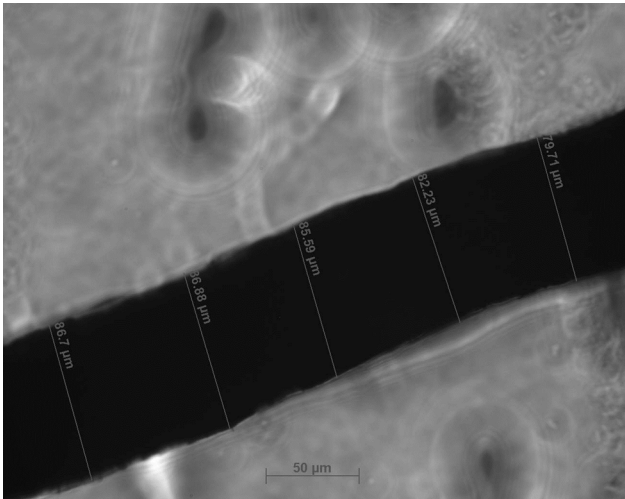
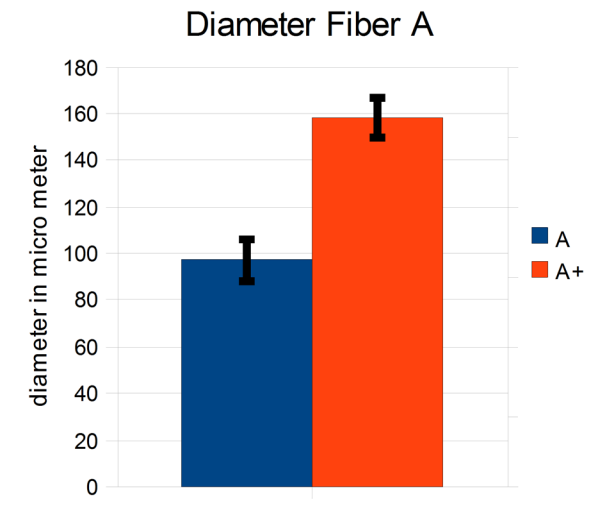
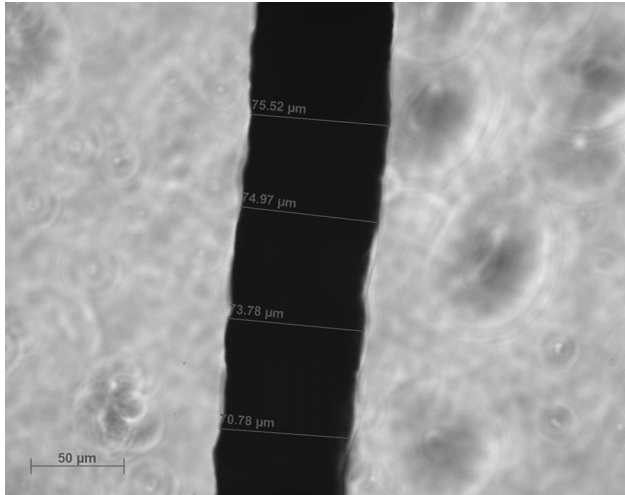


Figure 2: Fiber A before the crosslinking reaction

## 2.2 Raman

Fiber A:

The D-band of the starting fiber appears to be very low, as can be seen in figure 8. After the



*Figure 3: Fiber B before the crosslinking reaction*

Billup's reaction however, the D-band increases significantly. A closer look at the radial breathing mode (RBM) in figure 9 reveals that the signal at  $270\text{ cm}^{-1}$  completely disappears. This peak is considered to be the “roping peak” and is higher in intensity, the more bundles are present. Since the peak totally disappears, it is a good indication that a successful crosslinking reaction took place with the SWNTs now spaced apart from each other. This is strong evidence that this new expansion method to produce the 3D scaffold is working well.

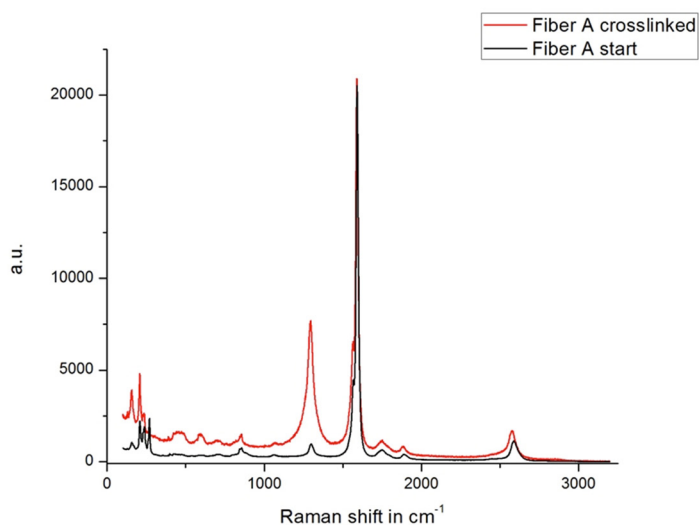


Figure 4: Raman spectrum (785 nm laser wavelength) of Fiber A before (black) and after the crosslinking reaction (red).

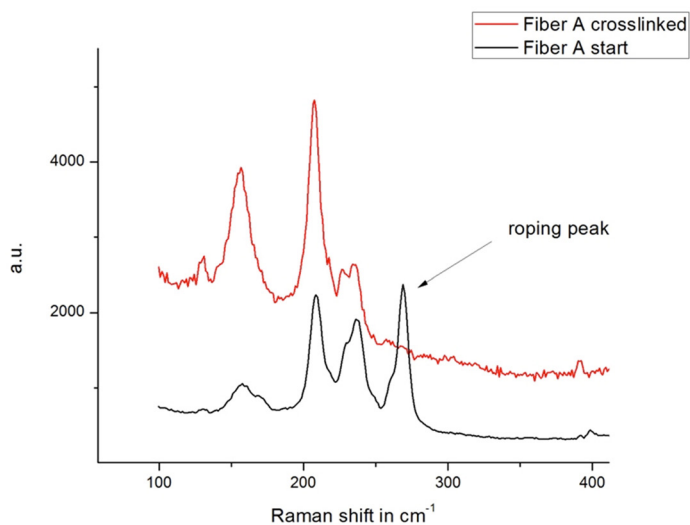


Figure 5: RBM mode of Fiber A before and after the reaction.

### 2.3 BET Surface Analysis

#### Fiber B:

BET measurements showed a decrease in surface area instead of an increase (starting material was  $121 \text{ m}^2 / \text{g}$ ). With heating however, the surface area increased slightly (see figure 12) with a white yellowish compound evaporating from the fibers, which had the same solubility properties than the starting material 4,4'-dibromobiphenyl. For measuring the surface area, the multipoint BET method was used.



Fiber A:

Surface area depending on temperature. It is worth to mention, that there still is starting material evaporating from the fibers, however in less amounts and at higher temperatures. This new method is already producing surface areas comparable to that for the well-developed oleum expansion.

120 °C	264 m <sup>2</sup> /g
200 °C	292 m <sup>2</sup> /g
400 °C	381 m <sup>2</sup> /g

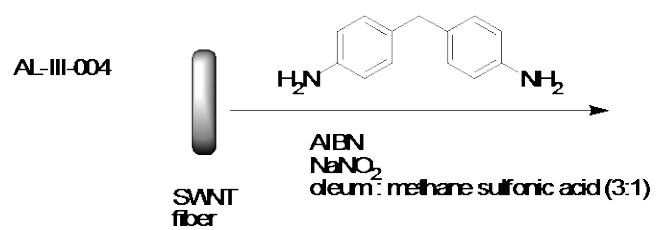
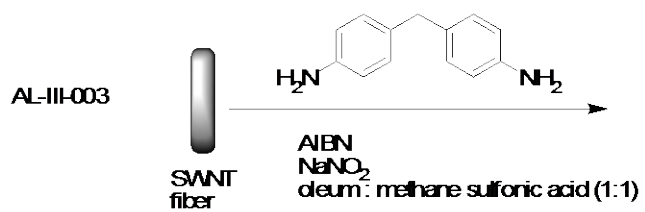
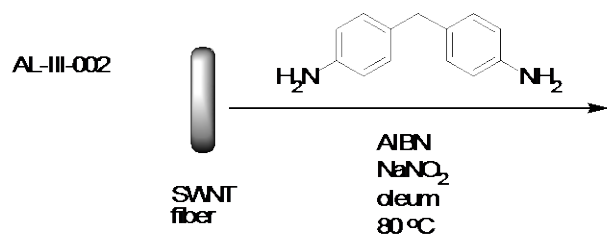
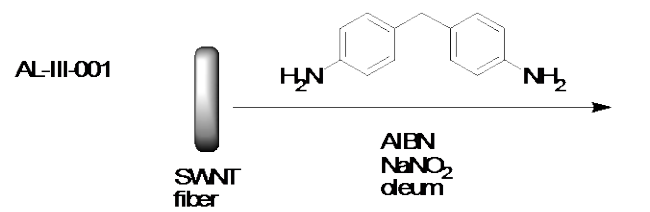
### **Spinning into methanesulfonic acid.**

An entirely new approach is being developed for the oleum-based nanoengineered scaffold. Ordinarily, the oleum=SWNT spinning dope is coagulated in a water bath which shrinks it as the acid is removed. Then this is re-expanded with new oleum. then the cross-linking chemicals need to diffuse in and the cross-linking is then initiated.. Such expansion may not be uniform, and involves multiple steps. In the new approach, the fiber is spun into methanesulfonic acid, which is a weaker acid than oleum, and will provide a more gentle reaction than that of the oleum in water, which is highly exothermic. (figure 7)

For the methanesulfonic reaction the cross-linking reagent is mixed directly into the spinning bath. This intercalates into the swollen fiber, and the coagulation/shrinkage followed by swelling of the fiber is bypassed. The radical initiator is then introduced and crosslinking commences.

In what is now essentially the creation of the SWNT scaffold in a one-pot reaction, this is an important step to scalability -- a concept always in mind -- in that the fiber that is collected is already expanded and cross-linked. Spinning a fiber and nano-engineering can be combined into a single continuous process!

In this first attempt we did not obtain complete fibers suitable for hydrogen uptake tests. In effect, the broken fibers form a granular material similar to most adsorbent media, although we are striving to develop all of this novel nanoscale engineering and maintain the fibrous integrity of the media. Our number one objective still remains the properly expanded on the nanoscale, which comes first, then we will endeavor to maintain the macroscale properties. In the near term, we can familiarize ourselves with handling the granular material to prepare for hydrogen uptake tests.



d

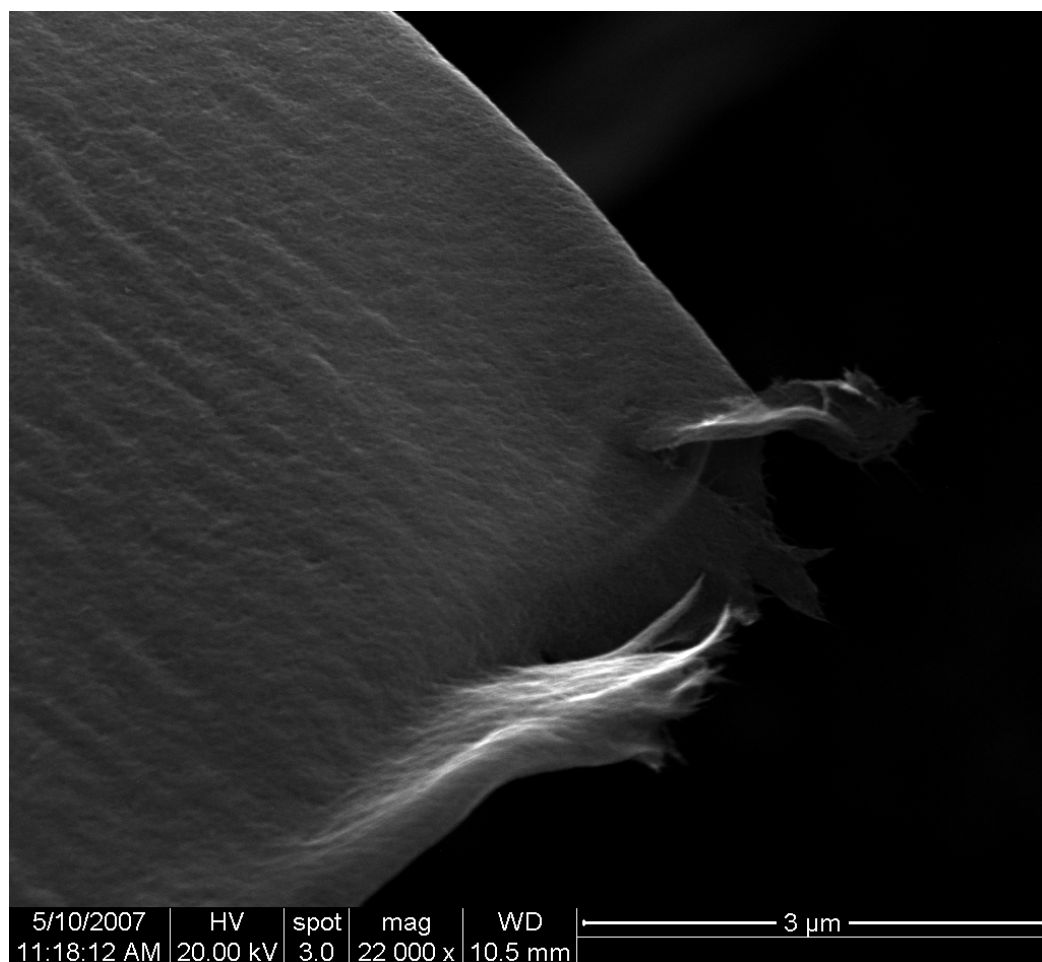


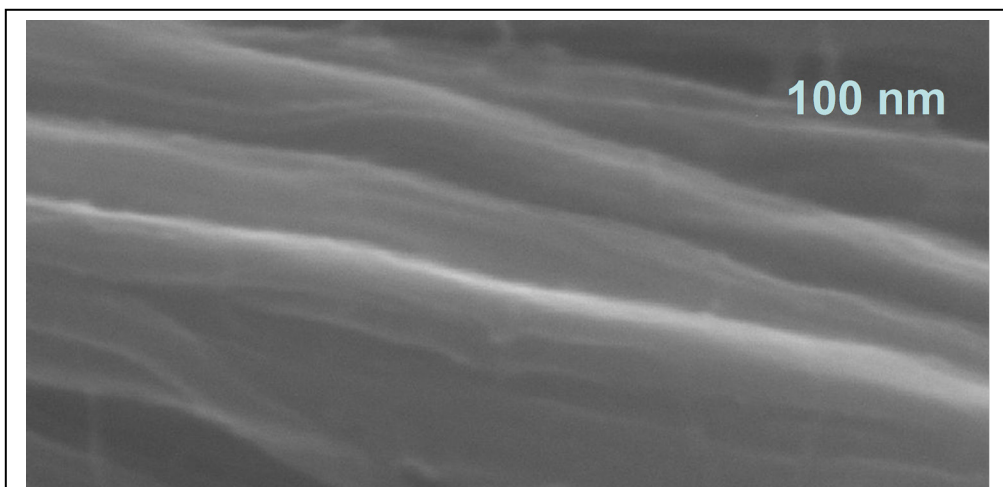
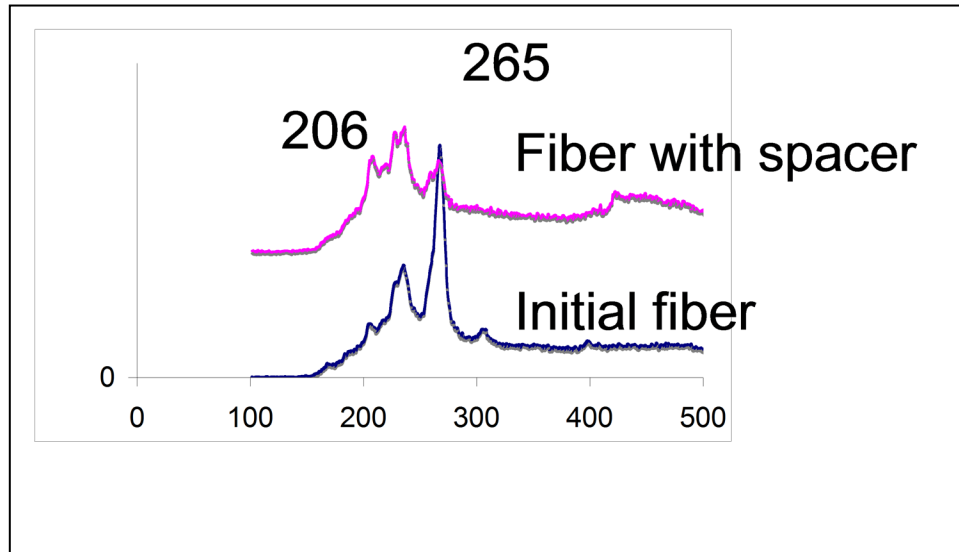
Figure 9. High resolution image of the new one-pot approach to making the SWNT scaffold. The fibrous nature of the crosslinked material is retained in the small scale structure, which is always important in any new approach we take.

### 1.1 Fiber crosslinking with Billup's alkylation method and the new dibromobiphenyl crosslink

In a 100 mL three necked, round bottom flask fitted with a dry ice condenser, 15 mg (1.2 mmol) HiPco-fibers were added to the reaction vessel under nitrogen atmosphere. Subsequently dry ammonia (75 mL) was condensed in the flask and 75 mg (10.8 mmol) of Li was added in small pieces. The solution was stirred for 2 hours in a dry ice-acetone bath and 4,4'-dibromobiphenyl (1.622 g, 5.2 mmol) was added slowly. The solution was homogenized for 2 hours at -78 °C and then at room temperature leading to slow evaporation of ammonia. The reaction was quenched by slow addition of water. The excess of 4,4'-dibromobiphenyl was dissolved in dichloromethane.

The fibers were washed several times with water and dried in the vacuum oven at 75 °C overnight.

The following figure shows the Raman spectrum which provides evidence that the nanotubes have indeed been separated, as the “roping” peak at 265 nm is greatly diminished.



**High Resolution SEM, 200,000x shows excellent alignment of the expanded nanotube fiber**

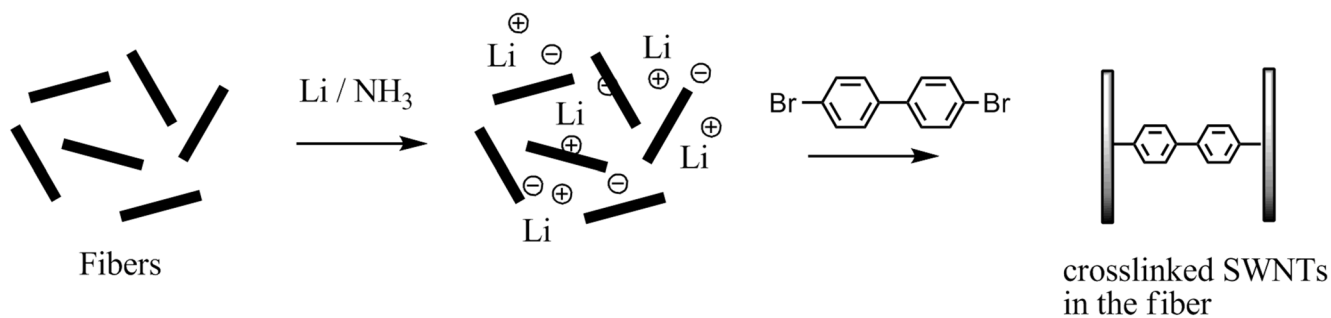
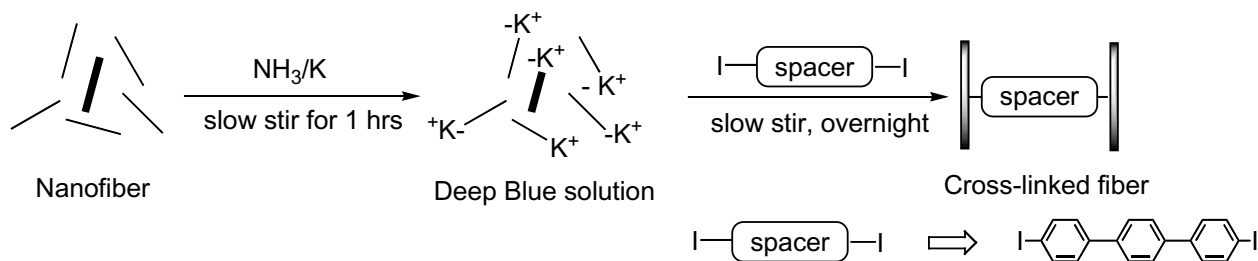


Figure 6: Reaction scheme for HiPCO fiber expansion using the Billup's alkylation method

## Alkali/ammonia based fiber expansion

In accordance with our plans to investigate diversification of our SWNT scaffold methods to overcome the solvent extraction problems associated with oleum, another fiber expansion method was developed. This uses the a potassium/ammonia bath. The larger alkali atom can help increase the spacing, and the lower electron affinity can help speed the intercalation process. This new demonstration that other, and larger, alkali metal atoms can expand the fiber is in accordance with our goal of adjustable expansion of the nanotube spacing (Figure 1)



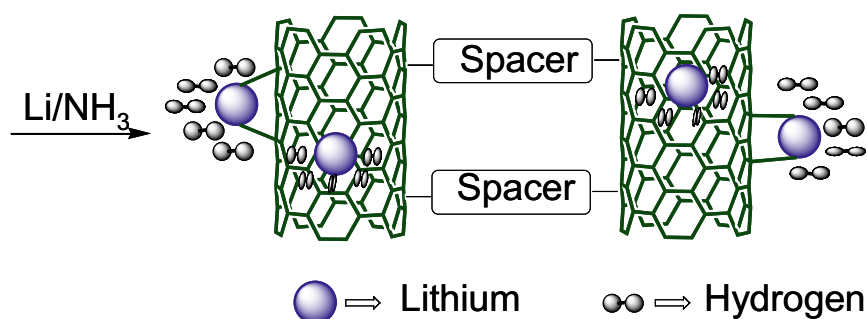


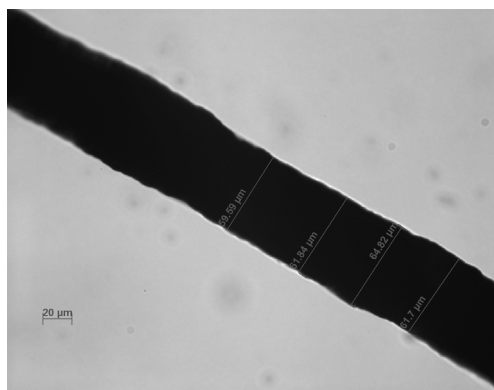
Figure 1. Top drawing: Potassium-based fiber expansion that has been recently been successfully performed in the laboratory. The CNT spun fiber is placed in a chilled bath of potassium dissolved in ammonia. The blue color indicates the presence of electrons solvated on the ammonia which leads to the intercalation. The addition of the iodo-triphenyl compound leads to the cross-linking of the SWNTs.

Bottom drawing: The crosslinked fiber which is produced from either a lithium ammonia chemistry, or from the new potassium/ammonia crosslinking chemistry is consequently subjected to lithium/ammonia bath, but in this planned second step, the lithium does not undergo subsequent reaction, but is left as the (charged) atomic species on the surface of the SWNT in the nanoengineered scaffold. The theoretically predicted charged induce dipole attraction of the hydrogen to the alkali metal is illustrated.

### Optical Microscopy of alkali expanded fiber

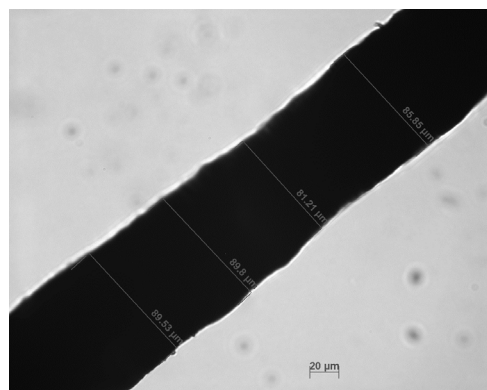
The spun fiber of pure SWNTs has been expanded by the alkali metal process described above. Figure 3 shows how this has been expanded without the use of oleum and had become larger. This demonstrates that there is more than one route to perform the 3D nanoengineering. In less than a year after the first oleum scaffold method was developed, a second one, based on an entirely different chemistry has now been proven. The enormous van der Waals attraction trying to pull them back together has been held at bay by the cross linkers. This binding force is unleashed to attract the hydrogen molecules more strongly than for carbon-based media that are not made of pure  $sp^2$  pi clouds.

### Unfunctionalized nanofibers



Average diameter H63 μm

### Nanofibers with spacers



Average diameter H85 μm

Figure 3. Optical microscopy of the expanded fiber. left: SWNT spun fiber before treatment. Right: Carbon nanotube fibers undergo swelling (35%) on covalent attachment of spacers. Functionalized SWNT scaffolds are self supporting and remain enlarged after solvent removal, in spite of the enormous van der Waals attraction trying to pull them back together.

### Raman data: the alkali expanded fiber scaffold

Raman spectroscopy is a powerful probe into the nanoscale structure of the fiber. This shows successful expansion and crosslinking of the fiber has been achieved (figure 4)

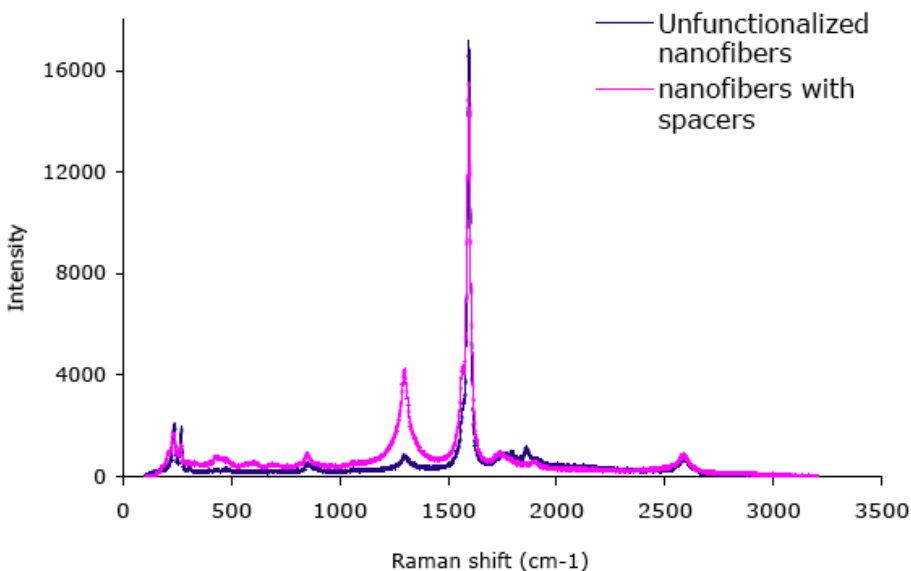


Figure 4. Raman spectrum comparing the SWNT fiber before and after functionalization with crosslinking. The blue trace shows the very small “D” peak at 1300  $\text{cm}^{-1}$ , for pristine sidewalls. The red trace shows that this peak grows markedly after crosslinking, proving that this is covalent bonding between the nanotubes, and not just debris holding the SWNTs apart. The 265  $\text{cm}^{-1}$  “roping” peak, just to the right of the 234  $\text{cm}^{-1}$  peak essentially disappears, so the red trace shows only the single peak in the low frequency shift region of the radial breathing modes. This is very strong evidence that the van der Waals interaction has been overcome, and that nanotubes have become individually separated from each other.

### Apparatus constructed for alkali metal uptake

In addition to this new method for crosslinking, this alkali metal method also provides the 3D nanoengineered scaffold for metal atom based molecular hydrogen to provide room temperature uptake.

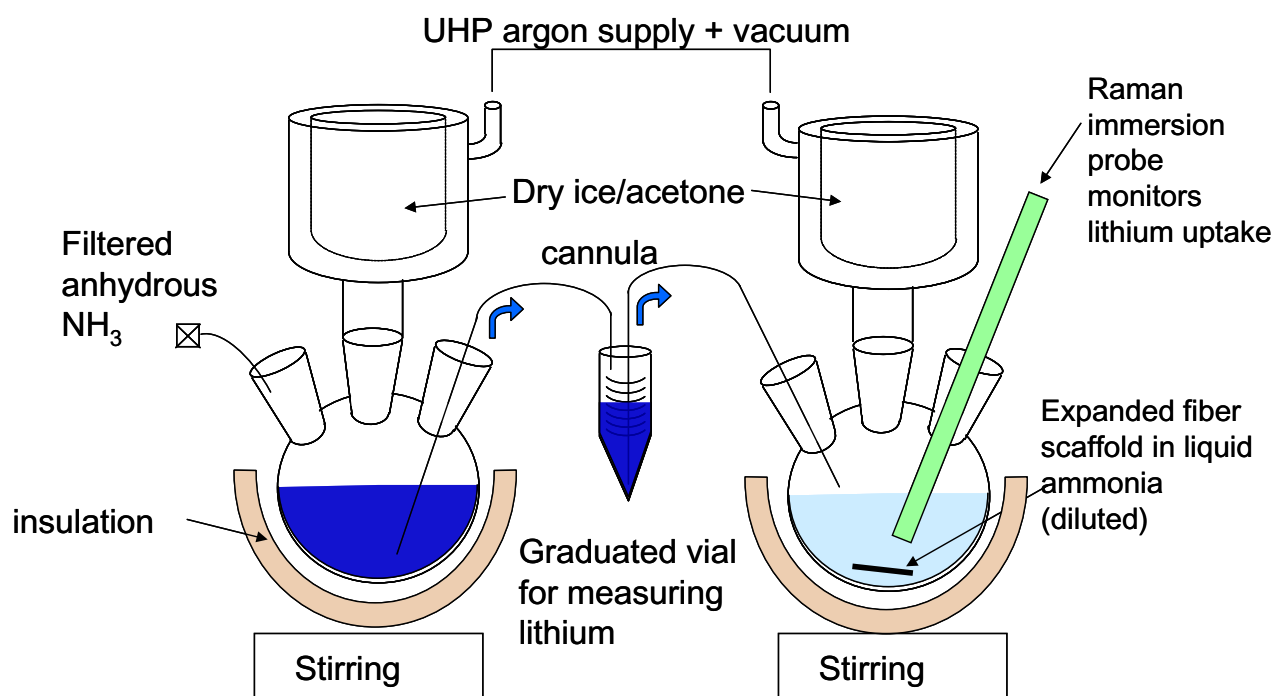


Figure 6. The proposed apparatus for quantitative addition of lithium to the cross-linked fiber that was constructed. The weighed lithium metal is placed in the flask on the left containing chilled liquid ammonia, to produce a solution of known concentration. The concentration can be verified by absorption spectroscopy on the characteristic blue color. This is transferred to a graduated vial under a blanket of inert gas. This simplifies the process of handling alkali metals and converts the measurement into one of measuring a volume of liquid rather than handling hygroscopic metals. The amount transferred from the graduated vial matches that of the mass of



the nanoengineered fiber and the amount of doping desired for the test. The doped fiber is then removed from the bath in an oxygen free glove box.

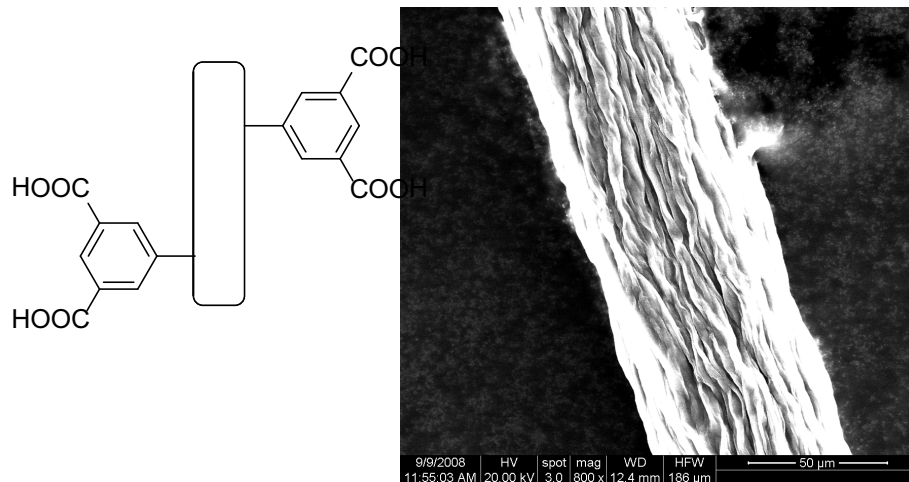
Due to our success with acid-based functionalization and spinning, we discontinued work on the lithium/ammonia functionalization

## **Isophthalic acid pre-spinning functionalization**

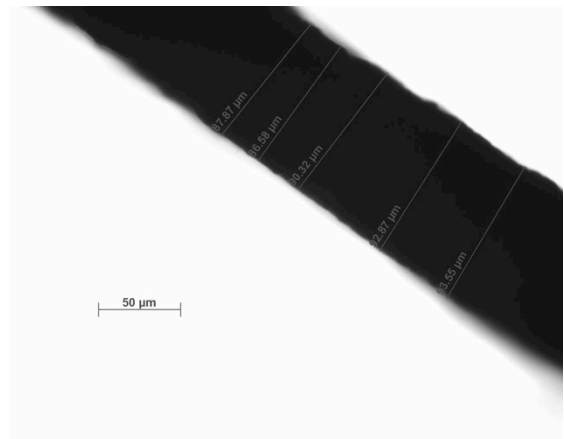
1. New type of CNT fiber has been made by pre-functionalization with isophthalic acid for more uniform pore spacing in the catalyst. This new scaffold was tested at NREL for the best hydrogen uptake, and largest deviation from Chahine's rule we have yet achieved.
2. A new approach to making graphene has been successfully tested, growing it from the gas phase using CVD rather than expanding mineral graphite
3. Metal uptake on nanotubes using potassium had been tested, and the Eklund shift of the Raman spectrum shows that successful electron transfer has taken place. This provides another tool in our toolkit of metal doping that should lead to RT hydrogen uptake
4. We attempted spillover on a parallel track to see if we could replicate the mercury catalyzed spillover reported at AMR 2008. We substituted very low cost graphene oxide, in place of the very expensive "carbon foam". We did not have good intercalation, and Ralph Yang reported that he could not reproduce the results, so we consider this a "no-go".

### **Use of isophthalic acid prefunctionalized SWCNTs provides proppants when the fiber is spun**

Crosslinked swollen fiber exhibits a 50% increase in diameter; corresponds to a 9 Å pore  
The spun fiber remains intact after the pore expansion process.  
The nanoengineered medium is a self-supporting, readily handled macroscopic object



The chemistry of the functionalization is indicated above.



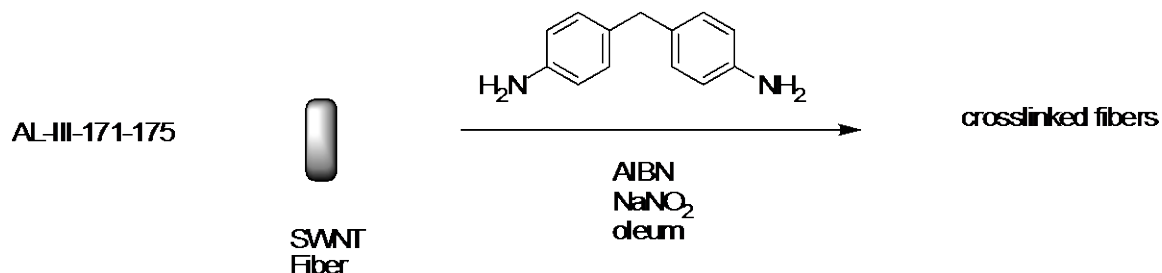
The spun fiber expanded from 62 microns left to 90 microns right, an increase of almost 40% diameter.

## 1. Crosslinking of fluorinated fibers with biphenyl

Fluorination of CNT fibers

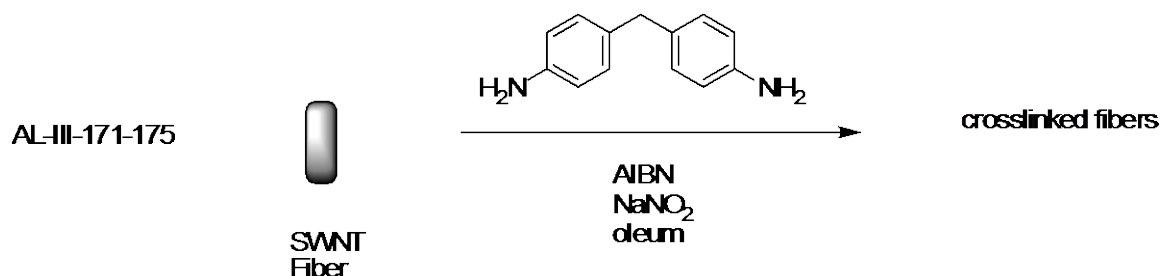
Crosslinking with biphenyl has been adapted to include fluorinated CNT fibers.

Fluorination continues to be a promising new method of expansion and functionalization of CNT fibers. A new type of crosslinker was demonstrated which uses an aminated biphenyl moiety. This also develops a methodology on a well-known substrate that may be useful for subsequent application to graphene-based materials.



### AL-III-171 – SWNT fibers on glass

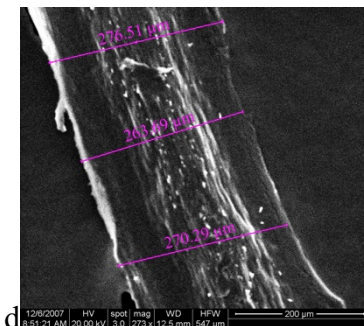
The fiber spinning process was modified with the spun fiber falling on a glass substrate rather than immersion in a water bath. This demonstrates that is feasible to slow the coagulation process that is very rapid in water and can be disruptive. However, the fluorination did not yield much expansion.



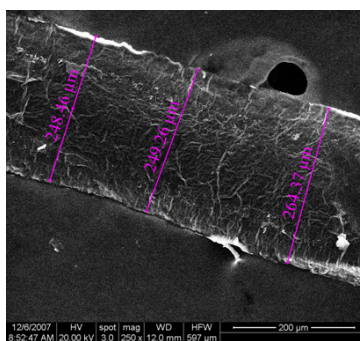
### AL-III-171 – SWNT fibers on glass

Sample	Raman	Diameter
AL-III-171-standard	0.04	280.1 μm
AL-III-171	0.14	278 μm

SEM image of fiber before functionalization : Average Diameter = 280.1  $\mu\text{m}$

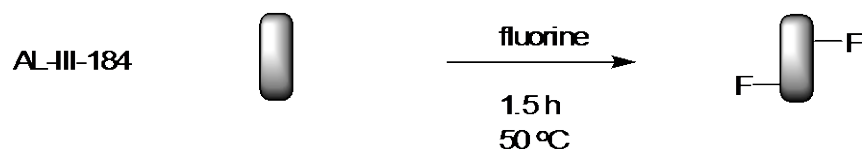


SEM image of fiber after functionalization : Average Diameter = 278  $\mu\text{m}$

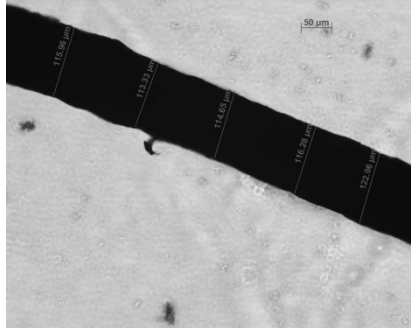


## 1.1 Reducing the amount fluorination

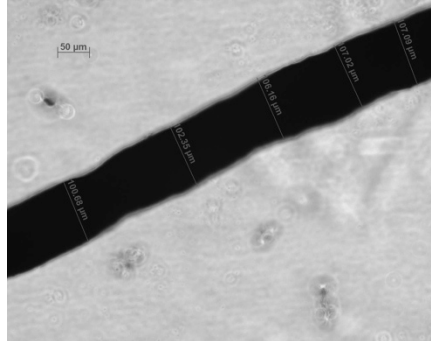
Since we did not obtain high hydrogen uptake with the fluorinated SWNT fibers and after further functionalization, they may be over-fluorinated in the expansion. A new approach was successful in reducing the fluorine content. This was done by both decreasing the fluorination time from 4 hours to 1.5 hours and also decreasing the temperature from 150  $^{\circ}\text{C}$  to 50  $^{\circ}\text{C}$ . This did reduce the fluorine content from about 30% fluorine compared to carbon to about 20% fluorine. The BET surface area went from 399  $\text{m}^2/\text{g}$  to 201  $\text{m}^2/\text{g}$ .



Optical Microscope image of fiber before functionalization : Average Diameter = 108.1  $\mu\text{m}$



Optical Microscope image of fiber after functionalization : Average Diameter = 100.5  $\mu\text{m}$



### Fluorine expansion spinning method tested

#### a. Production of spun fiber without oleum

#### b. defluorination to restore integrity of the pi cloud.

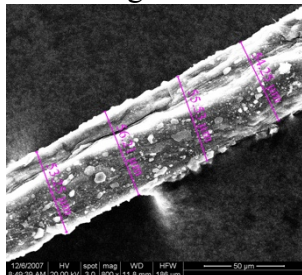
This research is focused on the fluorinated SWNT fibers and also trying functionalization on a variety of different types of fibers. Meaning, these fibers were spun from a dope other than the troublesome oleum (fuming sulfuric acid) and were spun into different coagulants. These changes in the fiber spinning process creates fibers with different properties including larger and smaller diameter, and also different degrees of oleum swelling.

#### AL-III-172 – SWNT fibers 10% chlorosulfonic acid spun into ether

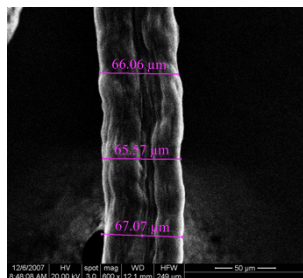
The fiber expansion was successful using the new spinning methodology without oleum.

Sample	Raman	Diameter
AL-III-172-standard	0.02	38.14 $\mu\text{m}$
AL-III-172	0.14	49.1 $\mu\text{m}$

SEM image of fiber before functionalization : Average Diameter = 38.14  $\mu\text{m}$



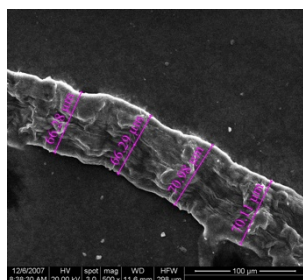
SEM image of fiber after functionalization : Average Diameter = 49.1  $\mu\text{m}$



### AL-III-174 - SWNT fibers 10% chlorosulfonic acid spun into ice chloroform

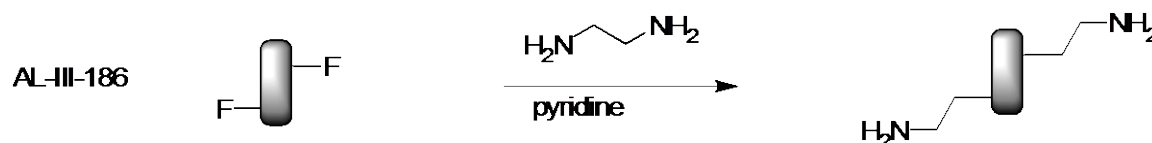
Sample	Raman	Diameter
AL-III-174-standard	0.04	114.4 $\mu\text{m}$
AL-III-174	0.04	129.8 $\mu\text{m}$

SEM image of fiber before functionalization : Average Diameter = 114.4  $\mu\text{m}$

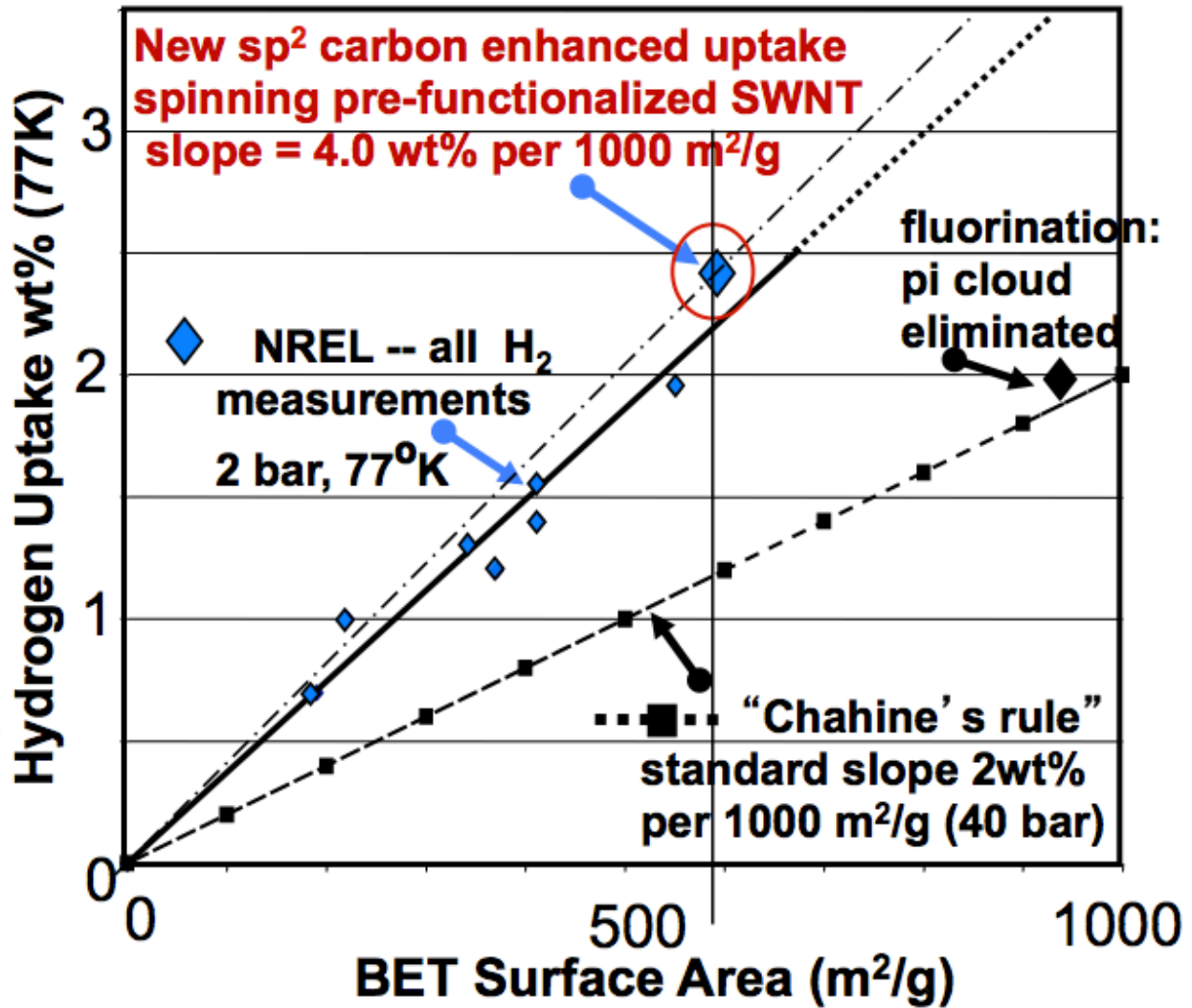


SEM image of fiber after functionalization : Average Diameter = 129.8  $\mu\text{m}$

These fluorinated SWNT fibers were then functionalized with ethylene diamine. The idea is that since there is a fewer numbers of fluorines on the SWNT fibers then the ethylene diamine reaction will not be as successful. This would hopefully leave more room for hydrogen adsorption. The surface area went from 418  $\text{m}^2/\text{g}$  to 407  $\text{m}^2/\text{g}$ . This is basically the same surface area within error of the instrument. From here, this work will use fluorinating for less than the 1.5 hours at room temperature. This should decrease the over-fluorination and prop the SWNT fibers up enough for hydrogen uptake.



Summary of these experiments: The crosslinking of fibers can be done on a variety of different types of fibers – meaning the fibers are spun from different types of dopes. We will continue to investigate the fibers that were spun onto glass, spun from 10% chlorosulfonic into ether, and spun from 10% chlorosulfonic acid into ice-cold chloroform. We see promise in these types of fibers. We are able to functionalize these larger and smaller diameter fibers, which will allow us to engineer our fibers to the optimal size.



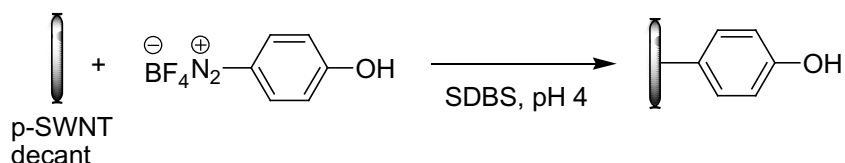
However, a rigid scaffold with excellent thermal conductivity is needed to provide for adequate gas flow and indefinite cycling without degradation.

We are able to successfully expand and crosslink nanotube fibers into a rigid and stable frame with chosen pore size. Uptake of hydrogen exceeds the slope provided by "Chahine's rule" by a factor of 2 or more indicating that properly engineered pores that are surrounded entirely by a pi cloud structure may have the capability of exceptionally large uptake per unit area, and research from other groups, both theoretical and experimental, supports this. We are able to project 8wt% to 10wt% uptake at 77K upon successful removal of the solvent. Extraction of the solvent after expansion is challenging, and we will engage in searching both for improved solvent extraction methods, and finding other expansion methods which use a more volatile solvent that can be readily removed.

## Functionalization developed as potential anchor sites for metal atoms.

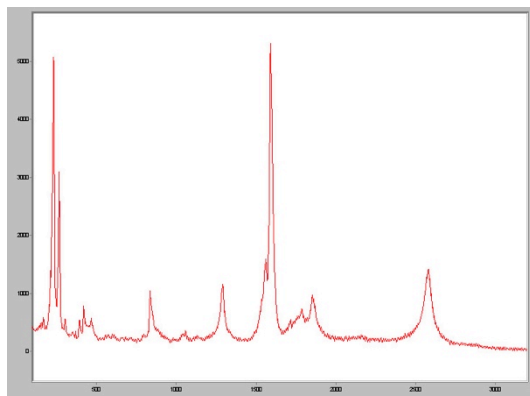
Several functionalization reactions have been tested. These are essential to determine the best species that can be attached to the sidewall for subsequent chemistry and providing an anchor for metal atoms.

### CDD-IV-195



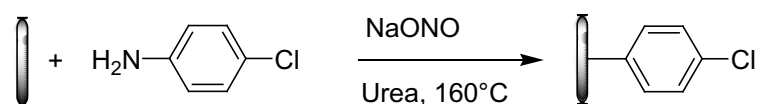
Even with the pH being adjusted, the G band did not shift at all, perhaps this was on a SDBS decant. During my past fluorescence experiments, I could manipulate the intensity of the sample via pH. This lends evidence that the surface of the tube is affected by the change in pH, therefore the phenol should be deprotonated, showing that the proton is acidic and the ionized version is stable. G is roughly  $1593\text{ cm}^{-1}$ , which is normal.

The solid Raman looks as follows:

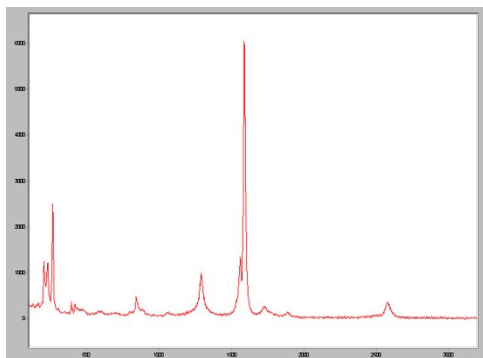


The strong radial breathing modes ca.  $250\text{ cm}^{-1}$  indicate undamaged sidewalls. Functionalization is modest, as the D/G ratio is modest.

### CDD-IV-199



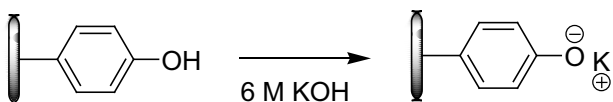




17% D to G ratio.

The D to G ratio was unusually low for this reaction (normal 30 to 40%). I used the old 4-chloroaniline, again showing modest functionalization.

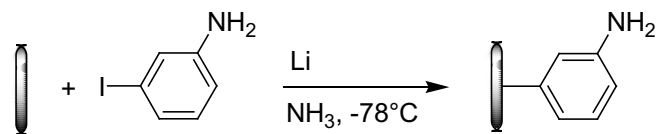
### CDD-IV-201



No noticeable shift in the G band suggesting that the charge remains localized on the phenol group. Oxygenated ligands probably keep the charge localized, which is less favorable for H<sub>2</sub> storage at RT.

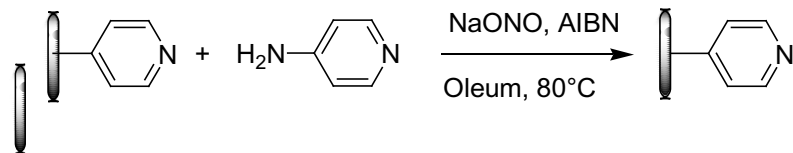
d

### CDD-IV-203



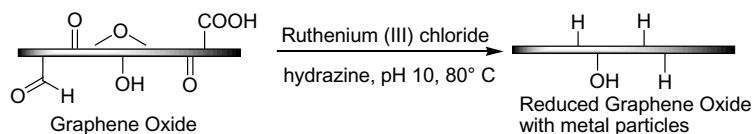
Creating material to be treated with LDA. Will make some material with the amine in the para position. This pyridine ligand is a good candidate for alkali metal uptake such as with lithium.

### CDD-IV-206



A new metal intercalant has been tested, and nano-particles were observed in the graphene sheets. Ruthenium has by far the most examples of “Kubas-type” binding of dihydrogen.

### CDD-IV-200



### Nickel doping of the SWNT framework

Nickel doping is now being added. Our first sample with 1.2% nickel doping has been tested by NREL and showed enhanced uptake of hydrogen, with a total uptake of 1.95 wt% at standard test conditions (2 atm). The increased uptake corresponds to at least two H<sub>2</sub> per nickel atom, assuming that all atoms are available. If some nickel atoms were buried, the remaining atoms would have to bind more than two H<sub>2</sub> molecules to account for the increased uptake for this sample. More nickel doped expanded frameworks have been prepared.

### Samples for hydrogen uptake

We have added more nickel to the fibers. One “bad fiber” was included.

We also heated some fibers to 1000 °C to be sure that we removed all of the sulfuric acid. We also did an oxidation on the fibers after functionalization to see if this would open more holes for hydrogen to be stored. Two of the samples, 193 and 194 have been doped with nickel to test for excess uptake by the metal supported on the framework

### Cross-linked SWNT fibers

The cross-link chemistry for each sample is indicated. We are testing the effect of the quality of the fiber alignment, with “bad fiber” indicating poor macroscale alignment. The BET uptake remains in the normal range. This demonstrates that entanglement of the bundles of nanotubes does not confer any special advantage in gravimetric uptake compared to well aligned fibers, which indicates that the adsorption is within the bundles and not on the exterior surfaces which would be more exposed for the criss-crossed bundles.

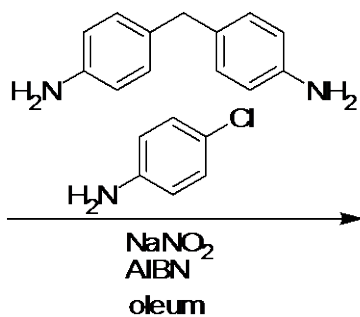
AL-I-148 We heated the fibers in the oleum to see if maybe that would help the functionalization. The results did not increase.

AL-I-157 We functionalized a “bad fiber” in which the SWNTs are not as aligned as the newer samples that we have been using. We then did a series of BET tests as shown below. This shows that the surface area does increase as we heat the fibers higher, suggesting that maybe we are removing some of the sulfuric acid.

ALI-157  
7-10-06



"bad" fiber



Functionalized Fibers

Heat to 150 °C	Vol of N <sub>2</sub> adsorbed 24.5 cm <sup>3</sup> /g	SA : 90.1 m <sup>2</sup> /g
Heat to 300 °C	Vol of N <sub>2</sub> adsorbed 30.5 cm <sup>3</sup> /g	SA : 110.5 m <sup>2</sup> /g
Heat to 460 °C	Vol of N <sub>2</sub> adsorbed 122.3 cm <sup>3</sup> /g	SA : 412.1 m <sup>2</sup> /g

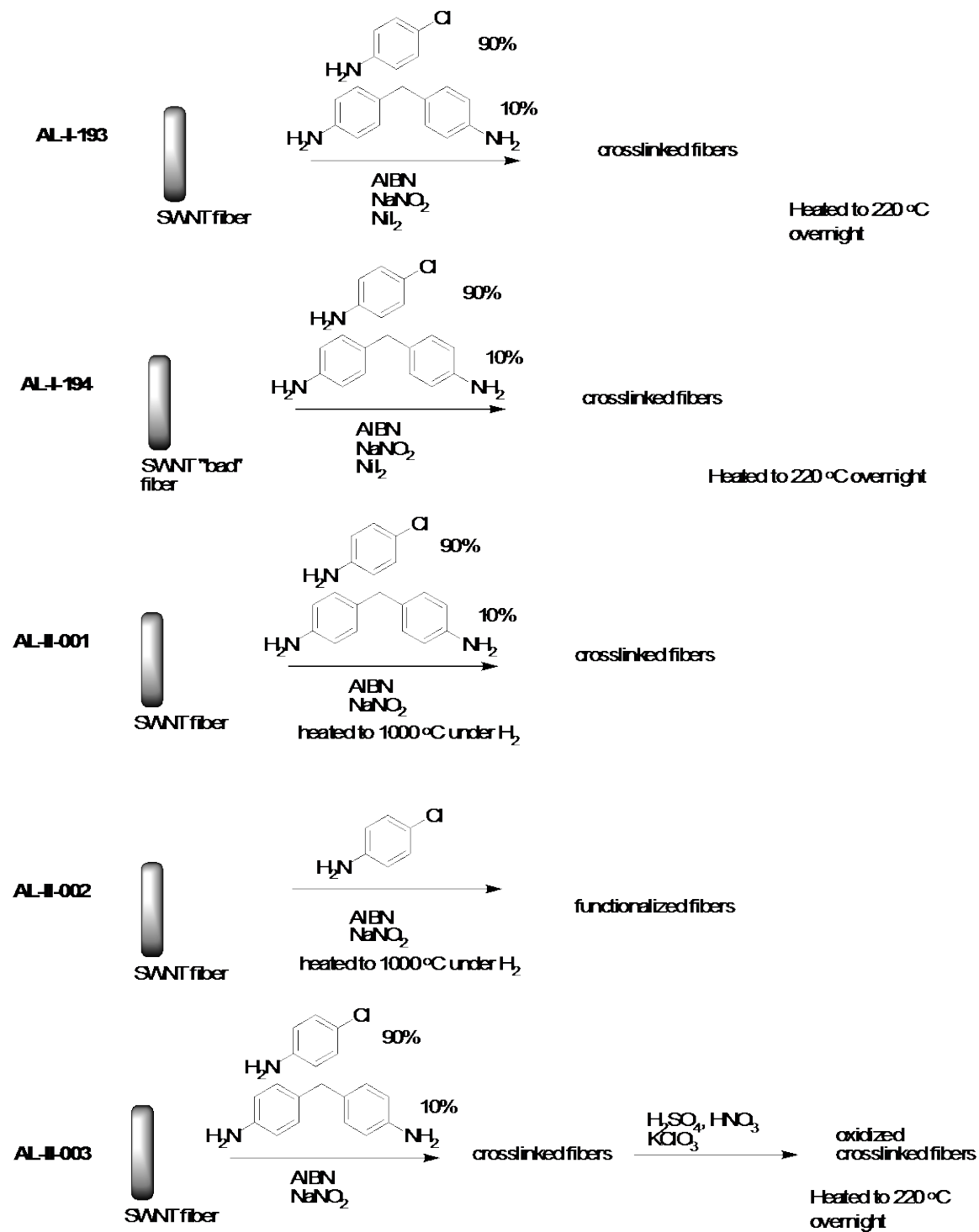
## **Samples for hydrogen uptake**

We heated some fibers to 1000 °C to be sure that we removed all of the sulfuric acid. We also did an oxidation on the fibers after functionalization to see if this would open more holes for hydrogen to be stored. Two of the samples, 193 and 194 have been doped with nickel to test for excess uptake by the metal supported on the framework

All of the samples that NREL heated to over 500 °C was done after July, including the 1.95 H-adsorption.

AL-I-148 We heated the fibers in the oleum to see if maybe that would help the functionalization. The results did not increase.

AL-I-157 We functionalized a “bad fiber” in which the SWNTs are not as aligned as the newer samples that we have been using. We then did a series of BET tests as shown below. This shows that the surface area does increase as we heat the fibers higher, suggesting that maybe we are removing some of the sulfuric acid



### Vertically aligned single wall nanotube arrays (VA-SWNT) array

This is also known as “carpet growth”. This is another approach to provide nanoengineered arrays of the fibrous rather than granular media that can take advantage of the high thermal conductivity of nanotubes.

The focus of the carpet growth project has been to find conditions that will grow the tallest vertical array of SWNTs, covering the largest possible area, in a given amount of time. The standard surface used is Si with a native oxide layer, coated with 10 nm of Al<sub>2</sub>O<sub>3</sub> followed by 0.5 nm of Fe. This wafer is rapidly inserted into a tube furnace with a hot filament, the purpose of which is to make atomic hydrogen that will rapidly reduce the metal on the surface. Growth runs have been done at different filament temperatures, and it has been observed that there can be too much atomic hydrogen for growth. Once the filament is carburized in the growth gases, a temperature (200-2300°C) can be assumed from the current. The current was varied until one was found that did not overwhelm the surface with atomic H while still growing the tallest possible carpet.

Once the optimal current was determined, the growth gases were varied. The best concentrations of gases that would grow, but not deposit amorphous carbon on the quartz tube were 10% methane and 0.5% acetylene, in H<sub>2</sub>. Also, a small amount of air (0.1%) was found to increase carpet height. These conditions will grow a 50µm carpet in 20 minutes, and the height is roughly linear to growth time. The area over which the carpet is grown is also maximized by these conditions. Tall carpets have been grown with acetylene only, but only over short areas.

With the best growth conditions determined, different substrates were used. If the process is to be scaled up, then a cheap surface is needed on which a large area of it can be coated with catalyst quickly. This can be done with metal foils. It was found that carpets could be grown on several different metal foils, like stainless steel, Ni/Fe alloys and Ti. The metals are also ideal in that they heat fast, keeping the catalyst particles from ripening and over-coating with carbon before they nucleate a tube. Upon scale-up, using sheet metal from a roll could allow several square feet of carpet to be produced in a few hours.

### **Test of Electrophilic fillers**

Initial studies have been carried out at Rice and NREL to investigate the possibility of enhancing the binding of hydrogen to the surfaces of SWNT by filling them with an electrophilic molecular species. SWNTs were partially filled with molecular iodine and bromine by exposing SWNT to the respective gases. These materials were investigated at NREL to determine if enhance surface binding of hydrogen was evident, but the first test indicates no significant enhancement for these relatively weak electrophilic fillers.

## 3a. Metal doping of SWNT

### Nickel doping of the SWNT framework

Nickel doping is now being added. Our first sample with 1.2% nickel doping has been tested by NREL and showed enhanced uptake of hydrogen, with a total uptake of 1.95 wt% at standard test conditions (2 atm). The increased uptake corresponds to at least two H<sub>2</sub> per nickel atom, assuming that all atoms are available. If some nickel atoms were buried, the remaining atoms would have to bind more than two H<sub>2</sub> molecules to account for the increased uptake for this sample. However, this did not help with uptake

We investigated the system of SWCNTs that were doped with lithium, sodium, potassium and calcium by Raman spectroscopy to give an explanation for the low hydrogen uptake numbers for lithium doped SWCNTs and predict how to design doped nano-engineered spaces build up by SWCNTs.

We used a buckypaper of purified SWCNTs that should act as an example for our nano-engineered spaces. Doping expanded fibers gave similar results. Metal doping of SWCNTs was performed in liquid ammonia at dry ice temperature with an excess of metal present. To prevent the nanotubes from being coated by MNH<sub>2</sub> salt, which remains in the flask after evaporation of ammonia, the material was put in a stainless steel metal mesh and lifted out of the solution before removing the dry ice bath. After transferring the doped SWCNTs to a sealed glass tube in a dry box, Raman spectra were taken.

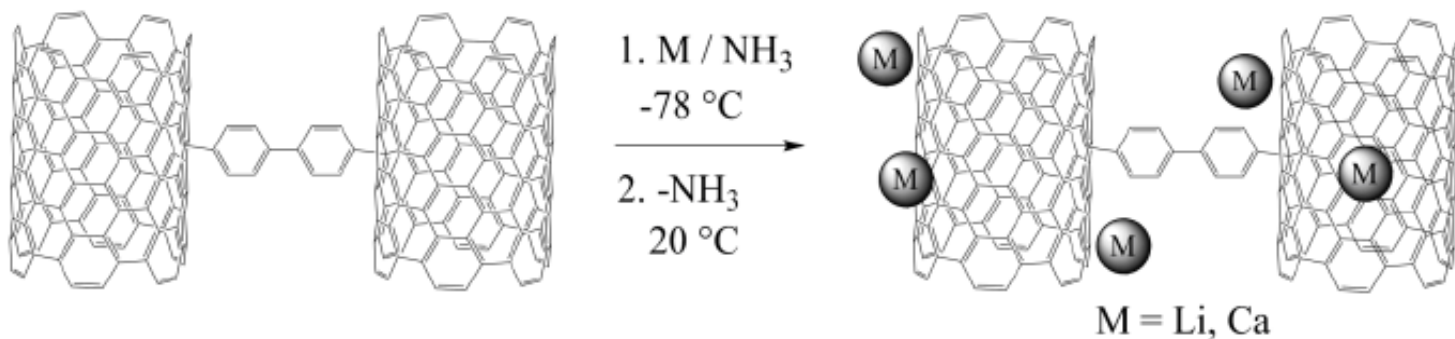
SWCNT doping by lithium in NH<sub>3</sub>: 10 mg buckypaper of SWCNTs functionalized with pyridine and degassed before at 250 °C for 18 h in vacuum, were trapped in a stainless steel metal mesh, which was put in a 100 mL nitrogen-purged and heat dried three-necked round bottom flask, equipped with two gas inlets, condenser and pressure compensation. Dry ammonia (75 mL) was then condensed into the reaction vessel. Lithium metal was added to the solution until a stable blue color appeared. The solution was stirred for three hours in a dry-ice-acetone bath. Then the metal mesh was pulled out of the solution and the liquid ammonia was evaporated at room temperature. The sealed reaction vessel was opened in a dry box and the doped buckypaper transferred to a glass vial, which was sealed air tight. The procedure was the same for calcium

Raman spectroscopy was used to prove interaction of the metal with the SWCNT. The shift of the graphitic (G) -band (Eklund shift)<sup>i</sup> was used for an indication of the relative amount of negative charge transferred to the SWCNTs. N -doping of SWCNTs lead to electrons in antibonding orbitals, weakening the carbon -carbon bonds, which causes a lower Raman shift for the G -band.

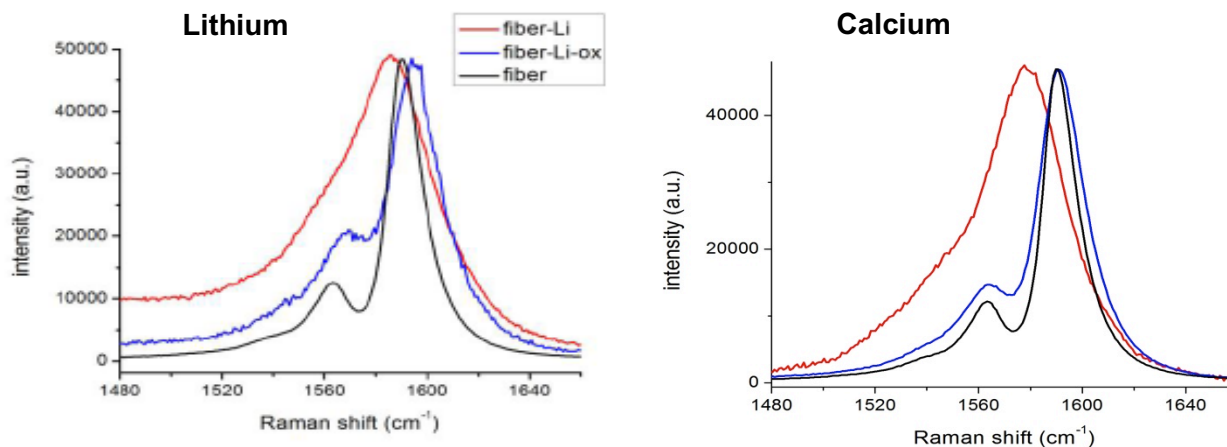
Lithium was used as dopant for SWCNTs in liquid ammonia. Both, the D –band as well as the G –band give valuable indication about the material. All spectra were baseline corrected as well as normalized to the height of the G –peak.

The position of the G –band after doping is in the range of 1582 – 1583  $\text{cm}^{-1}$ . But the shift is not the only thing about the G –band that can be observed. Broadening of the G –band is probably due to inhomogeneous doping, meaning that some SWCNTs are doped more than others.

Oxidation leads to a backshift of the G –band first and afterwards decrease of the D –band. The red spectrum are lithium doped SWCNTs with an Eklund shift of 9  $\text{cm}^{-1}$ . The next spectrum in black shows an Eklund shift of 4  $\text{cm}^{-1}$  and a slightly decreased D –band. The G –bands of the green and blue spectra are not shifted anymore, however, the green spectrum still shows a low D –band. The blue spectrum is the completely reoxidized material. Apparently first the negative charged tubes are oxidized and afterwards the lithium that interacts with the SWCNT surface. This indicates that the Eklund shift is due to lithium, that donates some of its charge but does not



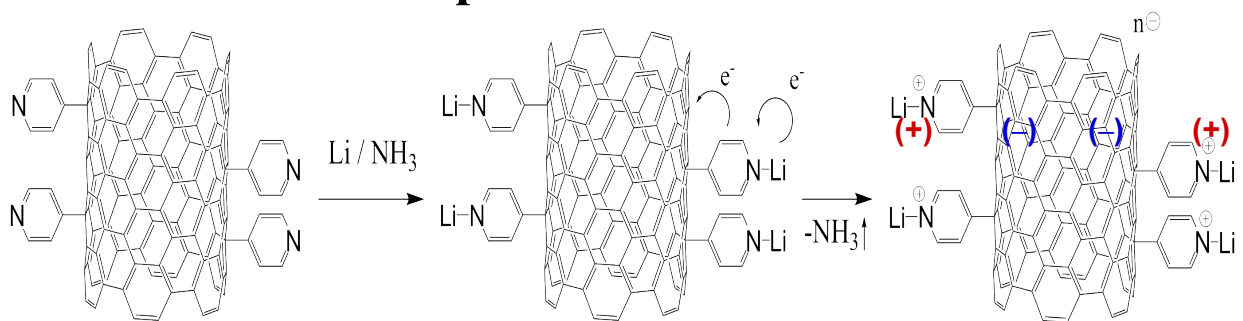
bind to the tube. The lithium that causes the high disorder in the Raman spectrum however, does not contribute significantly to the shift in G –band.



Expanded CNT fibers are doped with lithium or calcium in ammonia, 785 nm Raman excitation. The initial (black trace) G-peak shifts to lower frequency, which shows electron charge transfer (red trace) from the metal to the sidewall. It shifts back (blue trace) when the metal is oxidized and decouples. The large shift is indicative of strong electron transfer from individual atoms. This is not yet perfected; broadening of the peak indicates the metal has not fully penetrated the fiber to the core.



### 3b. An attachment point for the metal atoms

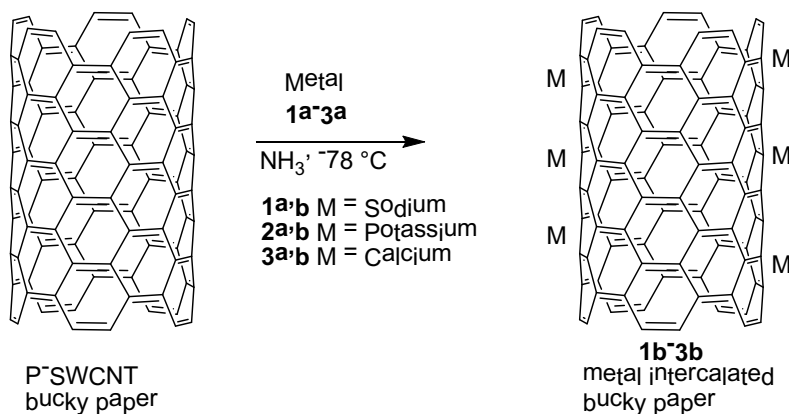


Our results suggest, that it is possible to introduce negative charges on SWCNTs, which according to calculations can increase the interaction energy between hydrogen and the surface of the carbon framework. Doping of expanded SWCNT fibers as well as hydrogen uptake experiments are ongoing experiments in our laboratory.

## 3. A Raman diagnostic for sodium intercalation of carbon nanotubes

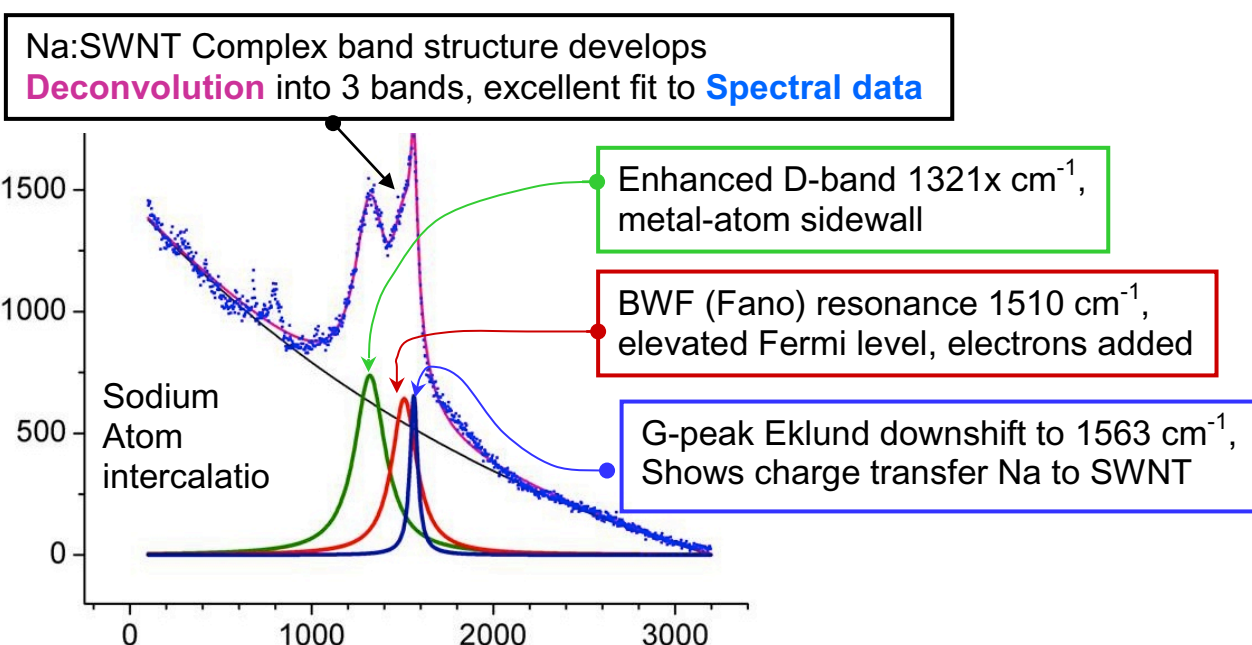
Alkali metal atoms intercalated into carbon nanotubes will donate charge to the nanotube wall, providing a positively charged atom that will bind hydrogen more strongly due to the polarization of the hydrogen. The metal is dissolved in ammonia, which transports the metal atoms onto the nanotube walls.

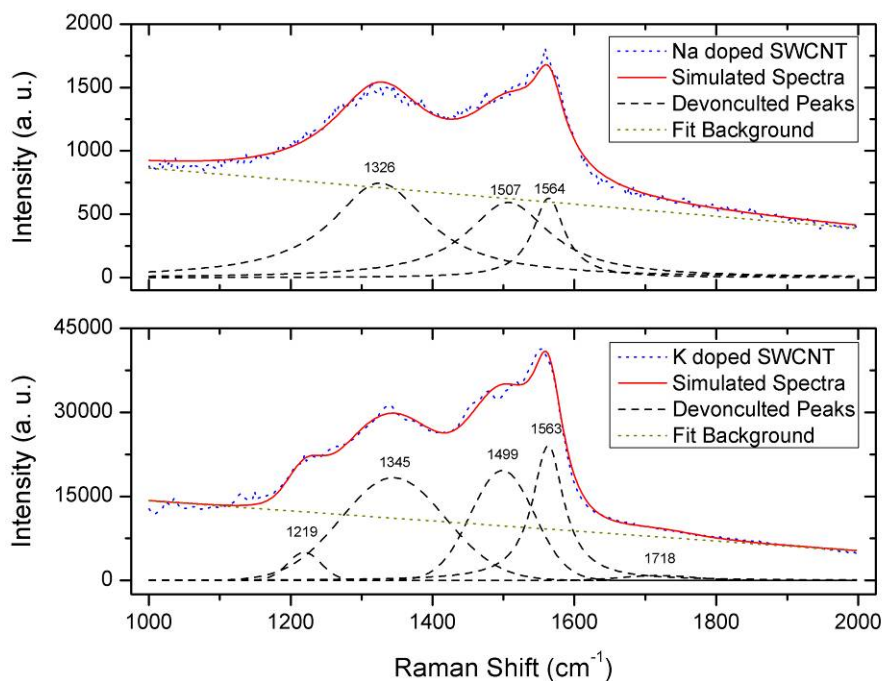
Since the metal atoms may aggregate in to clusters, this will be detrimental to this particular approach to store hydrogen near ambient temperatures. Such aggregation will reduce available surface area, and have a substantially less electron charge transfer to the SWNT per metal atom. Diagnostic methods that measure metal content, such as X-ray photoelectron spectroscopy (XPS) do not provide such charge transfer information. Sodium atoms provided best results in this case.





We have developed a new Raman scattering diagnostic that shows the Eklund shift due to charge transfer, and the development of a "Fano" resonance (AKA Breit-Wigner-Fano, or BWF resonance). This shows that the electron transfer is sufficiently large to move the Fermi level of the electrons into the conduction band. In addition, the disorder peak, at about  $1320\text{ cm}^{-1}$  becomes quite strong due to the radical anion that creates an  $sp^3$  site as a resonance structure with the  $sp^2$  carbon skeleton. Deconvolution of the spectrum reveals the three well-defined peaks that make up the overall Raman spectrum in the range of  $1100\text{ cm}^{-1}$  to  $1700\text{ cm}^{-1}$ . All of these Raman features considered together strongly indicate that the carbon nanotubes are decorated with individual atoms. This is an important new diagnostic to demonstrate successful intercalation

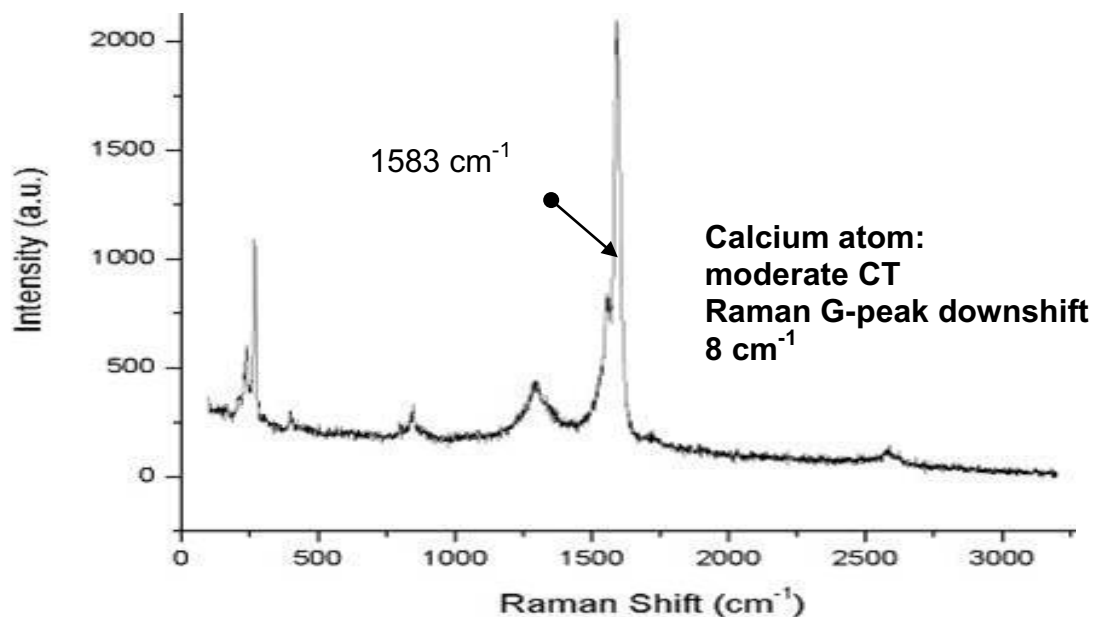




Potassium intercalation has now been shown to also be effective with charge transfer just as for sodium. The appearance of the middle peak indicates that the Fermi level has been raised into the conduction band, creating a new Raman feature and proving that there has been strong charge transfer to the CNT surface. This should considerably enhance hydrogen binding energy. However, the air sensitivity made the samples difficult to handle and preserve.

## 4. A Raman diagnostic for calcium intercalation of carbon nanotubes

Calcium metal intercalation was also tested. However the Eklund shift was considerably less, and the disorder peak was small. The Fano resonance, which usually appears ca. 1510 cm<sup>-1</sup> was not observed. This suggests that the calcium is not nearly as effective as providing charge to the sidewall as was sodium. This diagnostic is extremely useful in providing quick feedback as to the successful intercalation of the metal atoms, and in the case for calcium, it was less effective than for sodium. The 8 cm<sup>-1</sup> Eklund also shows a relatively modest amount of charge transfer.



### **CK details of metal atoms, downselected.**

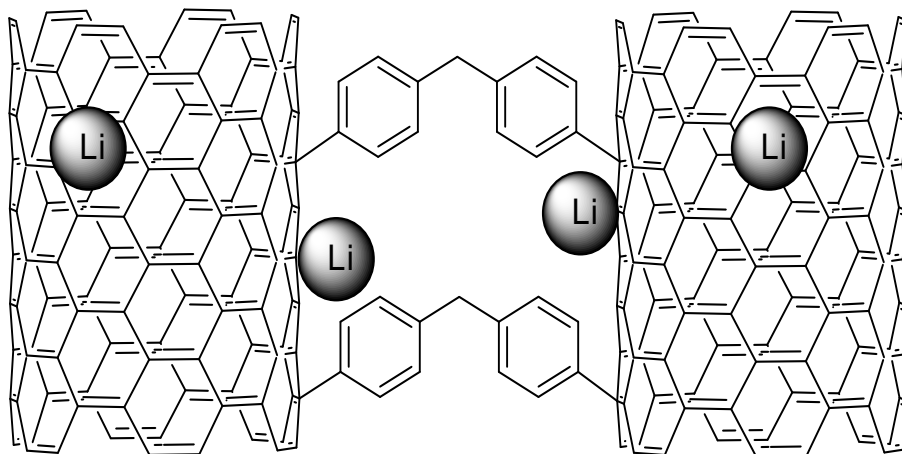
Our prior work with lithium intercalation into SWNTs sets the stage for using the rigid 3D framework as a support for a metal - hybrid adsorption material that will effectively store hydrogen at ambient temperatures. The SWNT fibers will be expanded with somewhat larger pores, as theory suggests that a pore size of 0.9 nm is close to optimum for lithium, whereas a somewhat smaller pore size of 0.7 nm is optimum for hydrogen uptake into the pure sp<sup>2</sup> carbon pore. Subsequently, we will investigate intercalation of transition metals, such as scandium, titanium, and nickel. Again, we will determine and optimize the pore size of our nanotube support scaffold for these larger atomic Kubas-type binding agents.

### **High density media achieves DOE volumetric goals (materials only)**

In addition, the density of our SWCNT fibrils was typically 1.3 kg/L, so that volumetric uptake was always higher than gravimetric uptake for our media when comparing the ultimate DOE goals, which correspond to a density of 0.7 kg/L and 7.5wt% for the complete hydrogen storage system when filled, which in turn corresponds to an overall density a little less than 1kg/L. Hence two primary goals for proof of principle for this novel approach to H<sub>2</sub> adsorbents were met, which is high absorption capacity per unit SA, along with a high-density media. Both goals track together and hence there is essentially no volumetric vs. gravimetric tradeoff when the nano-engineered sp<sup>2</sup> carbon media is used. We were not able to achieve high overall SA due to the difficulty in removing the solvent, as the very strong van der Waals attraction that we used to pull the H<sub>2</sub> into the pores also made it difficult to remove all of the solvent, and this is one of the problems that remain for future research. However we were able to achieve DOE 2010

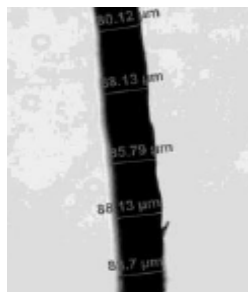
volumetric goals (materials only), and substantially exceed them when including the factor of  $1.3\times$  for increasing pressure from our test pressure of 2 bar to 40 bar, or 40 g/L compared to 28 g/L of the DOE 2010 target.

3. Metal uptake on nanotube had been tested, and the Eklund shift of the Raman spectrum shows that successful electron transfer has taken place. Pyridine functionalization has been used to provide an anchor point for lithium to prevent migration.

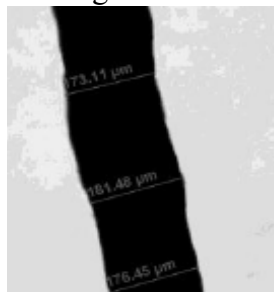


From 1850a-site-visit  
conceptualized Li doping  
reported in AMR 2008?

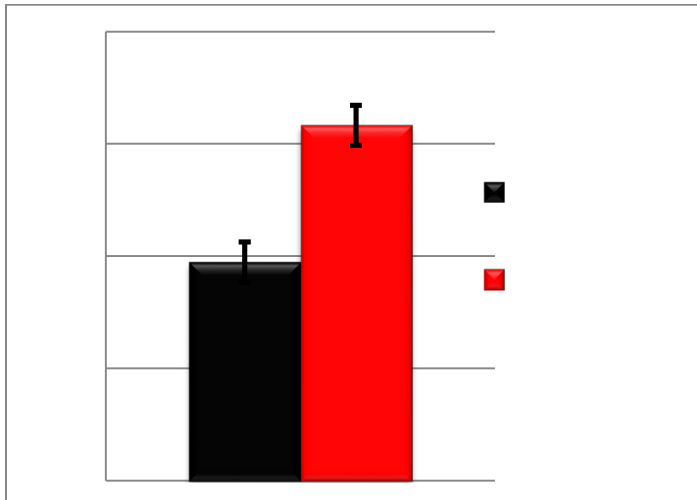
Dibromophenyl crosslinker used



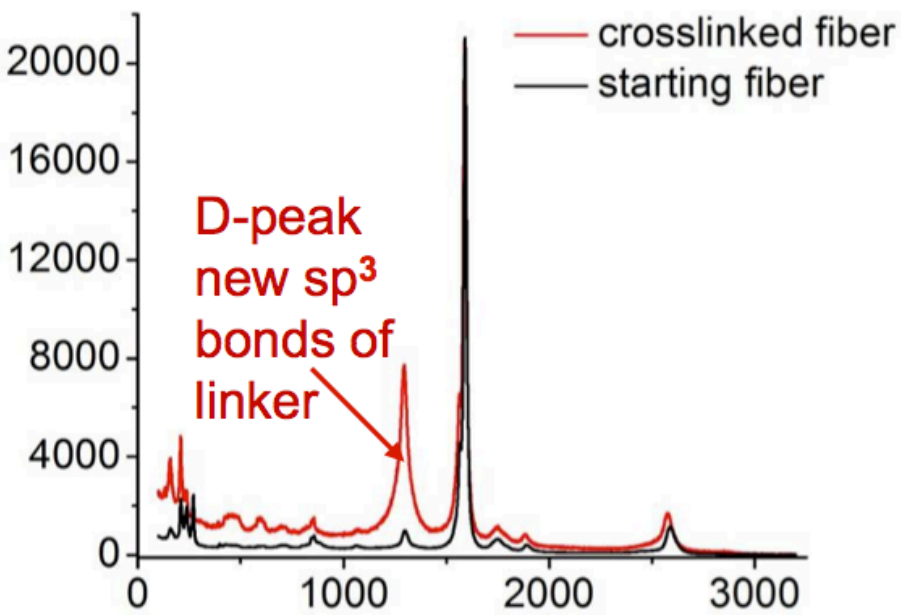
Starting fiber



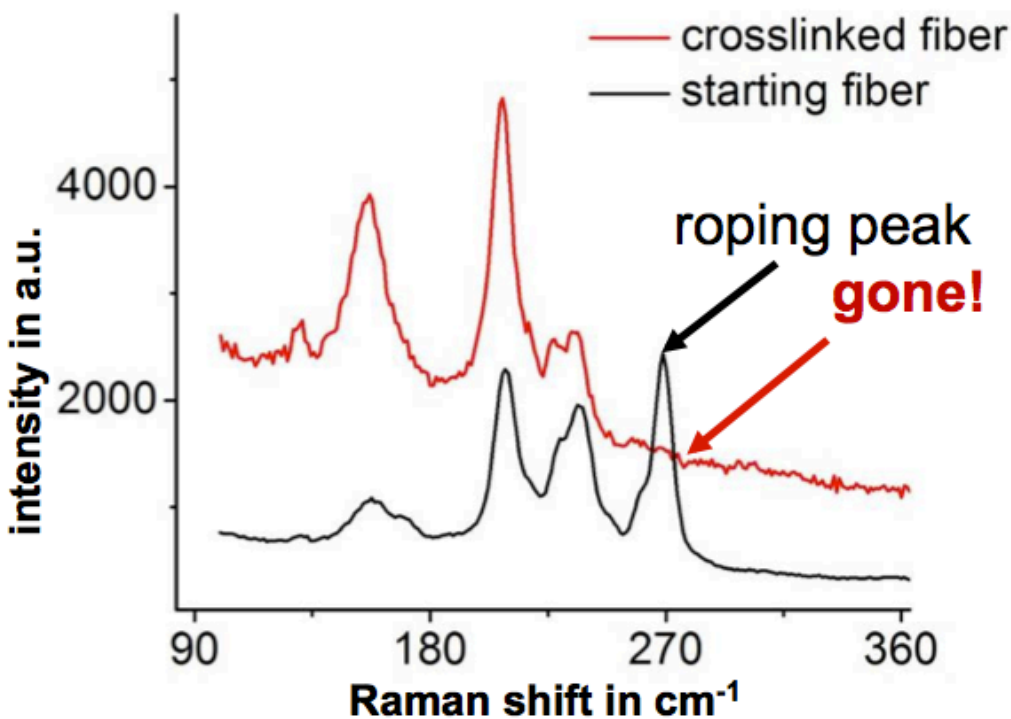
### Expanded fiber



the amount of expansion is illustrated. The diameter increased by 63%, and the cross sectional area that provides room for hydrogen uptake increased by 2.5x



### Raman after crosslinking



Raman spectra: Big increase in D-peak shows covalent bonding established  
Disappearance of the “roping peak” [Doorn 2005]  
This shows that DoE-2219ac-H2-Final-Report-Main

### Results for atom substitution

Instead of Kubas-type binding to enhance binding energy, we chose atom substitution in graphene to obtain enhanced binding, and this was successful with boron substituted and phosphorous substituted graphene, but not nitrogen substitution. (May1)

## Metal atom migration

An apparatus was constructed and characterized an apparatus capable of studying the temperature dependent behavior of metal atoms adsorbed to carbon nanotube carpets. The atoms are deposited in low pressure hydrogen to determine under what conditions they become mobile. Such mobility would compromise the ability to take up dihydrogen. The apparatus is capable of studying temperatures ranging from -100 C to 200 C.



Then this apparatus was used to explore the behavior of iron atoms as a proof of concept. The following sections detail the constructed apparatus, outline the experimental procedure, and then present and discuss novel results on the temperature dependent behavior of iron atoms.

### 1a. Apparatus

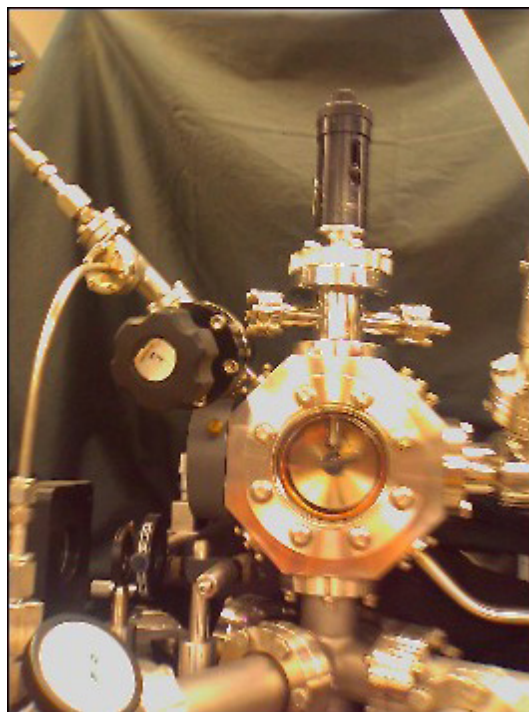
In order to perform this experiment, an apparatus needed to be constructed that was capable of the following:

1. High Vacuum. Metal atoms oxidize very strongly in the presence of O<sub>2</sub>. When the atoms oxidize, they are immobilized, making it impossible to determine if they would have aggregated in an oxygen free environment.

2. Temperature Control. Since the point of the experiment is to measure the temperature dependence of metal aggregation, it is imperative that the apparatus be able to precisely control the temperature of the nanotube carpet sample.

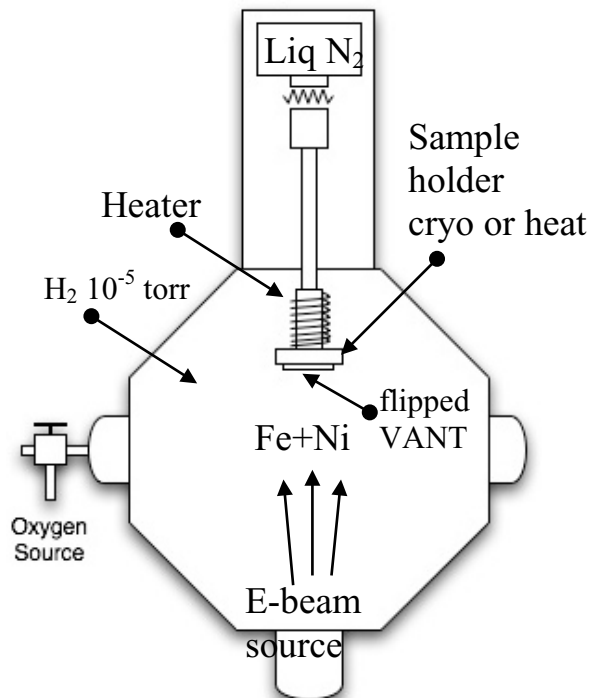
3. Metal Evaporation. There must be an evaporative metal source that is able to produce atomic metal and deposit it onto the carpet sample.

The figure shows the sample holder portion of the UHV chamber with the viewing port.



## 1b. Sample Holder

A vacuum chamber with an electron beam evaporator source has a new sample holder with this ability to attach to the existing vacuum apparatus. A schematic of the modified sample holder is



shown in the Figure

In order to precisely control the temperature of the nanotube carpet sample in the range -100 C to 200 C, the sample holder must have both heating and cooling capabilities, as well as a closed loop temperature controller that can precisely maintain a desired temperature with minimal drift. In order to accomplish this, the sample holder was designed to have both a heating element and a liquid nitrogen reservoir. As shown in Figure, heat is transferred from the aluminum sample arm through a copper heat pipe to the liquid nitrogen reservoir in order to cool the sample. The temperature control is provided by an external temperature controller using feedback from a thermocouple connected directly to the sample platform, as shown in the figure.

## 1c. Heating and cooling tests

The results from testing the heating and cooling abilities of the sample arm demonstrate that it is capable of maintaining a specific sample temperature within 1 degree Celsius for an indefinite period of time across the range of temperatures (-100C to 200C). This was the design range and was found to be adequate to see changes in aggregation behavior.

The main consideration in this procedure is to avoid the presence of oxygen during atomic deposition. In an oxidizing atmosphere, the metal atoms will deposit onto the nanotube carpet as metal oxides, which are inherently immobile. After deposition, they are then immobilized by adding oxygen.

The experimental oxygen level is carefully monitored using a Residual Gas Analyzer (RGA) which the atomic composition of the experimental atmosphere using a mass spectrometer, and a reducing atmosphere of hydrogen is established before performing the evaporation. Performing the experiment in a hydrogen atmosphere is also a more realistic condition since the goal is to develop a material that can be used in a hydrogen fuel tank.

Deposition thickness was determined using a quartz microbalance.

### 1d. Sample exposure

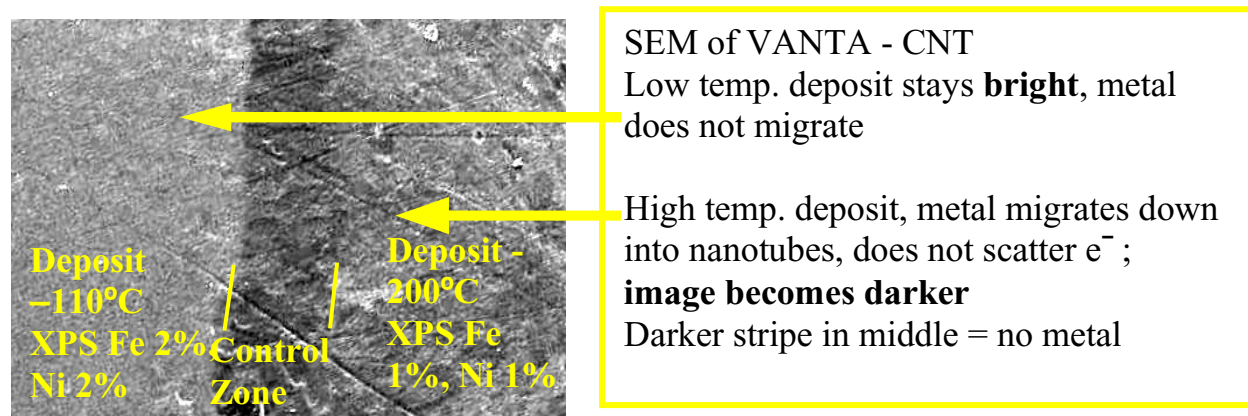
Both exposures were done on the same nanotube carpet, to minimize irregularities between samples. A copper shield was used to only expose part of the carpet to metal deposition at each temperature. This allowed the left and right halves of the carpet to be exposed at different temperatures. Further, since the shield covered the middle section of the carpet in both configurations, the middle became a control region, which was always shielded from metal deposition.

The SEM data was taken by transferring the nanotube carpets, to SEM sample holders using adhesive carbon tape. (XPS) was used to prove that metal had been deposited onto the carpets. XPS allows a quantitative measure of the elemental composition.

The test of aggregation depends on temperature. This was one using an iron/nickel metal alloy as the metal source. Three samples were tested, one at -112 C, one at 200 C and a third control sample. The preliminary findings indicate that there is a strong temperature dependence on migration. However, it is not the case that iron atoms do not aggregate at -112 C.

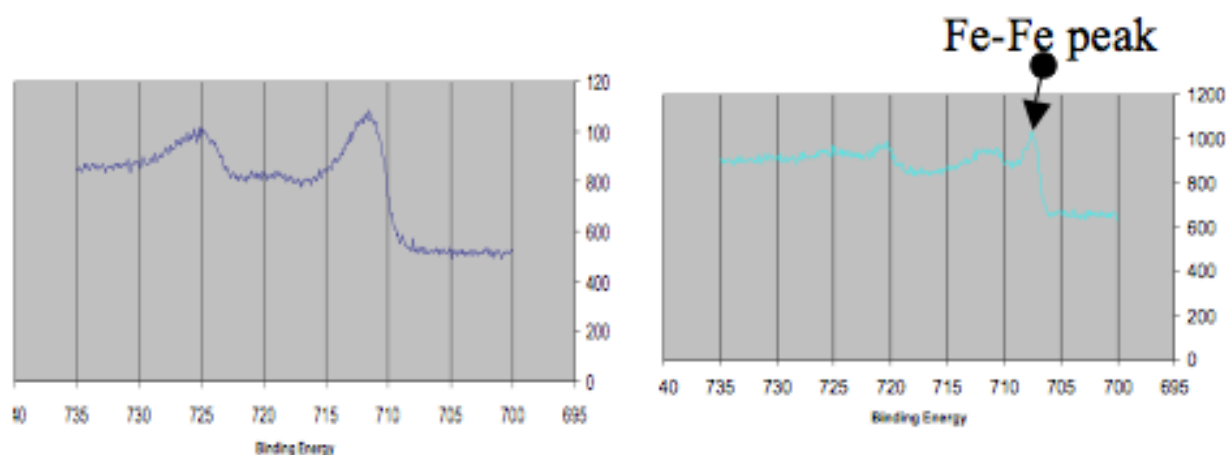
### 1e. Results

This is shown schematically in Figure 10. Figure 11 shows the two exposed regions as well as the central control section. The boundaries between the regions can be easily seen by the change in background color in the SEM image. The control section is noticeably darker than the other two sections, which makes sense because very few metal atoms were deposited there, whereas there is a layer of metal on both exposed sections. Metal scatters electrons very strongly, thus the layer should appear generally brighter than the surrounding carpet without metal.



The cold temperature sample was exposed to deposition at a temperature of -112C on average. The hot temperature sample was deposited at 200C with a temperature drift during evaporation of less than 1C. The middle section of the carpet sample remained shielded from metal during both evaporations, and as such remained relatively devoid of deposited metal.

Looking at the three regions of the sample, one notes that the control region is the darkest, followed by the hot region and that the cold region is the brightest in general. Assuming the hot and cold regions were exposed to about the same amount of evaporated metal, the fact that the cold section is brighter on average could indicate that the metal atoms are more uniformly spread out, whereas in the hot section there is a darker image overall since many regions have been partially or completely depleted of metal due to its migration deeper into the carpet where it can no longer be observed by SEM.



Left spectra, 25°C.

Right spectra, 600°C

XPS data shows extra Fe-Fe peak on right due to clustering

In addition to obtaining novel results demonstrating the temperature dependence of iron aggregation, this also served as a proof of concept that the apparatus was capable of providing data to answer this question for a variety of metal species. It also serves to demonstrate the efficacy of the procedure the author created, which can be easily extended to studying other metals. The final result of this work, then, is that a new method has been created and tested to study the temperature dependent aggregation behavior of metal atoms.

This suggests that such migration makes transition metal atoms unattractive for binding hydrogen on carbon scaffolds.

#### **Kubas-type binding and alkali metal atoms downselected**

We discontinued work on Kubas-type binding with transition metals, as we discovered that individual transition metal atoms will migrate and form useless clusters on SWCNT in the presence of hydrogen, and reported this at 2008 Annual Merit Review (AMR). We demonstrated that lithium and sodium atoms would spontaneously put charge on the SWCNT, with the idea that this would increase binding energy of the H<sub>2</sub>, and after substantial effort provided a Li

functionalized nano-scaffold sample to NREL, but it was degraded and showed the least enhanced uptake of any nano-structured sample. We down-selected this because lithium atoms make the media extremely air and moisture sensitive, with consequent difficulties and potential higher handling costs.

## Graphene scaffolds

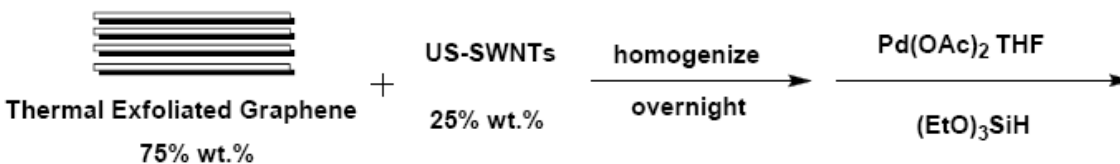
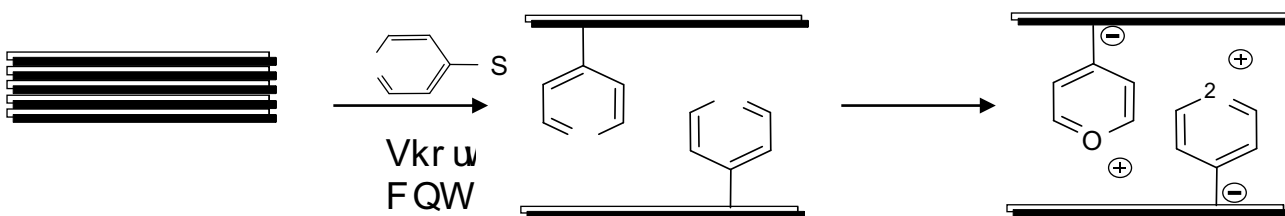
### **Redirect from pure SWCNTs to nano-structured carbon**

Our original goal was cloning single wall carbon nanotubes (SWCNTs) as a means to provide a source of uniform SWCNTs. We achieved high capacity production of very high quality SWCNTs, proved that cloning was feasible, and learned to spin fibrous SWCNT media. However, the strong van der Waals attractive force between the well-aligned SWCNTs did not have large enough pores to allow the hydrogen to enter. Utilizing substantial input from our research group and very helpful recommendations from the Hydrogen Sorption Center of Excellence (HSCoE) team at the National Renewable Energy Lab (NREL), DOE did a No Go on pure SWCNTs; with a redirect to produce nano-engineered pi-bonded carbon structures for Phase II. We developed solvent-based expansion of the SWCNT structures, followed by reaction with molecular proppants that were covalently bonded to the walls to make a porous  $sp^2$  carbon adsorbent with optimized slit pores. This used both our SWCNT production and fiber spinning capability that had already been developed. Theoretical work by other researchers indicated an ideal pore spacing to be about  $\sim 0.8$  nm, and we experimented with our nano-structured scaffolds with a variety of crosslinks and proppants to test and produce similar size pores.

Chemistry of carbon nanotubes is being transferred to graphene. We can now functionalize graphene. Chemistry can be subsequently be performed to make suitable binding sites for metals uptake. The graphene has been successfully cross-linked to make a new type of low-cost engineered nanospace. Preliminary experiments have been done to dope metals into the graphene. A new alternating-layer graphene-metal atom nanoengineered scaffold has been designed to attract hydrogen into the nanopore for high density uptake of dihydrogen at RT.

### Doubly enhanced uptake per unit SA

We were highly successful in proving our main goal as we consistently obtained much higher uptake per unit surface area than common physical H<sub>2</sub> adsorbents. For consistency and exceptional accuracy, all H<sub>2</sub> uptake measurements were performed by HSCoE on the same instrument at 2 bar of H<sub>2</sub>, as well as surface area (SA); all results are reported as “excess” H<sub>2</sub> uptake due to presence of the adsorbent media, not the total H<sub>2</sub>. “Chahine’s rule” that is used for most H<sub>2</sub> adsorbents is 1wt% per 500 m/g SA at asymptotic pressures (>40 bar) and 77K, whereas we routinely obtained higher (1.85× average) uptake at 2 bar. Allowing a generic 30% increase in uptake by raising the pressure from 2 bar to the asymptotic limit, this puts us at >2wt% per 500 m/g, or at least twice Chahine’s rule. When we fluorinated the sp<sup>2</sup> scaffold, which disrupted the π cloud, the enhancement was lost, and uptake reverted to 1.06 wt% per 500 m/g SA, ~same as Chahine’s rule. We proved that slit pores alone do not provide the enhanced uptake, but they act in concert with the sp<sup>2</sup> pi cloud as a nano-compressor to pack the pores with H<sub>2</sub>. Ozone perforated bulk SWCNT media provided 1.05 wt% per 500 m/g, also obeying Chahine’s rule, showing the randomly induced porosity in SWCNTs also does not cause the 2x enhanced uptake.



### 3.0 Graphene Functionalization

Graphene sheets (graphene oxide and reduced graphene oxide) were crosslinked with 4,4'-dibromobiphenyl, using the Billup's alkylation method. The crosslinking was carried out with graphene oxide (GO) produced by the Staudenmaier method of oxidation of graphite using KMnO<sub>4</sub> and with reduced graphene oxide (red GO), which is prepared by reducing GO with hydrazine in water at 90 °C.

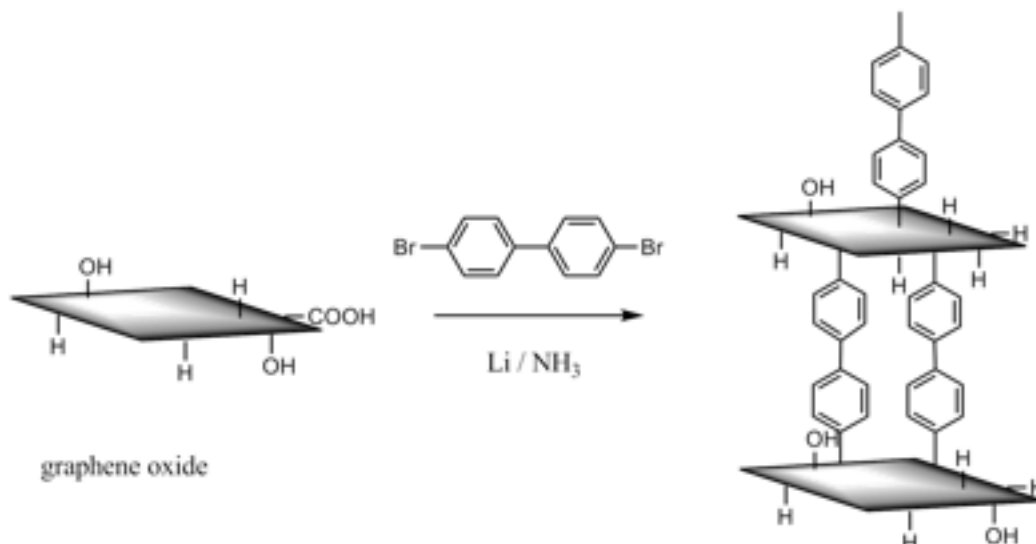


Figure 7: Crosslinking reaction with graphene oxide and 4,4'-dibromobiphenyl

In a 100 mL three necked, round bottom flask fitted with a dry ice condenser, 50 mg (4.2 mmol) graphene oxide were added to the reaction vessel under nitrogen atmosphere. Subsequently dry ammonia (75 mL) was condensed in the flask and 150 mg (21.6 mmol) of Li was added in small pieces. The solution was homogenized for five to ten minutes in a dry ice-acetone bath and 4,4'-dibromobiphenyl (6.45g, 20.7 mmol) was added slowly. The solution was homogenized for 2 hours at  $-78\text{ }^{\circ}\text{C}$  and then at room temperature leading to slow evaporation of ammonia. The reaction was quenched by slow addition of water. The excess of 4,4'-dibromobiphenyl was dissolved in dichloromethane. The reaction mixture was filtered over a teflon filter and washed several times with water. The product was dried in the vacuum oven at  $70\text{ }^{\circ}\text{C}$  overnight.

## 4.0 Characterization of the graphene oxide

### 4.1 Raman Spectroscopy

Raman spectra show an increase of the D peak in the crosslinked graphene oxide (figure 16) against the starting graphene oxide (see figure 15), indicating a successful functionalization.

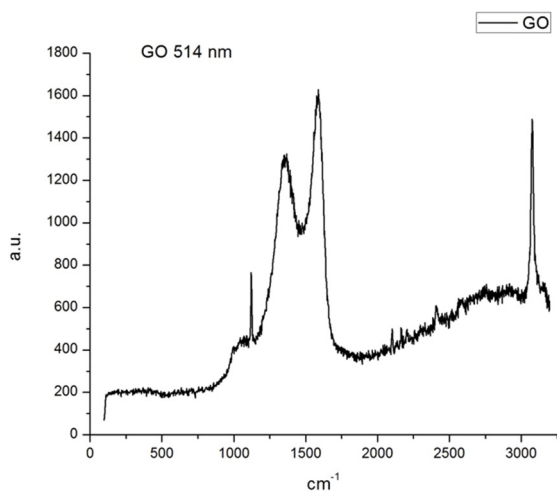


Figure 7: Raman spectrum of graphene oxide (514 nm laser)

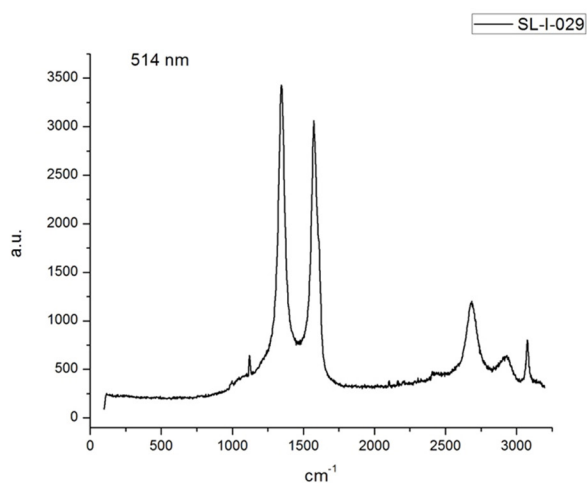


Figure 8: Raman spectrum of graphene oxide crosslinked with 4,4'-dibromobiphenyl (514 nm laser)

## 4.2 XPS

XPS data (spectra shown in figure 18 - 20) show, that there is still bromine in the material, which means still the edukt 4,4'-dibromobiphenyl. It is possible to calculate the amount of mol% linker and weight% linker in the material.

Reduced GO crosslinked with 4,4'-dibromobiphenyl:

	Mol %	Weight %
Carbon (in graphene)	69.9	61.9
Oxygen	18.2	21.5
Nitrogen	4.9	5.1
4,4'-dibromobiphenyl	0.5	11.5

GO crosslinked with 4,4'-dibromobiphenyl:

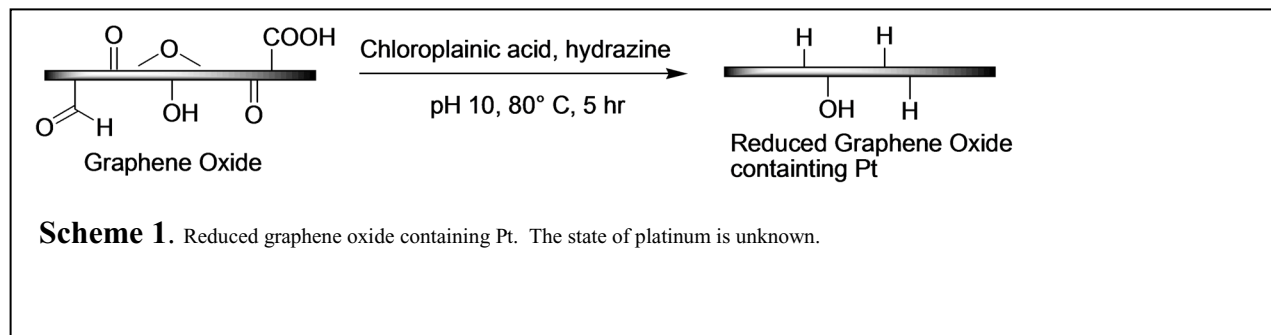
	Mol %	Weight %
Carbon (in graphene)	90.15	86.4
Oxygen	7.7	9.8
4,4'-dibromobiphenyl	0.15	3.6

## 5. Metal addition to graphene oxide



Transition metals are considered a key element in uptake of hydrogen by physisorption at room temperature. We are starting tests on metal uptake in a scaffold of graphene oxide.

Developing 3D nano-engineered scaffolds.

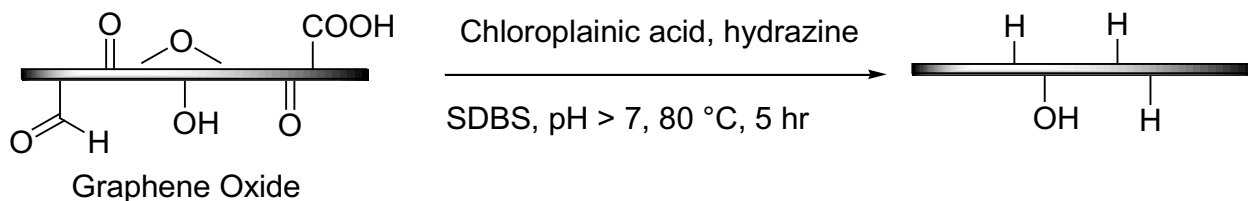


The scaffold material comprised of graphene oxide, reduced graphene oxide and functionalized Singled Walled Carbon Nanotubes (SWCNTs). The goal of the scaffold is to have a high surface area with the ability to keep metal atoms individual instead of clusters. In order to attain the two aforementioned goals, the scaffolds must first be loaded with metal. Examples of metals explored thus far are platinum, palladium below The most promising result has come from platinum, with a loading of 7.83% (Scheme 1.)

In some reactions, a **surfactant** was tested. After investigation, it was found that the surfactant was inhibiting the ability of the metal to physisorb on the surface of the graphene sheets. Reactions that did not contain surfactant were able to reach three times the amount of metal as the original reactions with the surfactant. Now that we know how to load metal with decent efficiency, we can produce a variety of samples if it is necessary.

Although these are heavier transition metals, the proof of principle is the first critical step. The low sensitivity to the environment makes it attractive to develop the technology for metal functionalization.

#### CDD-IV-156

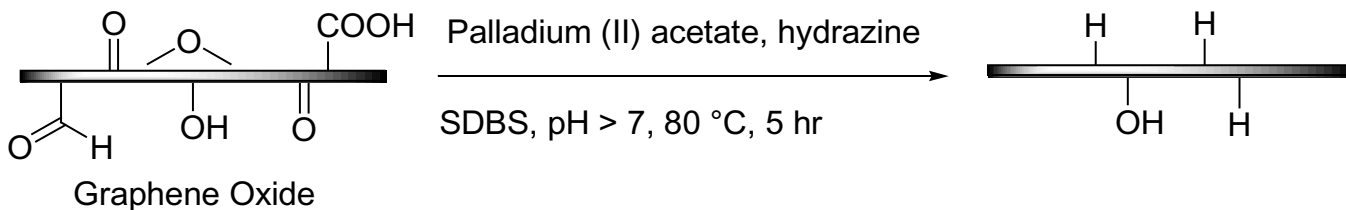


I used 100 wt % loading of metal in this reaction. I was able to increase the final loading, however we need better.

XPS Results:

C1s	O1s	Pt4f
86.76	10.47	2.77

**CDD-IV-157**

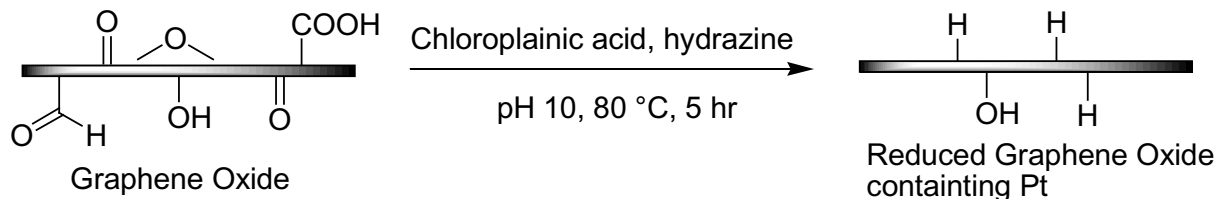


I used 100 wt % loading of metal in this reaction.

XPS Results:

C1s	O1s	Pd3d
81.42	16.91	1.67

**CDD-IV-163**



XPS Results:

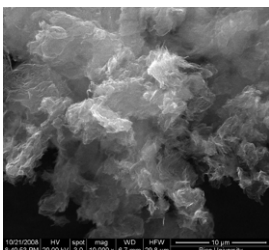
C1s	O1s	N1s	Cl2p	Pd3d
68.45	19.08	3.96	0.68	1.67

from AMR 2009

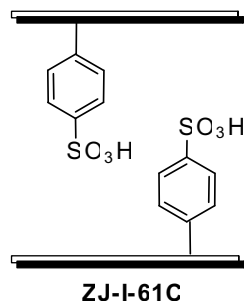
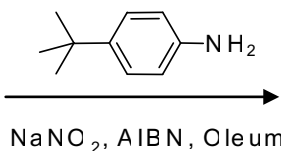
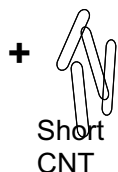
## 2. Graphene scaffolds from exfoliated graphite

These graphene nanoribbons were then crosslinked using the diazonium chemistry previously developed with single wall carbon nanotubes (SWNT) to crosslink them. However, the surface areas were not as large as desired, ranging from 150 to 300 m<sup>2</sup>/g.

Higher surface area was achieved using cut CNT to help prop open the graphene sheets.

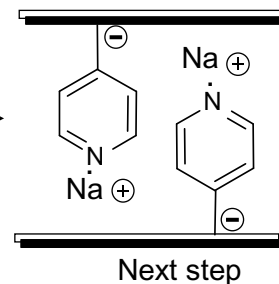
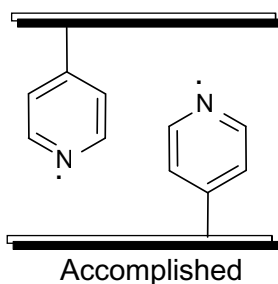
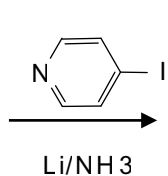
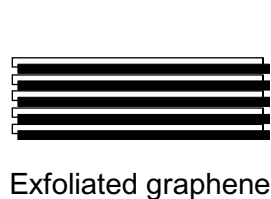


Exfoliated graphene:  
short SWNT for proppant  
75:25 ratio



[Publication Functionalization of graphene sheets; Tour 2008]

Exfoliated graphene has been successfully functionalized with pyridine, which provides a parking spot for sodium to provide dipole induced dipole enhancement of H<sub>2</sub> binding energy.

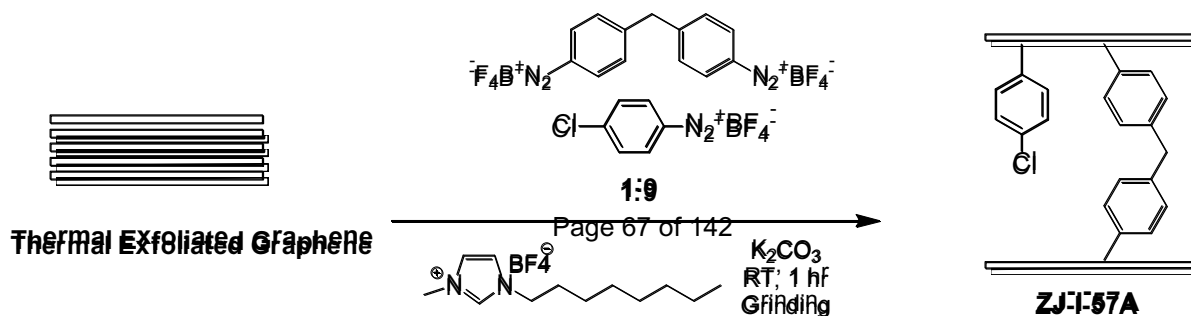


Pyridine functionalization to make alkali atom “parking spot”,  
showing alternate lithium/ammonia functionalization

## 2. Graphene scaffolds from graphene oxide.

Thermally exfoliated graphene is crosslinked to make a new type of scaffold of sp<sup>2</sup> carbon. It starts out as graphene oxide (GO) so this material is termed TEGO.

Several crosslinking schemes have been tested to keep the layers open.

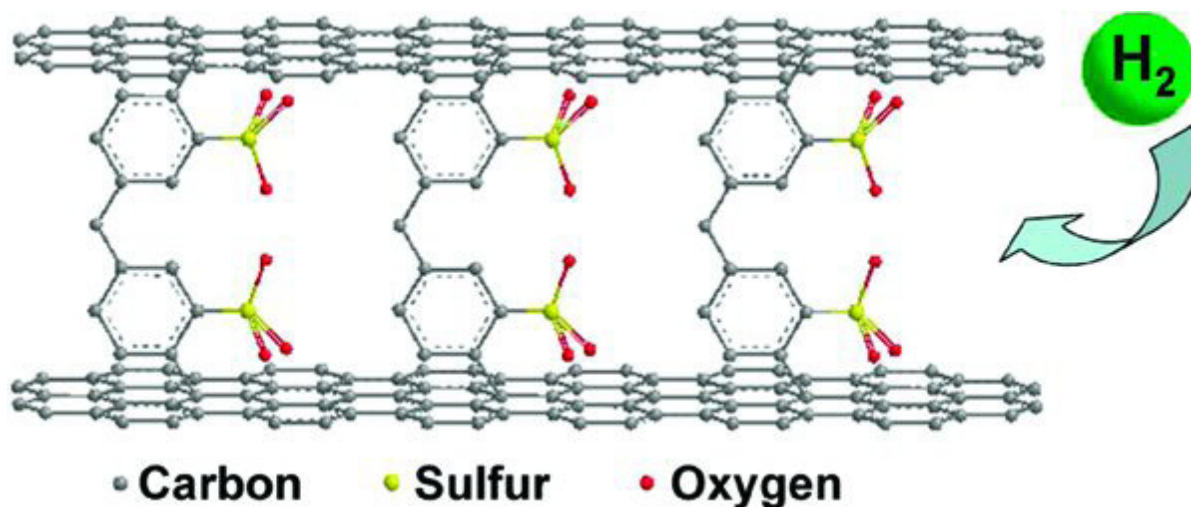


Surface areas comparable to that from SWNT scaffolds have been achieved. However, heating to high temperatures is not necessarily beneficial. In all samples, 400°C to 500°C was optimum, with detrimental effects at higher temperatures. This generally produced much larger surface area than that from the graphene nanoribbons.

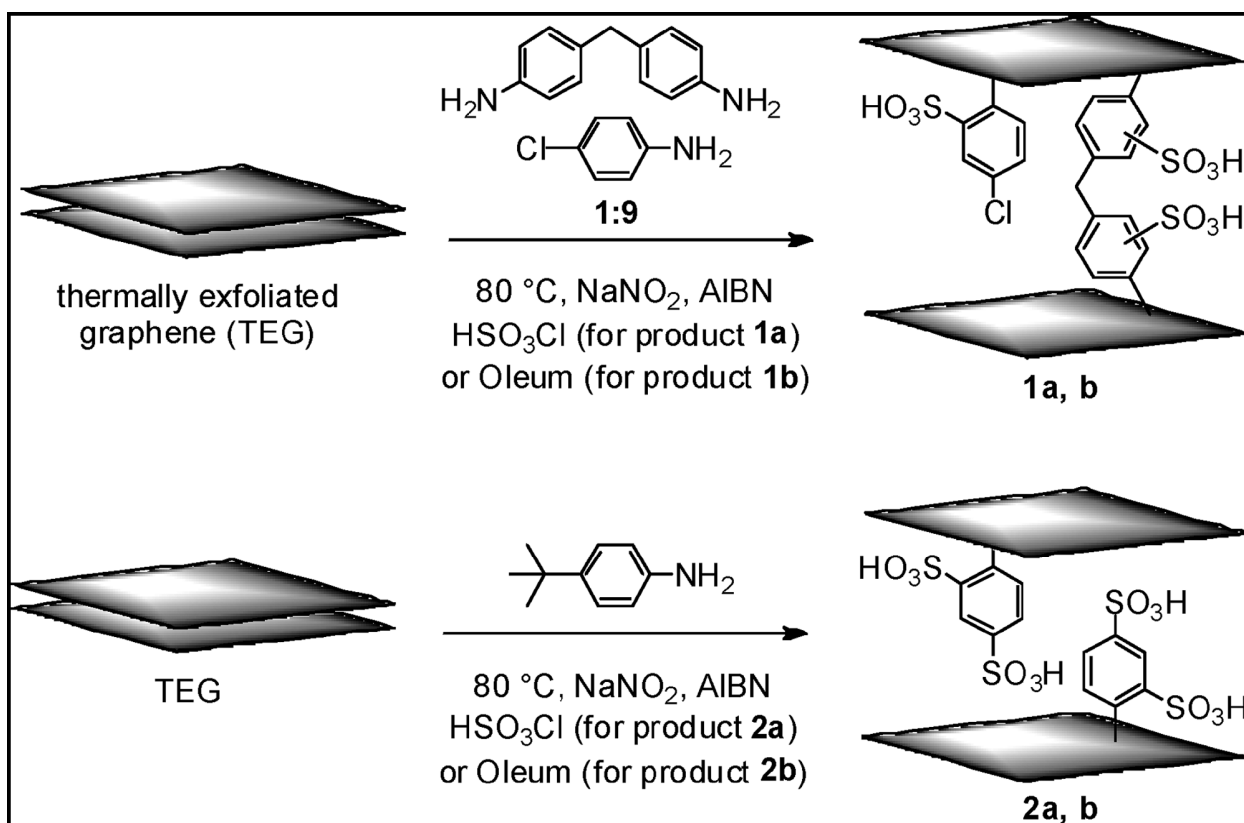
Degas temperature/Surface area (m <sup>2</sup> /g)	200 °C	300 °C	400 °C	500 °C	600 °C	700 °C	800 °C
ZJ-I-57A TEGO di-/Cl-Ph- 1:9 diazonium Grinding in ILs	314.75	324.69	375.83	362.73	355.35	369.67	355.17
ZJ-I-57B TEGO dianiline Stirring in Oleum	23.47	26.88	<u>399.12</u>	394.89	314.29	255.34	234.13
ZJ-I-57C TEGO di-/Cl-aniline 1:9 Stirring in Oleum	97.06	183.98	485.81	<u>562.83</u>	488.53	405.46	377.55
ZJ-I-57D TEGO t-butyl aniline Stirring in Oleum	509.88	546.63	560.46	<u>560.97</u>	553.23	557.53	559.60

1. Phenyl sulfonated and bi-phenyl sulfonate spacers and crosslinkers have been used with the acid-expanded graphene.
2. SEM shows the layered nature compared to the disordered starting graphene material
3. Incorporation of the crosslinking material is verified by X-ray photoelectron spectroscopy, Fourier transform infrared, and thermogravimetric analysis
4. A plot of uptake vs. surface area shows an approximate 2x enhanced uptake for the nano-scaffold media.

## 1. Conceptual drawing of (TEG) sheets with H<sub>2</sub> uptake



## 2. Diagram of crosslinked thermally exfoliated graphene (TEG) sheets for H<sub>2</sub> uptake



Functionalization and Cross-Linking of TEG Sheets in Chlorosulfonic Acid Products 1a and 2a; and in Oleum products 1b and 2b.

### 3. SEM images Crosslinked thermally exfoliated graphene (TEG) sheets

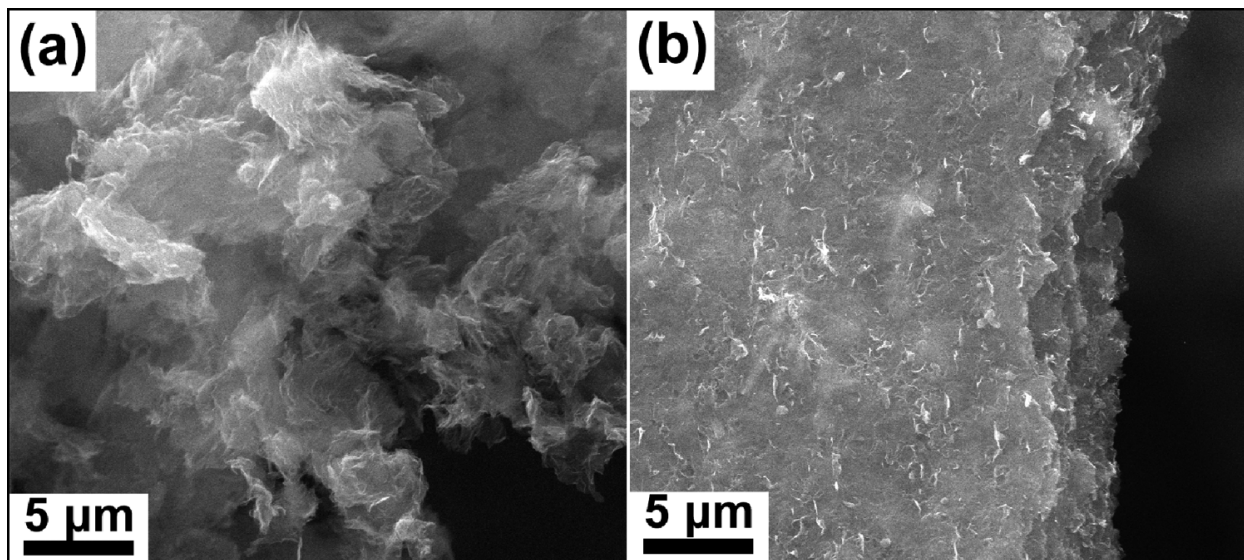
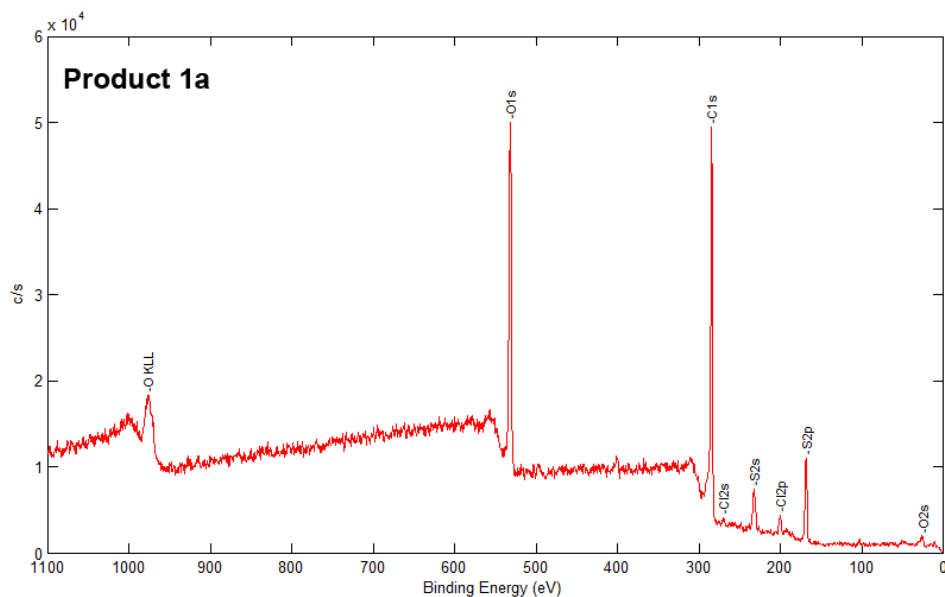
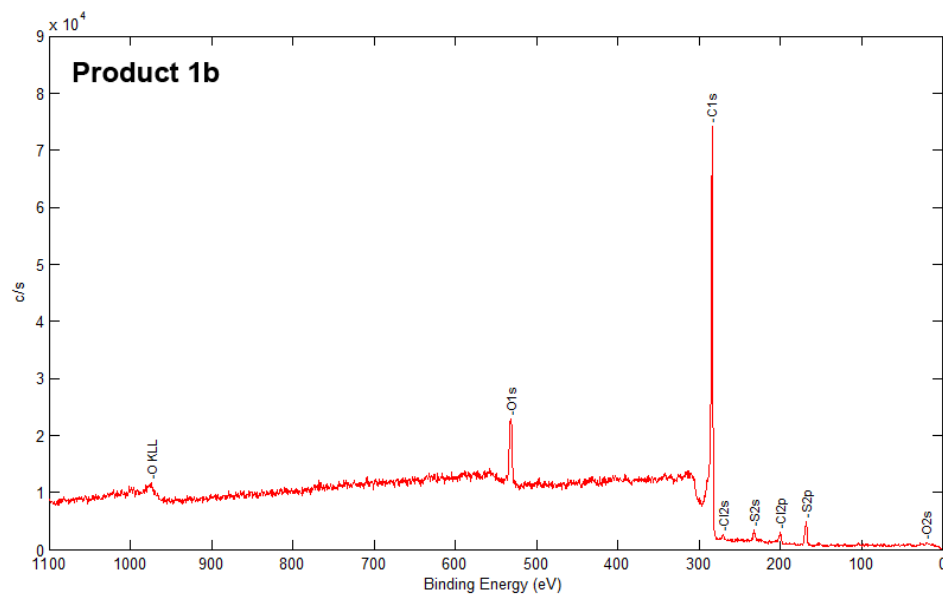


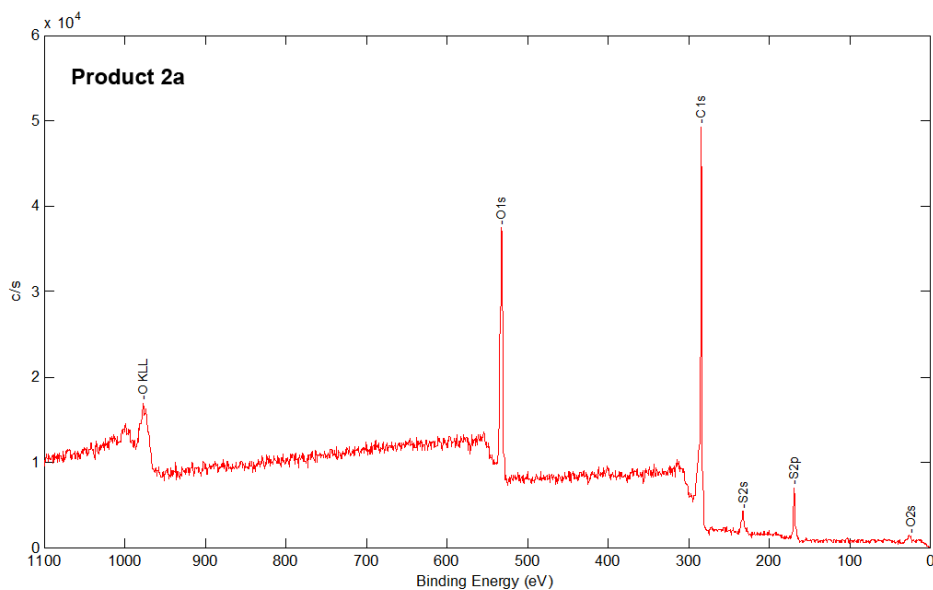
Figure 1. SEM images of (a) original TEG sheets which are fluffy and disordered and (b) layered stacking structure after organic cross-linking functionalized-TEG product 1a. Additional products 1b, 2a, and 2b have the same layered-stacking structure as product 1a.

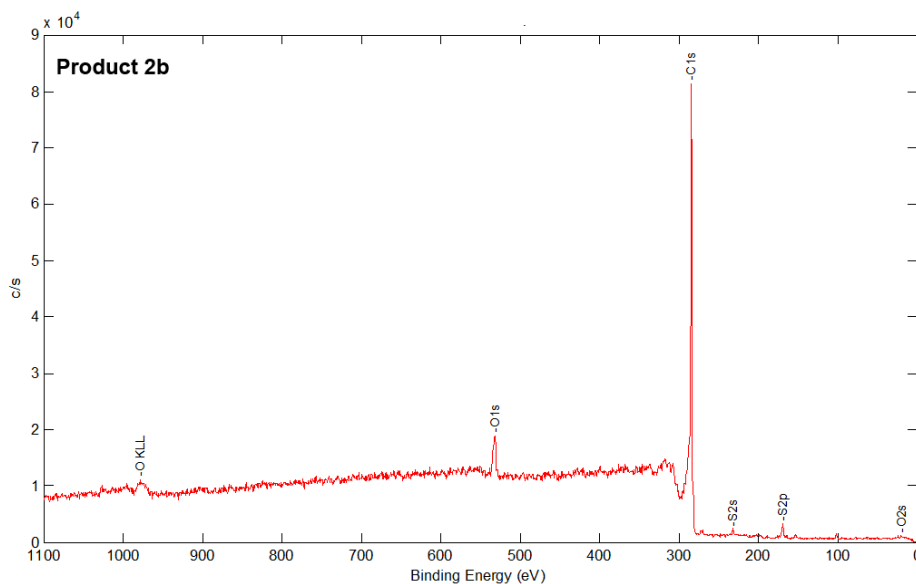
#### 4a. High Resolution XPS of the cross-linked (TEG) sheets





#### 4b. High Resolution XPS of the cross-linked (TEG) sheets (continued)



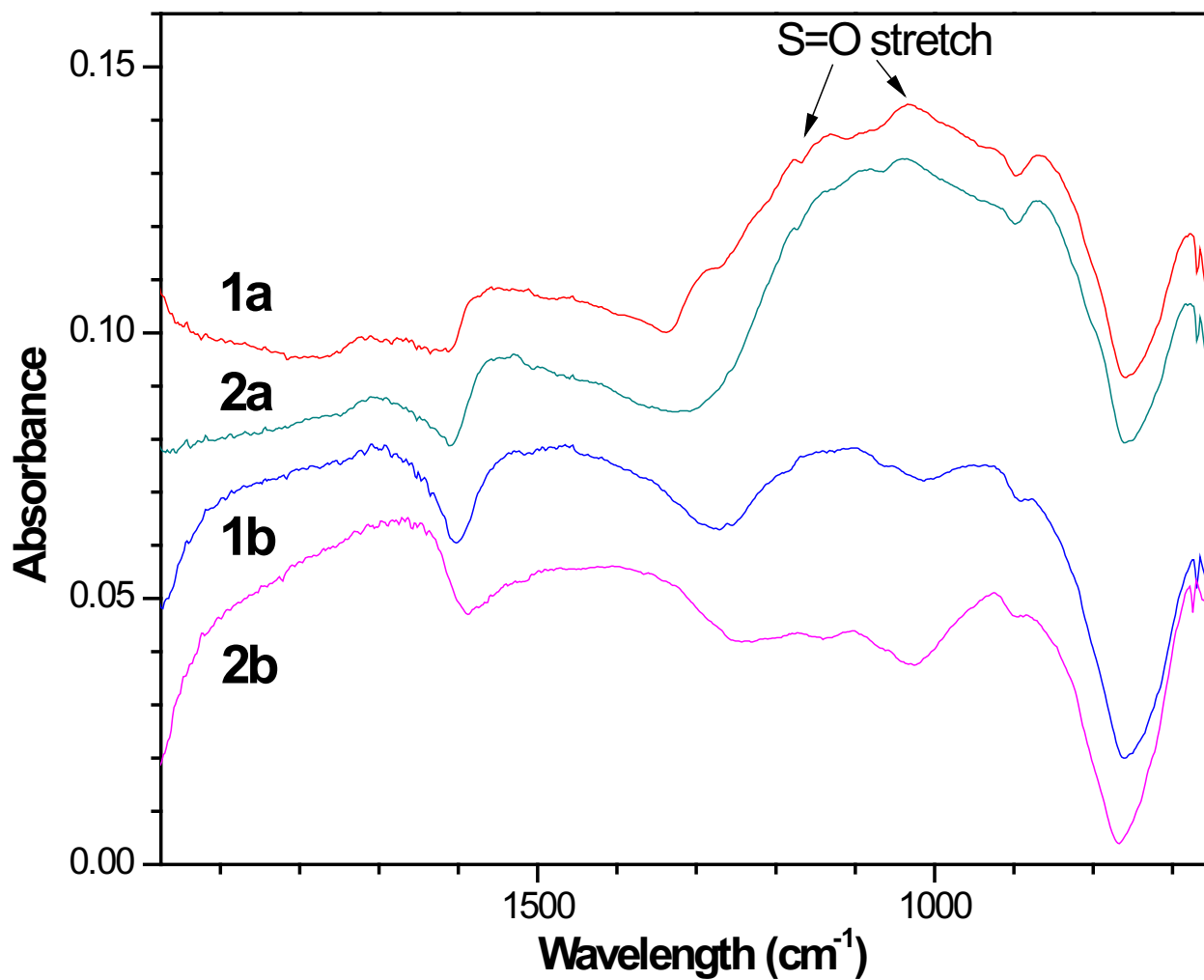


High-resolution X-ray photoelectron spectroscopy (XPS) demonstrates the presence of the spacers and cross linkers.

The XPS of products 1a and 1b showed the atomic percentages of chlorine as 1.7% and 0.8%, respectively. Meanwhile, S 2p peaks were detected in all four products: 1a, 6.3%, 1b, 2.2%, 2a, 4.2%, and 2b, 1.7%, indicating that the aryl rings were sulfonated to varying degrees by the super acid solvents; the degree of sulfonation was higher in chlorosulfonic acid than in oleum. The functionalized aryl groups can serve as inter-layer spacers between graphene sheets while the sulfonic acid groups could generate partial charge transfer with the graphene planes. Both could be good factors for increasing adsorption of H<sub>2</sub> to the surface of f-TEG sheets.

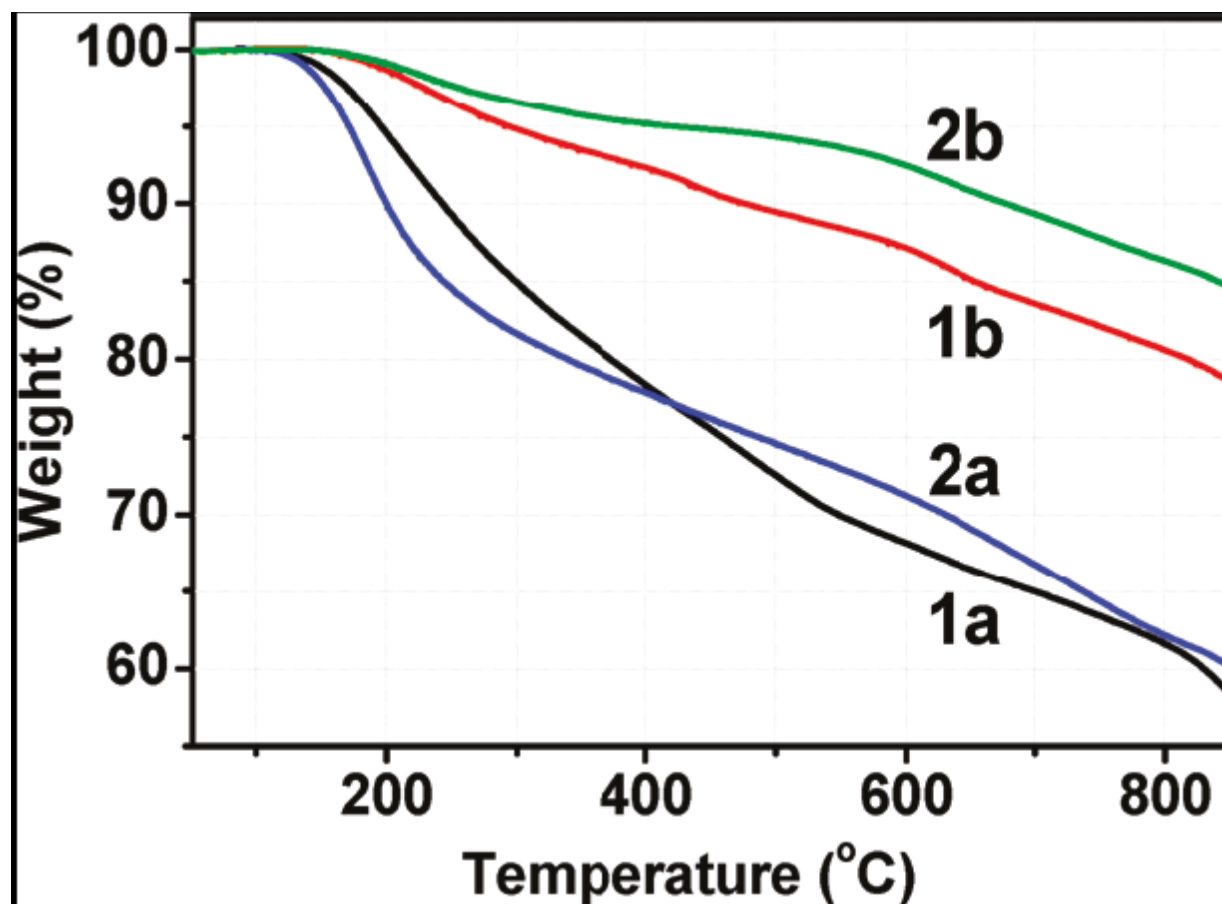


## 5. Fourier Transform Infrared Spectrum of the scaffolds



The Fourier Transform Infrared Spectrum of the scaffolds shows the presence of the sulfur - oxygen double bond that establishes the presence of the sulfonated group of the graphene spacer and cross-linker

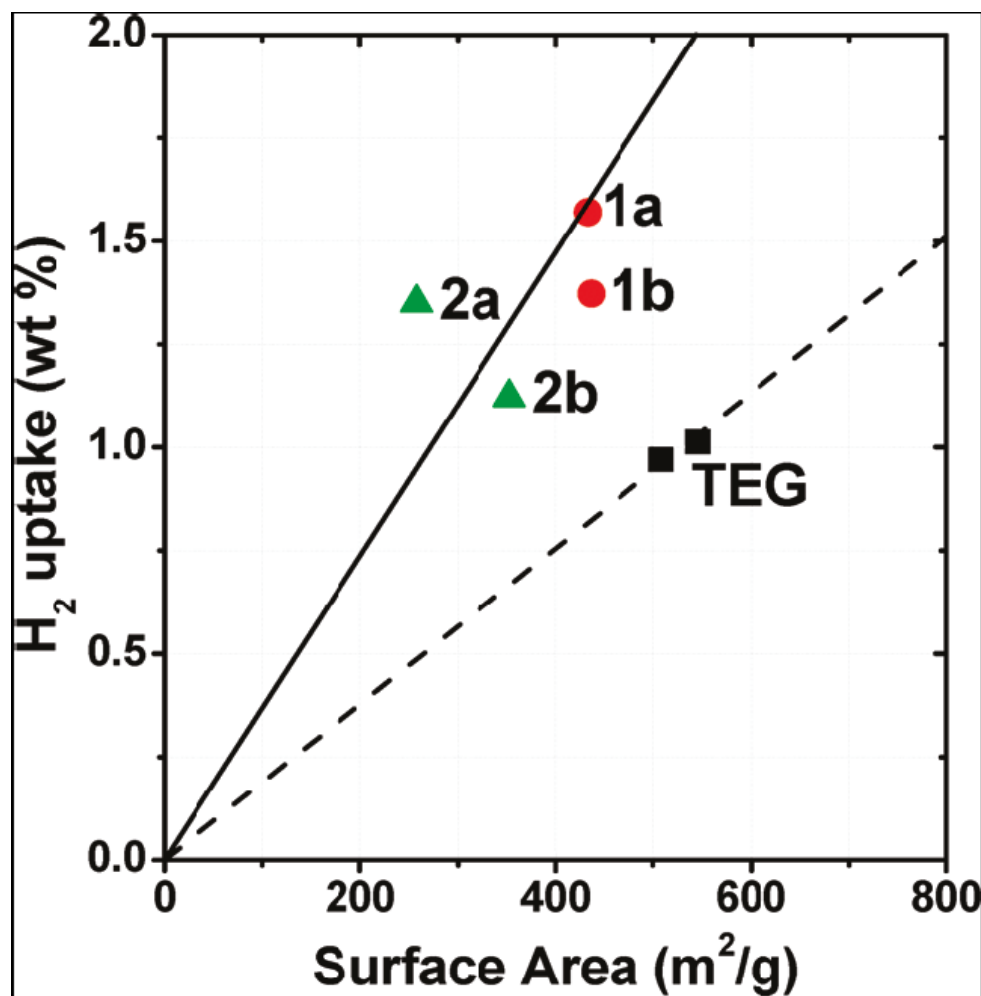
## 6. Thermogravimetric analysis of the graphene scaffolds



Weight loss upon heating shows the removal of the functional groups.

The weight loss of the f-TEGs was as follows: 1a, 42%; 1b, 21%; 2a, 40%, and 2b, 15%. The weight loss of 1a and 2a was higher than in product 1b and 2b. The data show that the degree of functionalization in chlorosulfonic acid is higher than in oleum, and this is consistent with the results of XPS data and the recorded solubility of graphene in those solvents

## 7. Enhance uptake due to expanded graphene scaffolds



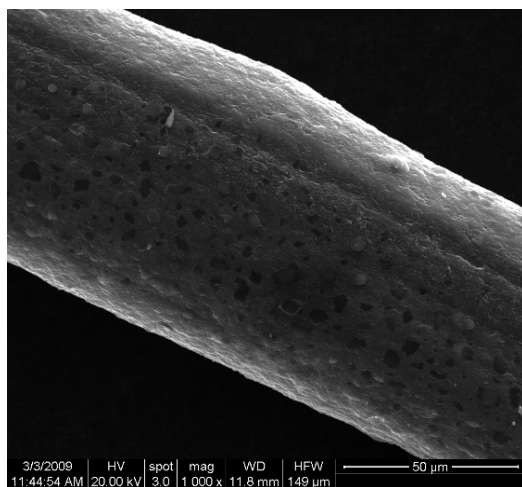
Specific surface area determined from nitrogen BET at 77 K versus hydrogen uptake capacity at 77 K and 2 bar. The data of different materials are represented by different symbols: black squares, original TEG; red circles, products 1a and 1b; and green triangles, products 2a and 2b. The solid line is the fit and extrapolation from the data of f-TEG products. The dashed line correlates to the data of original TEG. The slope for the functionalized material is about twice as steep, showing enhanced uptake per unit surface area for f-TEG.

## 8. Publication

The above data was included in a manuscript (along with supplemental information) that has been accepted for publication:

Zhong Jin, Wei Lu, Kevin J. O'Neill, Philip A. Parilla, Lin J. Simpson, Carter Kittrell\*, and James M. Tour\*, "Nano-Engineered Spacing in Graphene Sheets for Hydrogen Storage" ChemMater 2011 ; DOI:10.1021/cm1025188 (proof)

Graphene nanoribbons (GNR) can also be spun into fibers, using the same acid-based spinning techniques as used for SWCNTs.

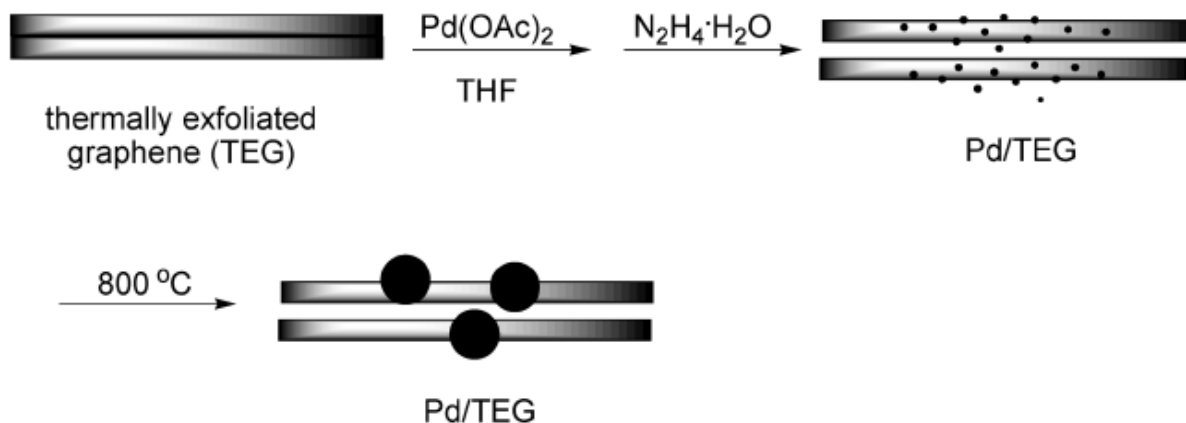


## 4. Palladium Catalyst

A Pd Catalyst particle that is very small, ca. 2 nm, can be mobile, and can move to the hydrogen to hydrogenate/dehydrogenate the graphene surface. Particles in the range of 1.5 nm to 3 nm have been made, and some mobility has been observed in this first demonstration of feasibility of the mobile catalyst.

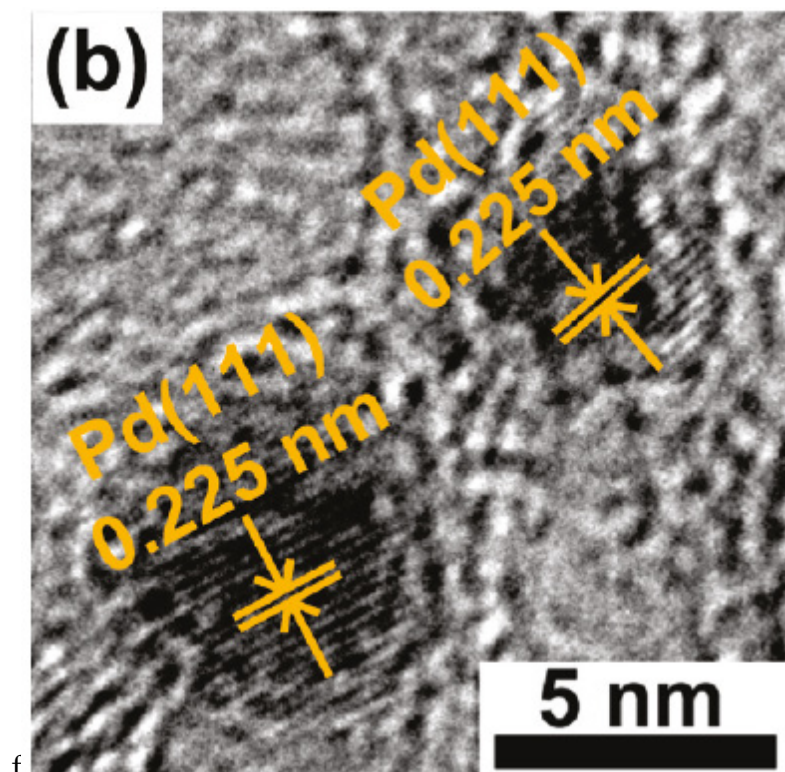
1. Pd nanoparticles which can catalyze the dissociation and binding of hydrogen to adjacent surfaces have been synthesized
2. TEM images show small particles and diffraction shows crystal planes that correspond the Pd lattice spacing.
3. Heating to 800 C under STEM observation shows the Pd particles will move and aggregate.
4. X-ray diffraction confirms coalescence into larger particles with well defined crystal domains. This places an upper bound on the temperature of processing a Pd intercalated sample. Fortunately this temperature is quite high, and the particles were stable at lower temperatures.

### 1. Palladium decoration of graphene sheets



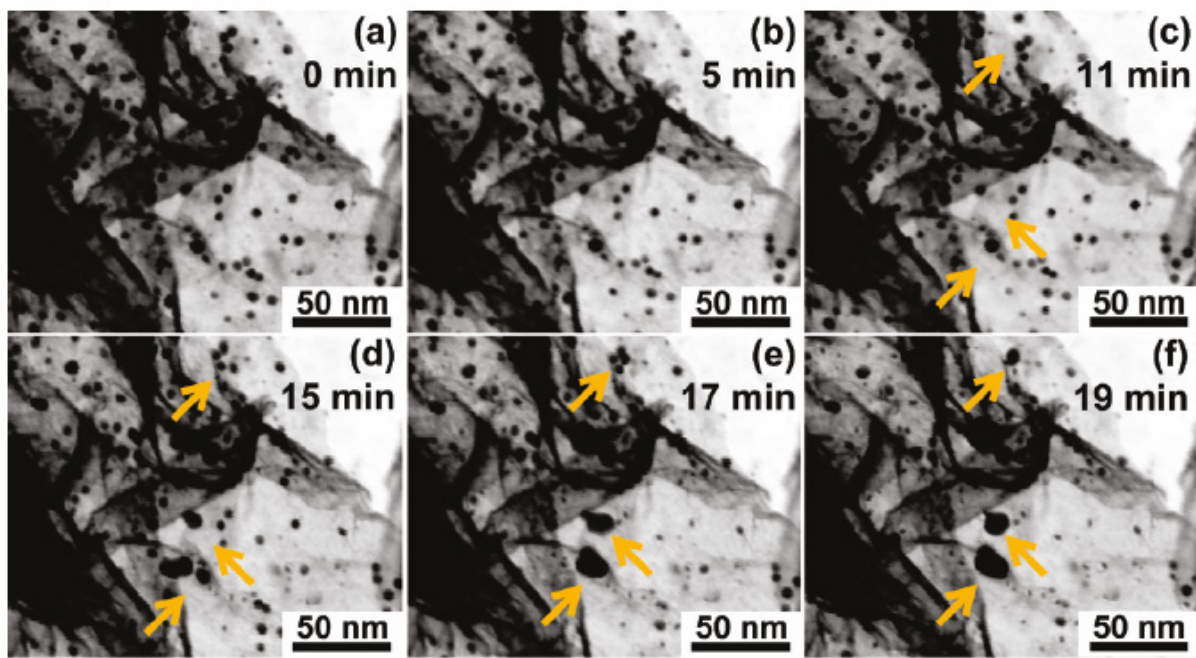
Palladium will catalytically dissociate hydrogen which in turn will help it bind to adjacent carbon materials. It is essential that the Pd be well dispersed in small nanoparticles if sufficient hydrogen uptake can be achieved. The reaction above precipitated Pd nanoparticles onto graphene sheets. The subsequent annealing at 800 C shows that the particles will aggregate at elevated temperatures. This limits the processing temperature of the decorated material. However, this limiting temperature has proved to be quite high.

### 3. Palladium decoration of graphene sheets



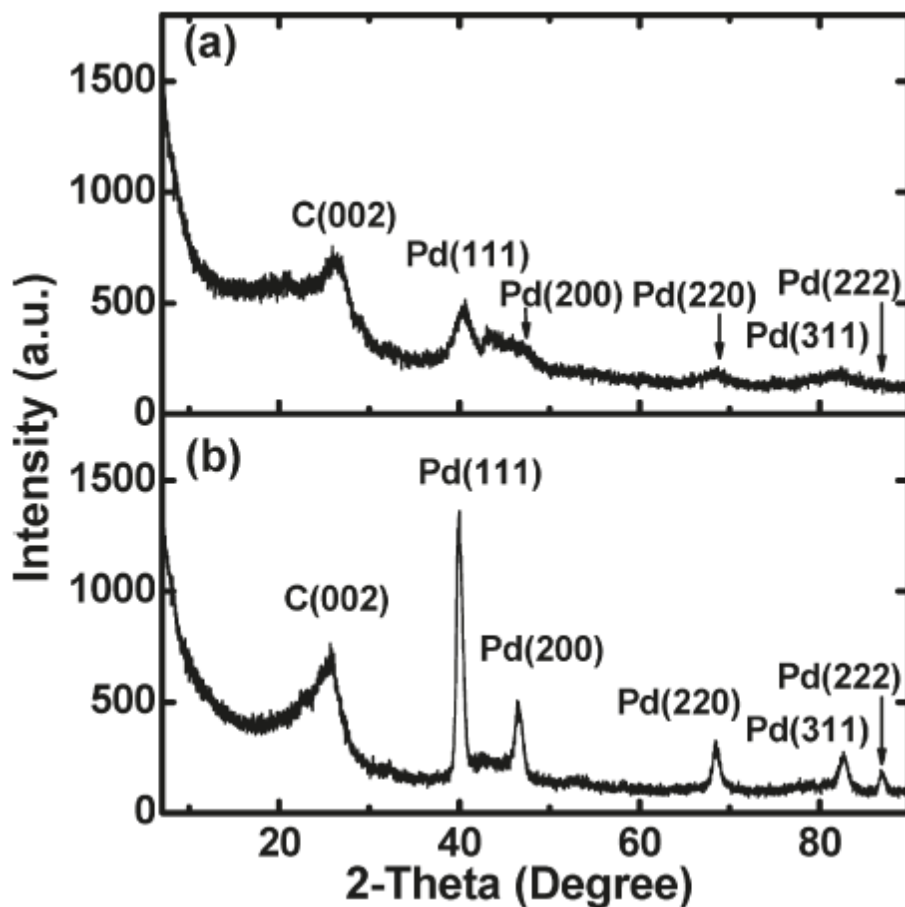
This is a high resolution of the Pd particles, which shows that the particles are only a couple of nm in size. The lattice fringes may be clearly seen due to the crystal structure of the Pd nanoparticles.

#### 4. Palladium decoration of graphene sheets

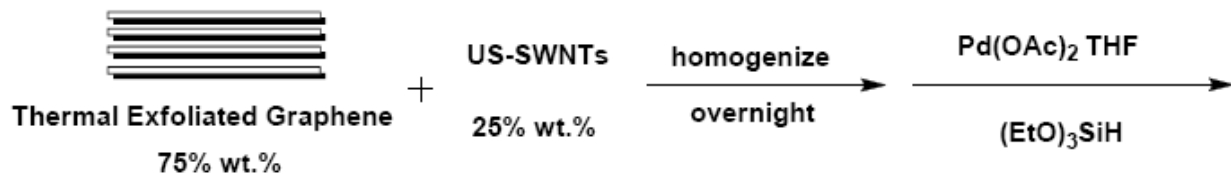


This is a sequence of STEM (scanning transmission electron microscopy) images taken when the sample is heated to 800C. This is sufficient to cause the Pd particles to migrate and aggregate. The arrows show where particles have moved together and fused into larger aggregated particles. The upper arrow shows a group of four particles that fuse into a single larger particle in 19 minutes.

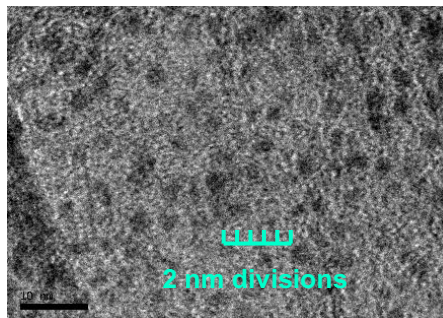
#### Palladium decoration of graphene sheets



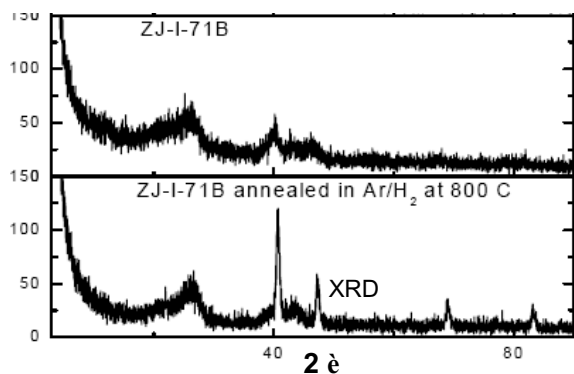
This is an X-ray diffraction spectrum of the Pd particles before and after annealing. The weak and broad peaks in (a) are characteristic of very small crystal domains. The sharp feature that develops at 40 degrees in (b) is indicative of a development of a larger crystal structure. This confirms the observations of coalescence in the STEM sequence. The absence of such coalescence at lower temperatures indicates that small Pd nanoparticles can be deposited and are stable if not annealed at too high of a temperature.



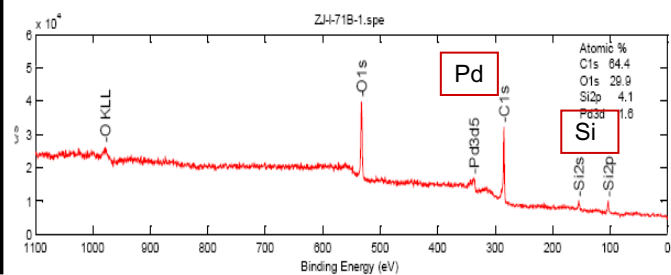
**Pd nanoparticles in graphene (TEM)**  
range 1.5 to 3 nm dia. Pd about 5wt%;  
scale bar 10 nm.



The TEM image shows that the catalyst particles are sufficiently small to be mobile. Due to the mobility, it was not attractive to continue along this line, and use of Pd nanoparticles was downselected.



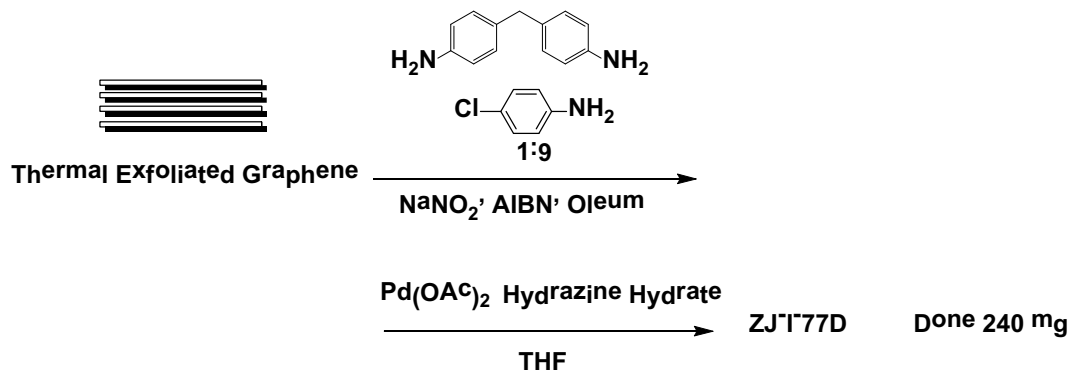
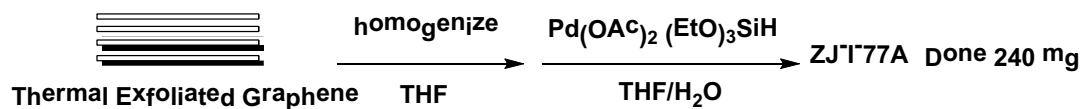
X-ray diffraction before and after shows formation of the nano-crystalline Pd catalyst particle at 40°



X-ray photoelectron spectroscopy reveals small amounts of silicon proppant along with the palladium.

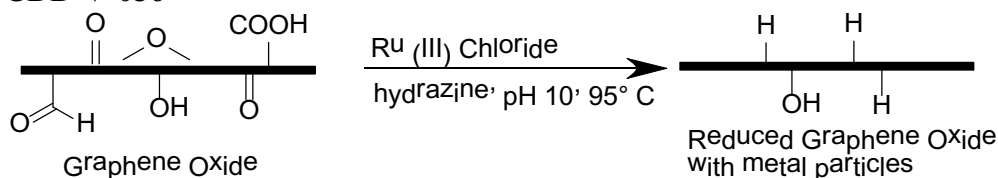
X-ray spectroscopy shows the particles become nanocrystallites, and XPS shows that Pd is present in the sample.





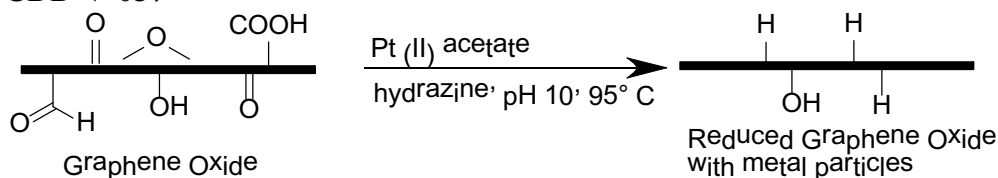
## 4. Spillover with mercury catalyst

### CDD-V-056



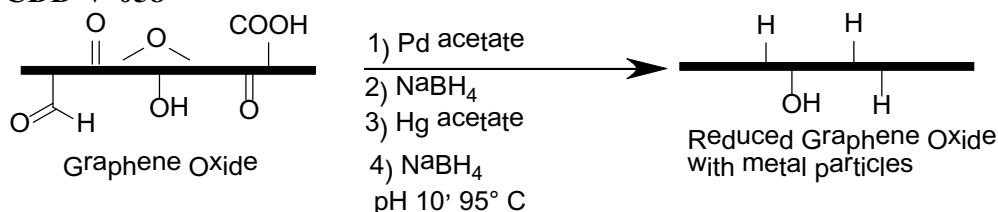
This reaction looks like it worked properly.  
I ran this on a 200 mg scale, enough to send to NREL.

### CDD-V-057

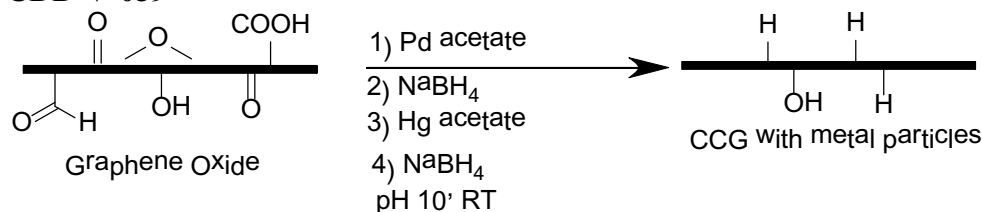


This reaction looks like it worked properly.  
I ran this on a 200 mg scale, enough to send to NREL.

### CDD-V-058



**CDD-V-059**

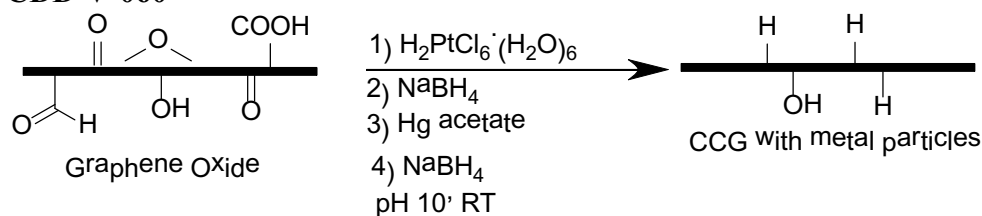


The Pd was dissolved in concentrated HCl before adding to the graphene solution.

-----  
Atomic Concentration Table  
-----

C1s	N1s	O1s	Pd3d	Hg4f
[0.314]	[0.499]	[0.733]	[5.637]	[7.512]
49.13	0.86	49.82	0.17	0.03

**CDD-V-060**



-----  
Atomic Concentration Table  
-----

B1s	C1s	N1s	O1s	Pt4f	Hg4f
[0.171]	[0.314]	[0.499]	[0.733]	[6.080]	[7.512]
2.95	62.41	0.57	33.95	0.05	0.07

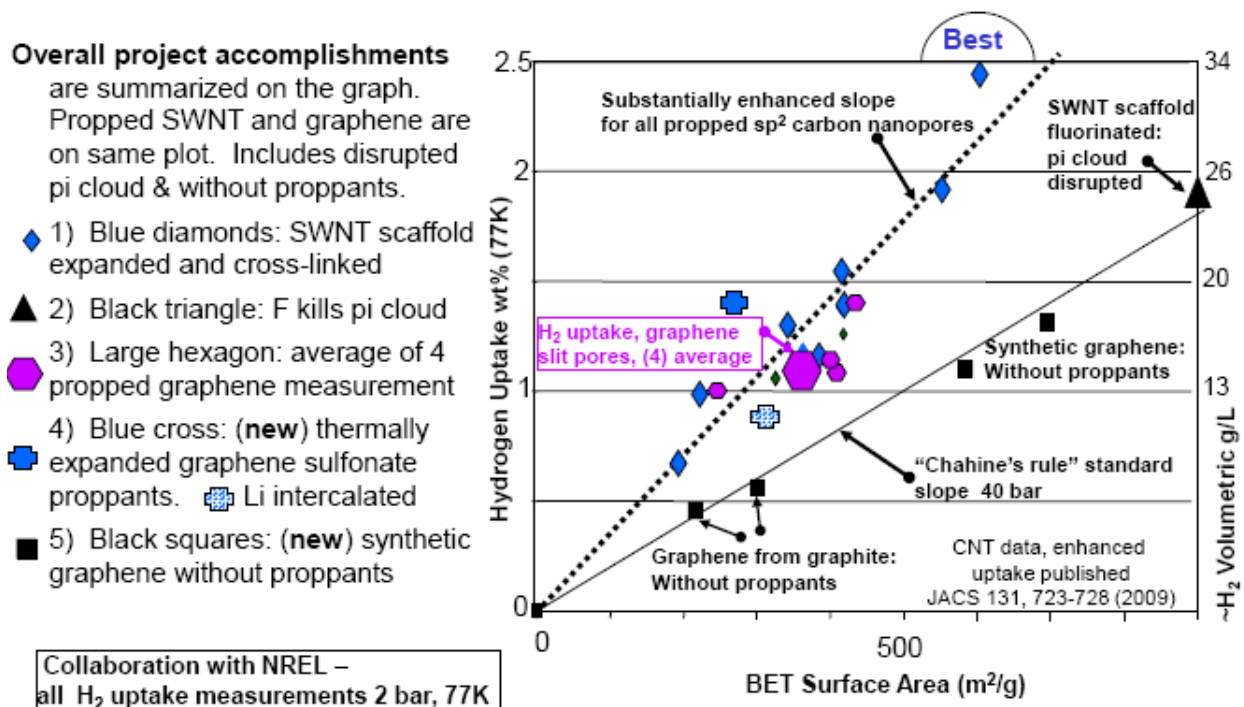
The Pd was dissolved in concentrated HCl before adding to the graphene solution.

We attempted to make the mixed Pd and Hg catalyst as reported at the DoE AMR 2008 meeting, and reproduced by Mike Miller in his report there. This was reported to have good hydrogen uptake at room temperature. We thought that this reaction could be transferred from their carbon foam to graphene oxide, both of which have a high oxygen content. However, we did not observe good intercalation of the catalyst particles, but rather they formed large 10 nm aggregates on the surface, and consequent H-uptake measurements showed no significant uptake at RT. At the September meeting at NIST for HSCoE, Ralph Yang reported that he could not reproduce the results with the mercury catalyst on the original carbon foam, so it does not appear fruitful to continue to try to extrapolate this to graphene oxide.

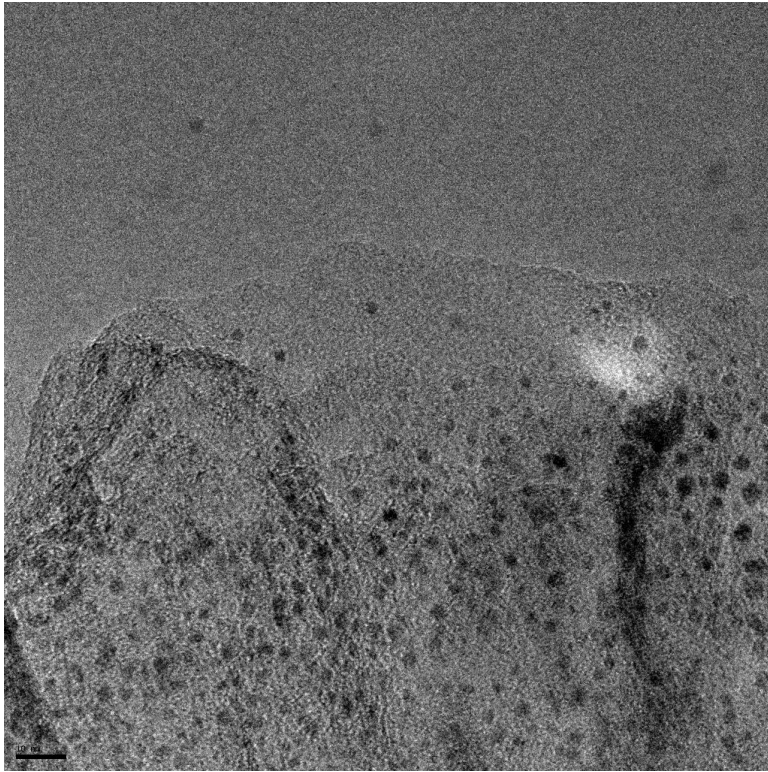
We added this to our “no-go” list.

## Overview of enhanced uptake in propped nanopores

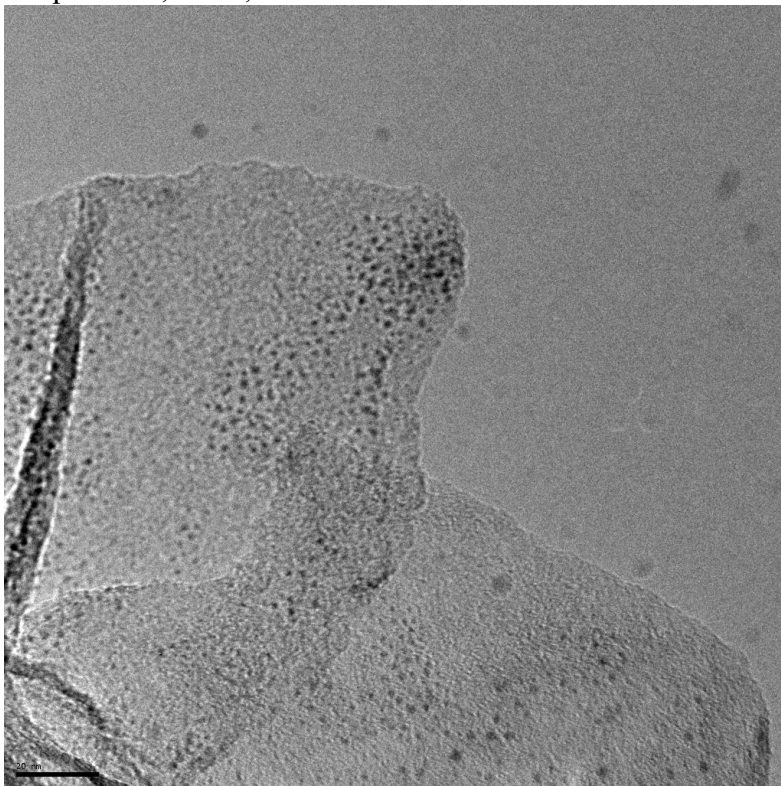
The graph displays new graphene data along with previous data from propped carbon nanotubes, showing the consistent enhancement in uptake per unit surface area for all  $sp^2$  carbon media. This shows how graphene scaffolds compare with earlier scaffolds using SWCNTs and in general, they fall on the same slope, overall. The large hexagon shows an average behavior. Lithium intercalation proved detrimental to the uptake, but this was a single experiment, and we discontinued this approach due to its severe sensitivity to air, and oxidation renders it ineffective, just adding mass.



Design of engineered nanospaces using  $sp^2$  material has shown unusually high  $H_2$  uptake per unit surface area. Best uptake is 2.4wt%  $H_2$  g/L as the  $sp^2$  carbon is a high density material.



PD particles, TEM, scale bar 10 nm

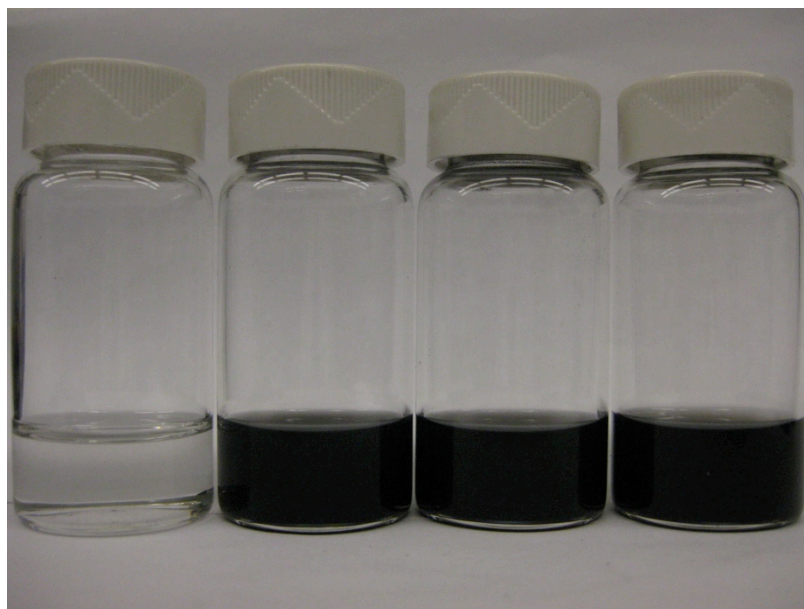


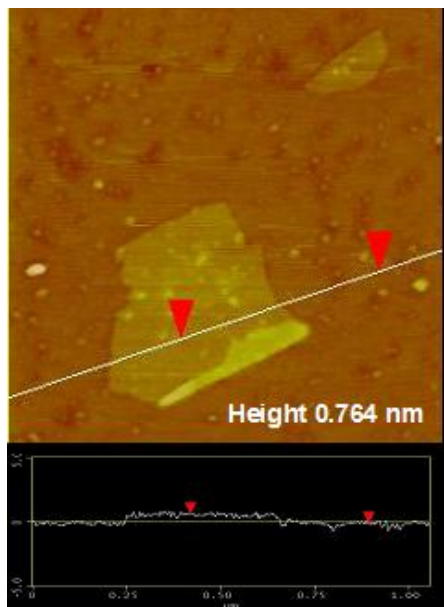
Scale bar, 20 nm

From John's weekly Report28

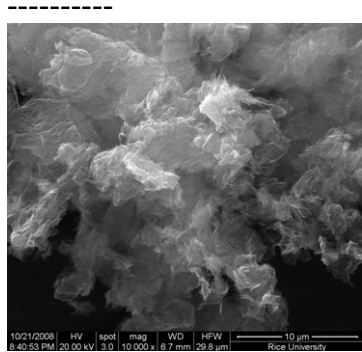
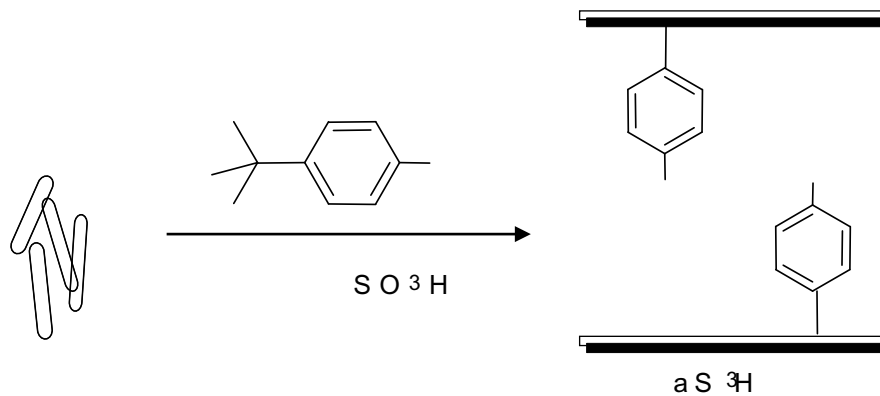
Since  $sp^2$  carbon has unusually high van der Waals interactions, we believed that  $H_2$  could be more densely packed into the pores of dense nanostructured  $sp^2$  carbon materials, and with this new approach, volumetric and gravimetric capacities are no longer a tradeoff, but remain in sync as the density of the media (including  $H_2$ ) is  $\sim 1$  kg/L. In addition, nano-engineered slit pores with identical covalently bonded molecular proppants provides a rigid, crystal-like nano-engineered structure where the slit pores are the same size, with no undersize pores that add mass to the media, or oversized pores with an “empty” middle that is wasted volume.

A uniform size pore is essential to pack in the  $H_2$  more densely than simple physisorption on a surface, which we determined to be about twice the diameter of the  $H_2$  molecule, and allowing for the width of the carbon framework the center-to-center spacing is 0.8 to 1.0 nm. In essentially all cases, whenever we made such nano-structured pores, the  $H_2$  uptake per unit surface area was about double that for  $sp^2$  carbon without spacers. when plotting volumetric vs. gravimetric uptake, this enhanced slope was observed for both single wall carbon nanotubes and **propped open graphene sheets**. As a general rule for physisorption at 77K,  $H_2$  uptake is about 1wt% per 500  $m^2/g$  SA at the asymptotic pressure limit (typically  $>40$  bar) whereas we observed an average of 1.8wt% per 500  $m^2/g$  SA at only 2 bar. We obtained additional confirmation for our nearly 2x enhanced uptake by fluorinating the nano-structured SWNT scaffold, and the uptake per unit area fell by 2x and returned to that typical of carbon sorption media. The partial fluorination of 1:3 F:C atoms was sufficient to disrupt the pi cloud, and the special enhancement of the pi cloud was eliminated, confirming that not only nano-structured media, but specifically nano-structured  $sp^2$  carbon is essential for such enhanced uptake per unit SA.

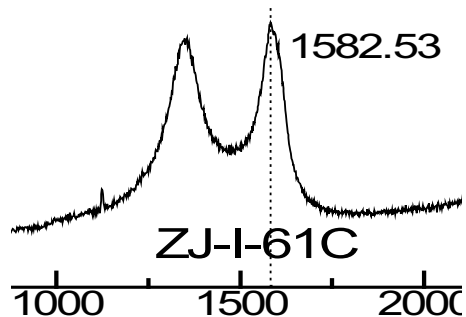




-----



-----

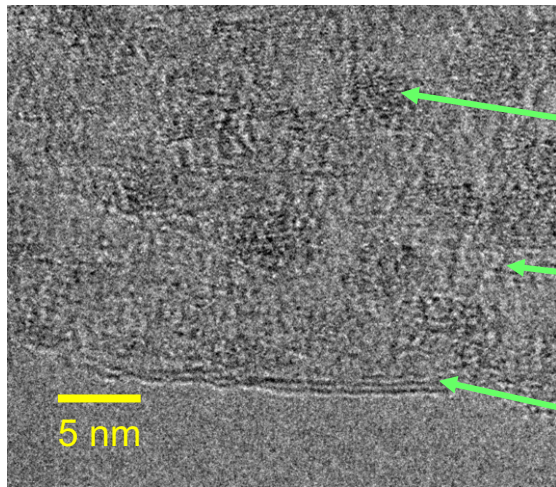


AMR 2009 propped graphene

Overall: The primary focus continues to be towards producing the 3D nanoengineered materials which will be suitable for intercalation of metals for near RT uptake of di-hydrogen. A new technique has been developed for substitutional doping.

1. A method of chemically synthesized graphene has been developed that is liquid based. This produces good quality graphene, as shown in TEM. This also provides a route for intercalation of different elements to enhance binding energy.
2. Thermal exfoliation of graphene oxide has been improved. Proppants have been added using a phenyl t-butyl group that is converted into a phenyl sulfonate group. solubility. This holds the graphene sheets apart to allow room for the hydrogen to enter.
3. A new method for boron substituted in the graphene has been developed using the chemical synthesis and addition of boron-containing precursor. The boron is well distributed, is shown when imaged with element-selective TEM. The graphene sheet structure is retained. The purpose is to provide for enhanced binding energy uptake at higher temperatures.

## 1a. Chemically synthesized graphene



HRTEM image of synthetic graphene ZJ-I-85C

● Darker spots: 5 to 10 layers of graphene

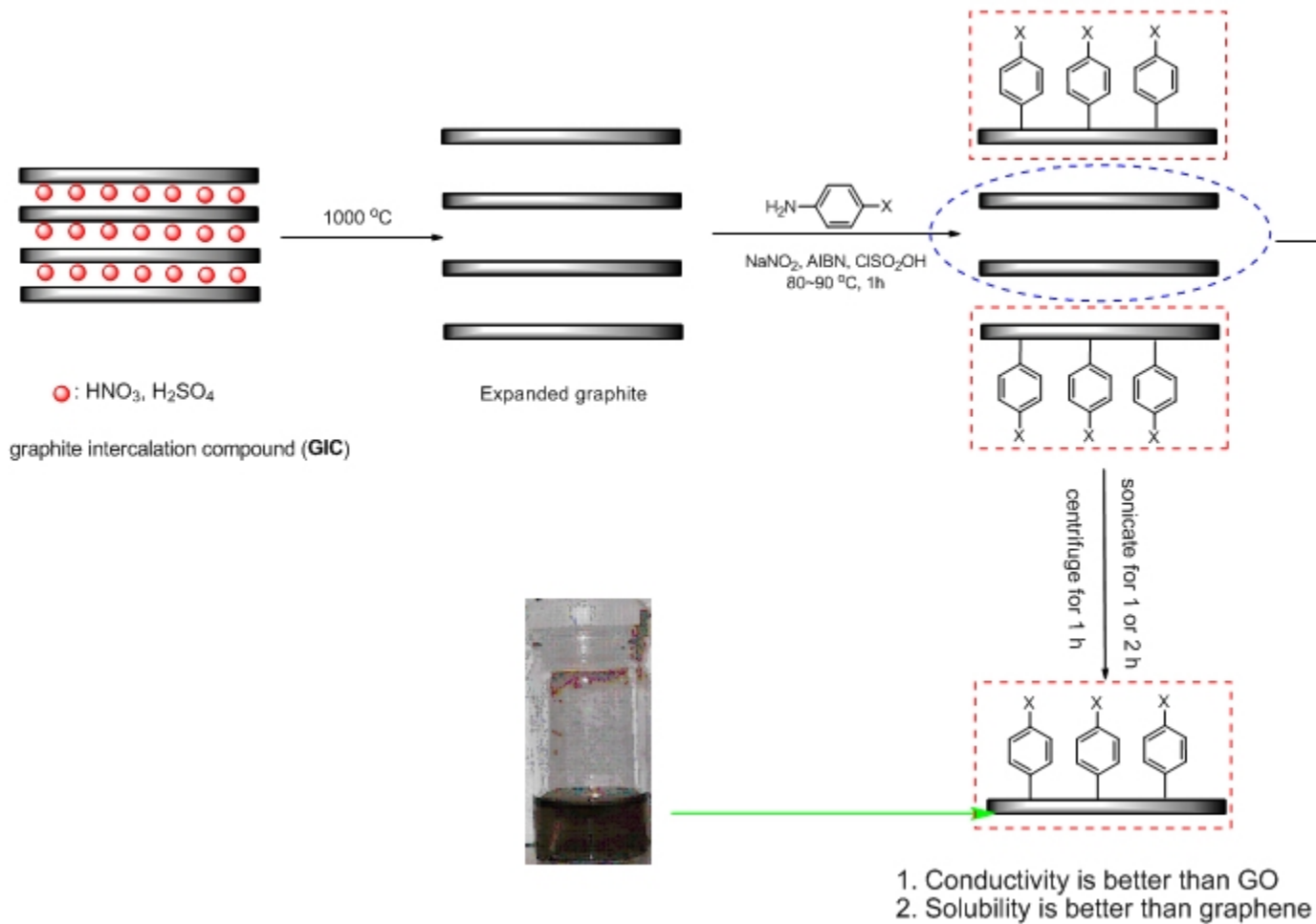
● Lighter areas 2 to 5 layers of graphene

● Edge shows 2 to 3 layers of graphene

A liquid based chemical synthesis method has been developed for graphene. A TEM image is above. The overall thickness is a few graphene layers, with several spots being thicker. The edge of the image reveals striations of a few layers of graphene. Several samples have been sent for testing,

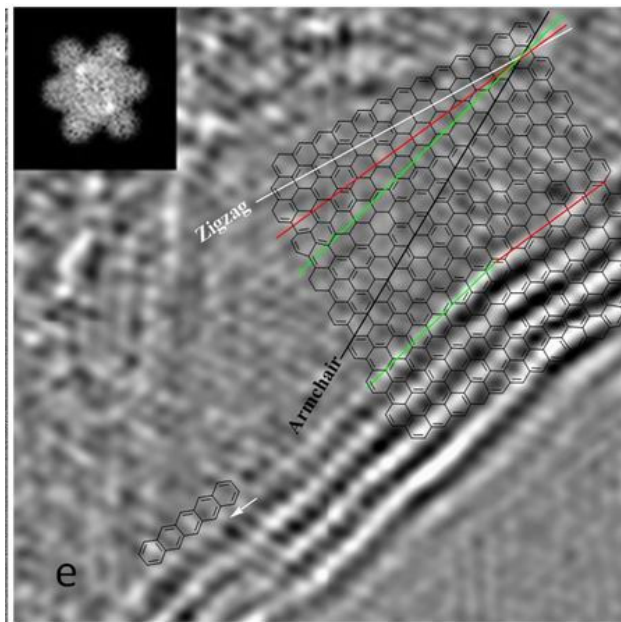
## 3a. Chemically assisted exfoliated graphite (CAG)





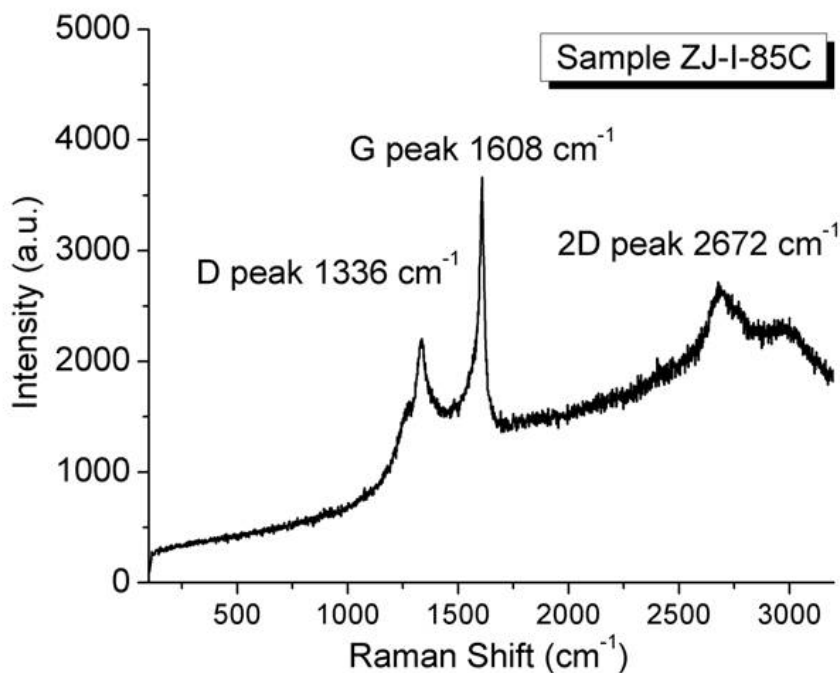
Chemically assisted exfoliated graphite helps separate the graphene sheets. The diazonium functionalization helps keep the graphene sheets separated and improves solubility.

### 3b. TEM of CAG on edge



The high resolution TEM image shows the layered structure of the chemically assisted exfoliated graphite

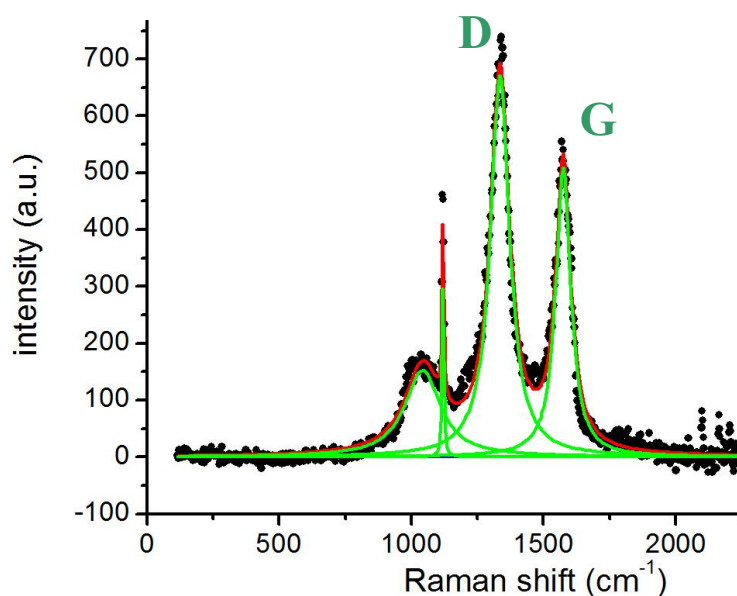
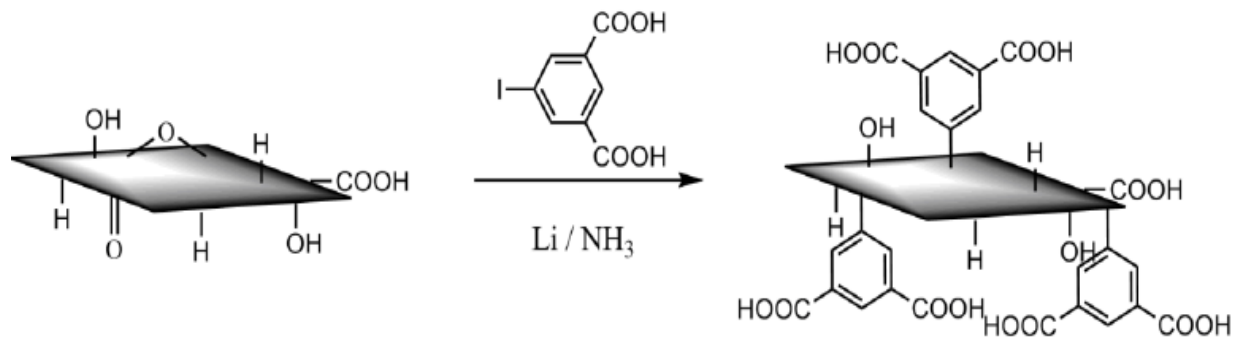
## 1b. Raman spectrum of chemically synthesized graphene



Raman spectrum of the chemically synthesized graphene. The sharp G-peak shows excellent  $sp^2$  graphene character. The relatively weak D-peak indicates that there is a small number of defect sites. This material has not been functionalized or propped open. The 2D peak is relatively small, indicating that there are several layers together. Higher numbers of layers attenuates the 2D peak.

## 4a. Functionalization of graphene

Single sheet graphene is the “New kid on the block” for nanoengineered materials [Nature, July 2006], due to oxidation [Yakobson 2007a] Graphene, like SWNT, has superb thermal conductivity. Electrostatic assembly into nano-ribbons has been demonstrated. Graphite is oxidized with very low cost reagents: sulfuric acid + oxidizers like chlorates or permanganates, to make water soluble graphene oxide (GO). We have now begun applying well-developed SWNT organic synthesis methods to create carbon-carbon covalent bonding of functional groups to graphene.

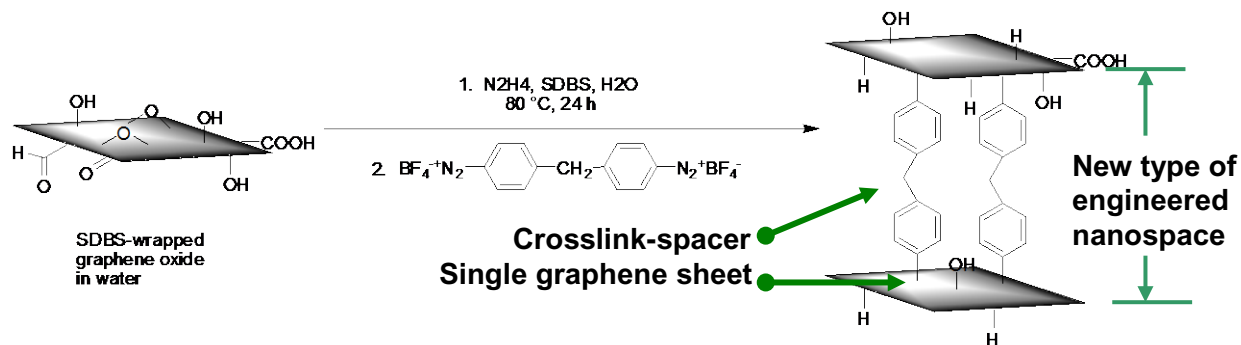


Lithium – aryl iodide reaction leads to covalent C–C bonding of isophthalic acid to a graphene sheet. Raman spectra (514 nm excitation) shows a strongly enhanced “D” peak, due to the new sp<sup>3</sup> hybridization of the graphene. Green lines = fit to peaks, D:G ratio 1.4:1 This shows that the covalent attachment was successful. Our expertise in SWNT sidewall functionalization now being transferred to the newborn field of single sheet graphene functionalization chemistry.

#### 4b. Crosslinking the graphene, technology transfer from carbon nanotubes

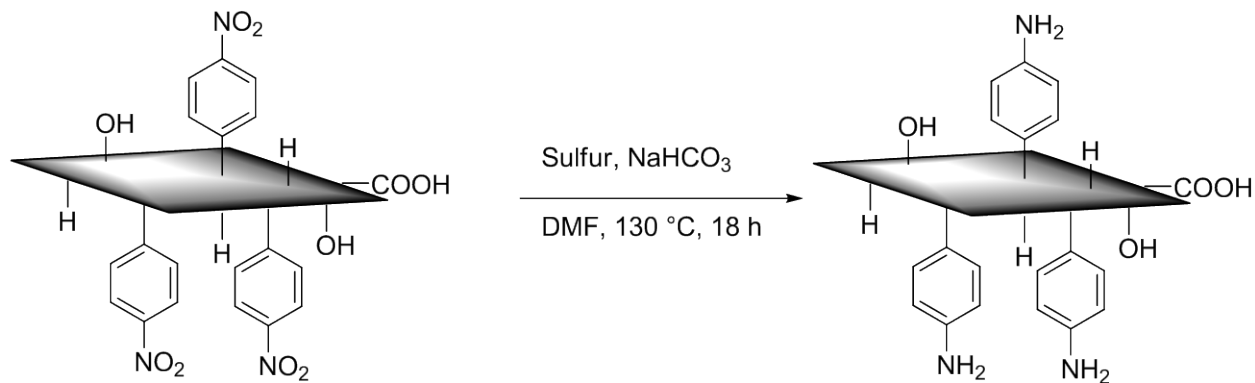
Diazonium chemistry for functionalizing SWNT sidewalls now put to work functionalizing and crosslinking graphene sheets. Broad knowledge of the chemistry of SWNTs is proving

invaluable for rapidly developing single sheet graphene chemistry to make an engineered nanospace for dihydrogen at room temperature.

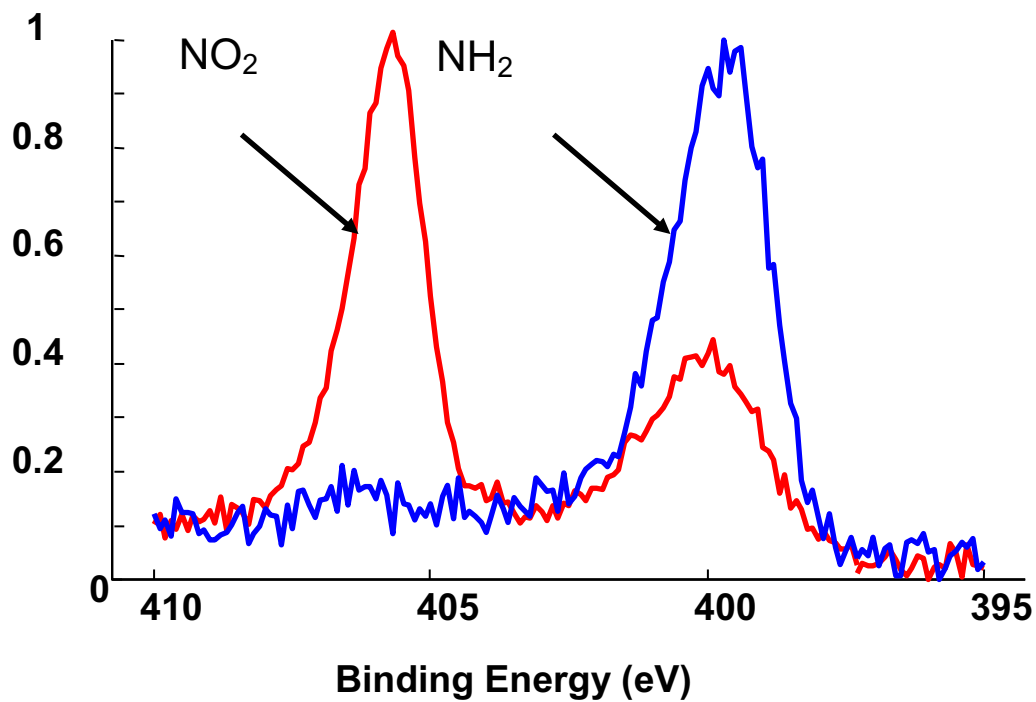


The same bifunctional diazonium salt that has been used so successfully on SWNTs has now been demonstrated for graphene as well, with spaced apart graphene sheets created.

### 4c. Chemistry on graphene

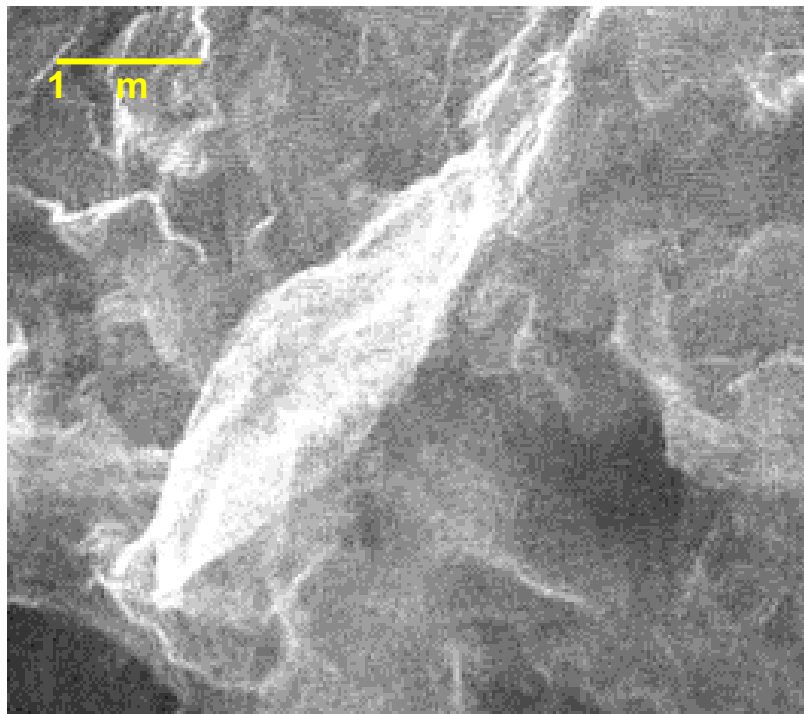


Conventional chemistry may be performed as well. This will be very beneficial in modifying the graphene structure to accept metal atoms.

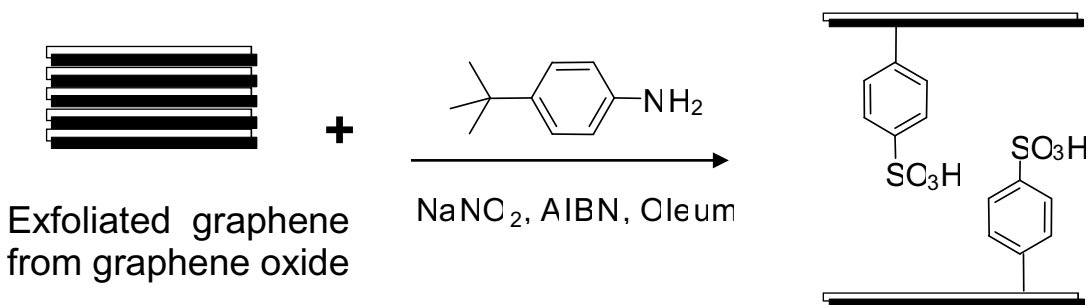


Chemistry on graphene: XPS data shows phenyl nitrate at 406 eV (red) and conversion to phenyl amine 400 eV (blue). Since metal atoms readily bind to amines, this produces appropriate binding sites.

## 2a. Propping open a graphene scaffold

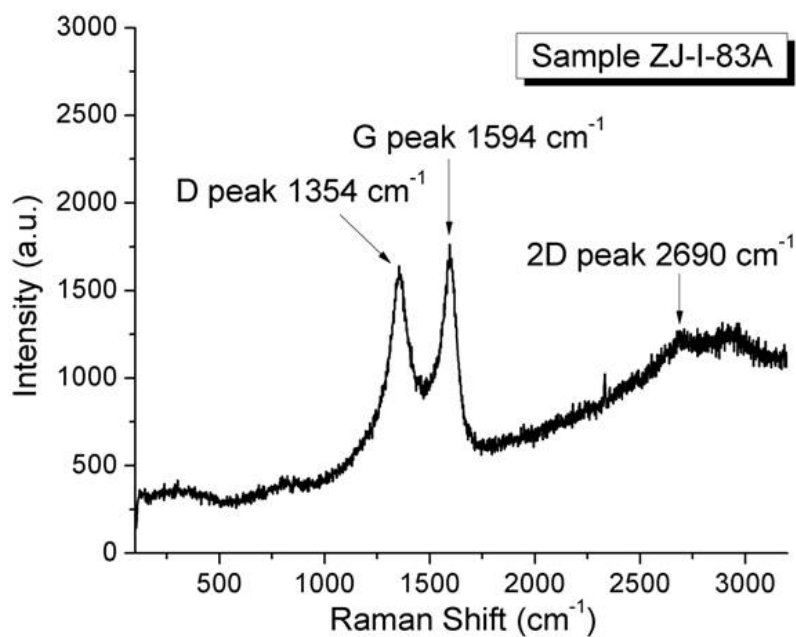


Thermally exfoliated graphene derived from graphene oxide. The large flake-like structure may be readily seen in this SEM image. Sample JZ-I-83A



The exfoliated graphene is propped open by addition of functional groups. The t-butyl groups are converted into sulfonate groups during the acid treatment.

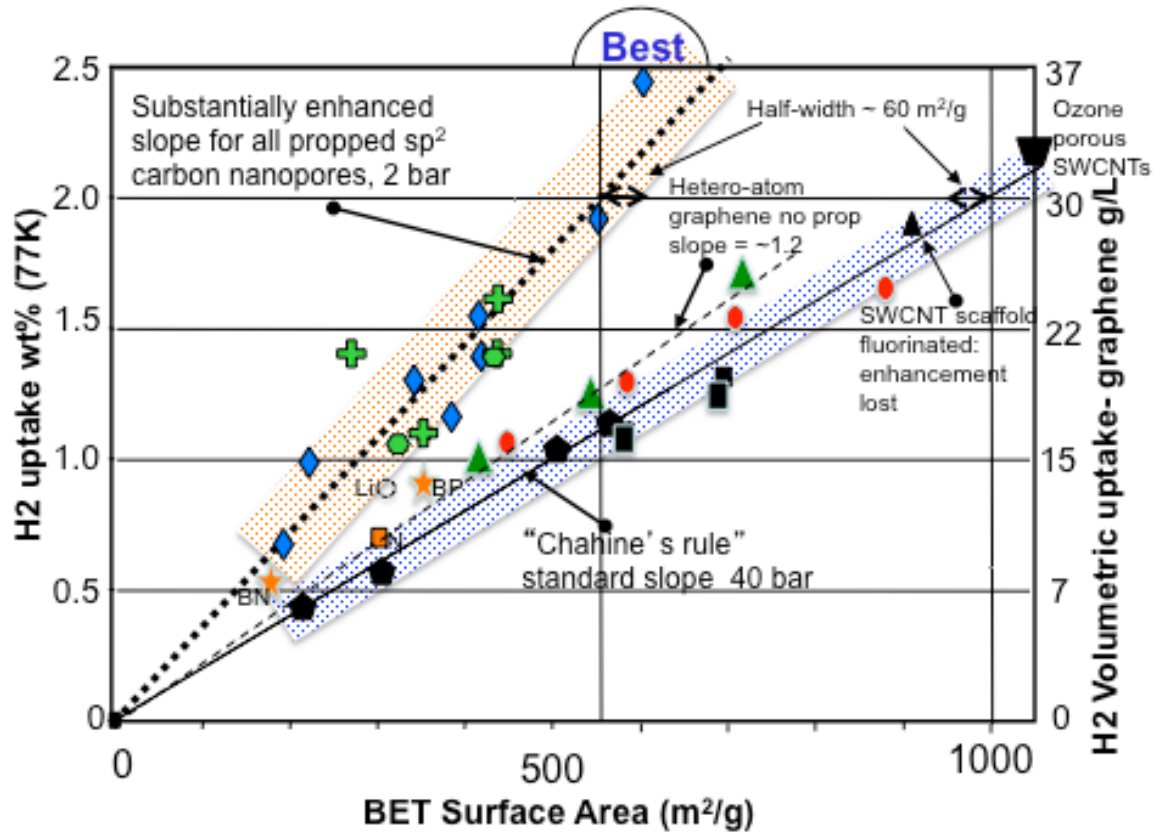
## 2b. Raman spectrum of propped graphene scaffold



The Raman spectrum shows a fairly sharp G-peak indicating the dominant sp<sup>2</sup> carbon structure, and the strong D-peak is due to the functionalization.



### Enhanced Uptake in nanostructured sp<sup>2</sup> slit pores



**Overall accomplishments are summarized on the graph.**













All of the propped and/or crosslinked graphene-like carbon samples are clustered around the steeper slope of nearly 2x enhanced uptake per unit SA.

All of the graphene and CNT media without proppants follows the Chahine's rule slope of 1wt% per 500 m<sup>2</sup>/g SA. Fluorination of a scaffold disrupts the pi cloud, drops to lower slope. The Li intercalated is in between due to degradation by moisture.

Heteroatom B, P substituted graphene has higher binding energy 8.5kJ/mol, slightly higher uptake, ~1.2 slope

The Chahine's rule slope of 1 = 1wt% per 500 m<sup>2</sup> /g, and not fitted to the data

The half-width of the shaded areas shows how well the data fits the slope. the deviations tend to be in absolute SA, so that the greater the uptake, the less the deviation from the average slope

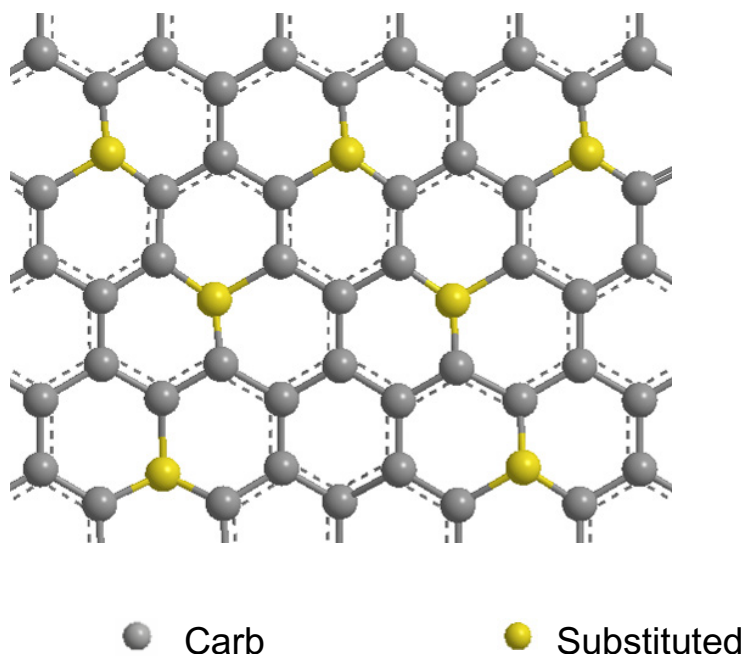
-  Blue diamonds: SWNT scaffold expanded and cross-linked (8)
  -  Black triangle: Fluorination kills pi cloud of SWCNT scaffold enhanced uptake is lost
  -  Green hexagon: propped graphene aniline sulfonate & diphenyl crosslink (2)
  -  Green cross: TEG phenyl sulfonate link & proppants (4)
  -  Dotted circle: Li intercalated SWCNT scaffold (sample probably degraded due to moisture)
  -  Black squares: synthetic graphene without proppants (2)
  -  Black pentagons: thermally exfoliated graphene (natural), without proppants (4)
  -  Orange square: Nitrogen substituted graphene without proppants
  -  The ozone perforated bulk SWNTs is from Phase I, before nano-engineered scaffolds
  -  Red dots: Boron hetero-atom doped graphene, enhanced binding energy (4)
  -  Green triangles: Phosphorous hetero-atom doped graphene, enhanced binding energy (3)
  -  Orange Texas star: Double hetero-atom substituted graphene suggests greater enhanced uptake, perhaps due to charge separation which will polarize the H<sub>2</sub> molecules.
- BN = boron + nitrogen; BP = boron + phosphorous

## Atom substituted graphene, B, N, P

Our second major effort was increasing the binding energy of the H<sub>2</sub>, so that higher temperatures could be used for physisorption. By using atom substitution into the graphene lattice, this will “dope” the structure producing a partial charge. This charge will induce polarization into the H<sub>2</sub>, providing an additional binding force of charge-induced polarization. When the binding force is higher, the H<sub>2</sub> will adhere at higher temperatures. A 5.4 atom% substitution with boron (p-doped) increase binding energy from a typical 5.5 kJ/mol to 8.6 kJ/mol and a 7.5 atom% substitution with phosphorous (n-doped) increased this to 8.3 kJ/mol. A 18 atom% substitution with nitrogen provided no significant enhancement. However, we had difficulty with low SA of only 180 m<sup>2</sup>/g for the nitrogen sample, so this lack of enhancement for nitrogen substitution should not be considered definitive. The B-substituted media had 700 m<sup>2</sup>/g which makes the binding energy more reliable, and the P-substituted media with 400 m<sup>2</sup>/g is also acceptable.

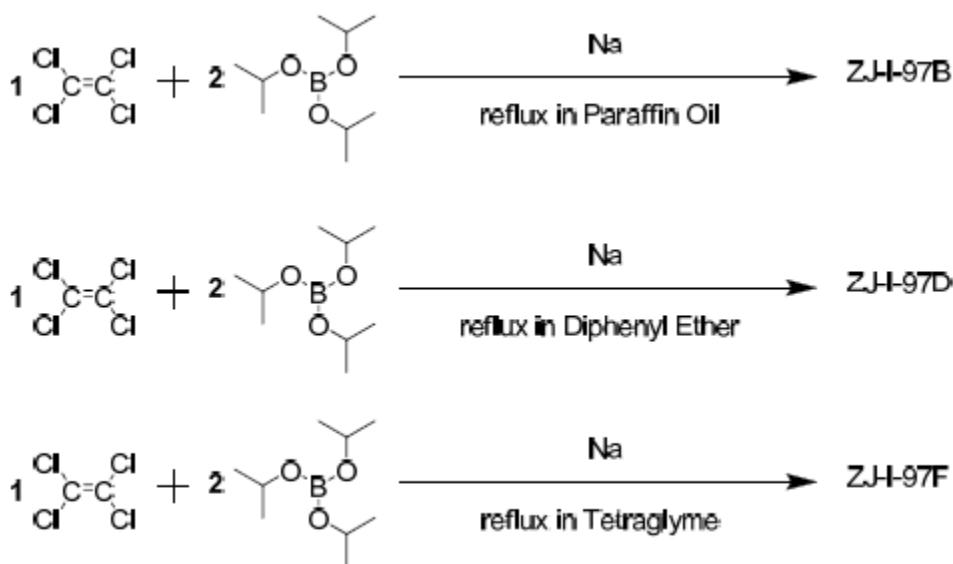
### 1a. Atom substitution in synthetic graphene sheets tested for hydrogen uptake

This generic illustration shows the concept of atom substitution, which includes boron, nitrogen or phosphorous, which is a useful guide for the remainder of the report.

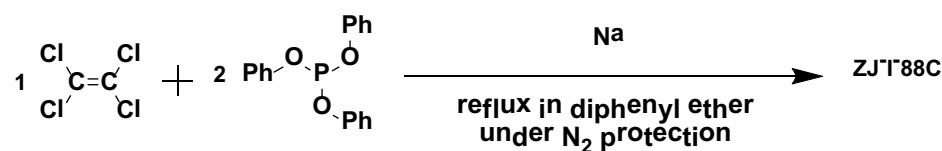
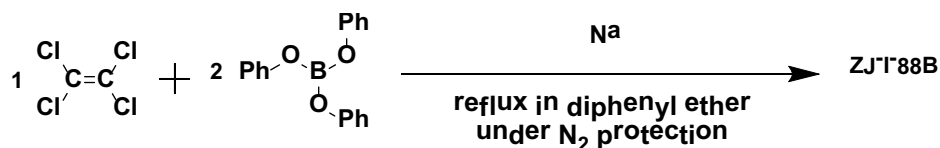


1. A new method for boron substituted in the graphene has been developed using metallic sodium in a liquid reflux bath. Phosphorous substitution is new.
2. The versatility of the metallic sodium extraction of the chlorine in the liquid phase has proven to be very versatile, and nitrogen and boron can be simultaneously added to the carbon structure. TEM shows the small disks of substituted graphene.
3. Chemically assisted exfoliated graphite helps separate the graphene sheets. The diazonium functionalization helps keep the graphene sheets separated and improves solubility.
4. CVD grown graphene has been improved, with a good quality Raman spectrum indicating high quality graphene sheets.

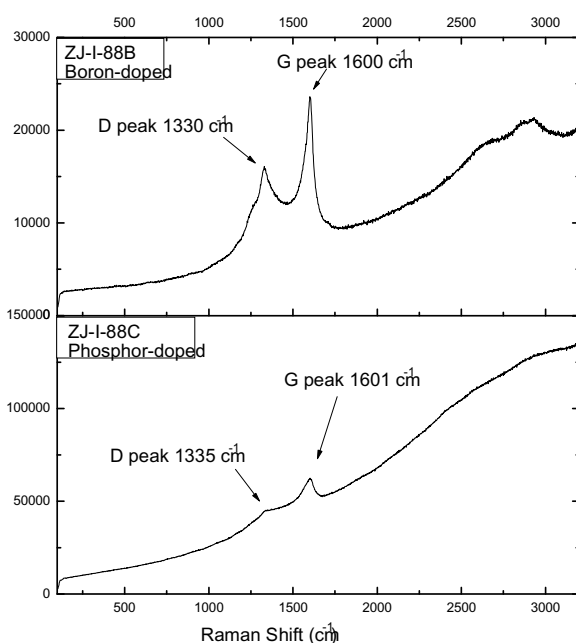
## 2a. Typical chemistry of making atom substituted graphene flakes.



# 1. Boron and Phosphorous doped graphene



**Raman spectra.**



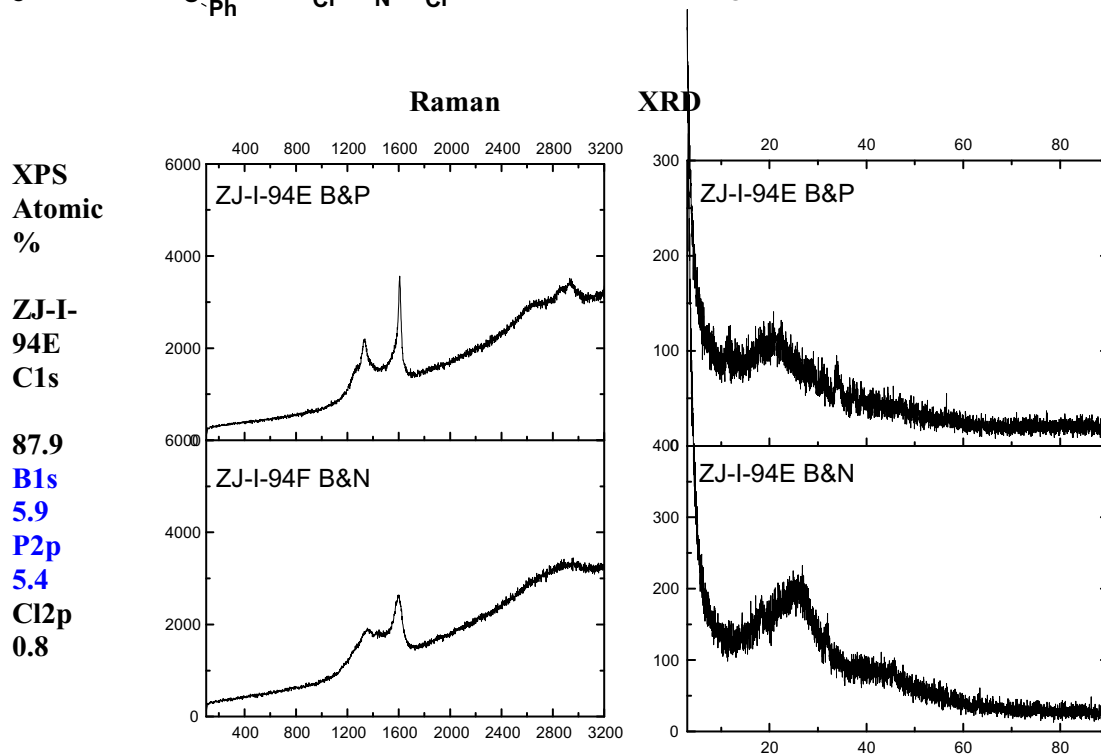
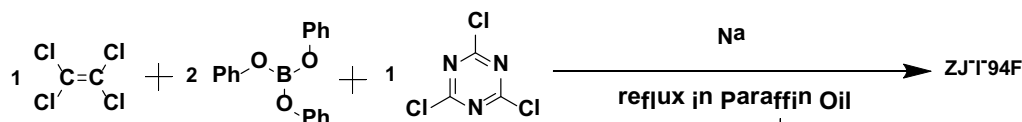
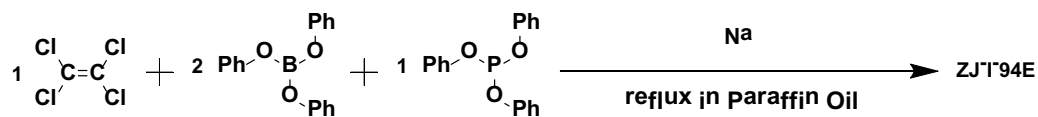
**XPS Atomic %**

**ZJ-I-88B**  
**C1s 94.3**  
**B1s 5.4**  
**Cl2p 0.3**

**ZJ-I-88C**  
**C1s 92.4**  
**P2p 7.5**  
**Cl2p 0.1**

A new method has been developed to make boron doped graphene, using a solution-based chemistry rather than gas phase CVD. The sodium metal extracts the chlorine atom, causing the carbon to become reactive. The G-peak in the Raman spectrum shows that  $sp^2$  graphene-like carbon has been made. Sample 88B contains 5.4% boron. Sample 88C contains 7.5% phosphorous. These substitutional species should provide doping and enhanced binding energy for the hydrogen.

## 2a. Boron, Nitrogen, Phosphorous doped graphene

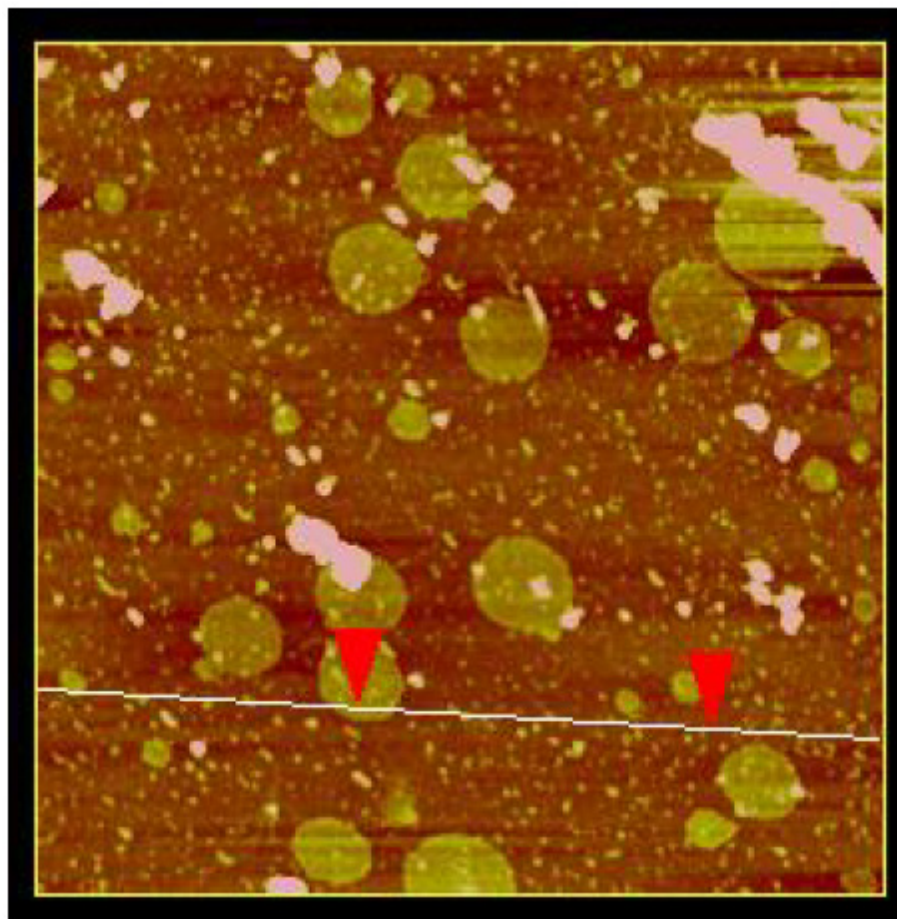


This shows the versatility of the metallic sodium reflux technique, which allows simultaneous substitution with more than one atomic species. This may lead to charge separation and enhanced hydrogen binding energy. The Raman spectrum exhibits the characteristic G - peak of graphene, and X-ray diffraction shows the 26 degree scattering angle for graphene.

prepared by refluxing paraffin-oil.

Boron-doped scaffold; Sample: ZJ-I-88B

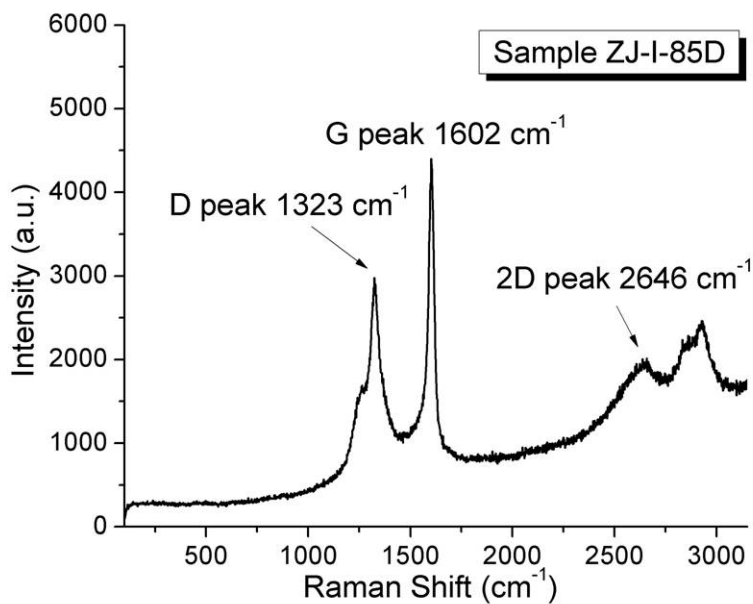
This shows that the chemical synthesis makes small graphene sheets with atom substitution.



Surface distance	1.810 $\mu\text{m}$
Horiz distance(L)	1.807 $\mu\text{m}$
Vert distance	1.572 nm
Angle	0.050 $^\circ$

Small graphene flakes were observed everywhere on the surface which have low height less than 2 nm, so these are thin flakes as expected for graphene.

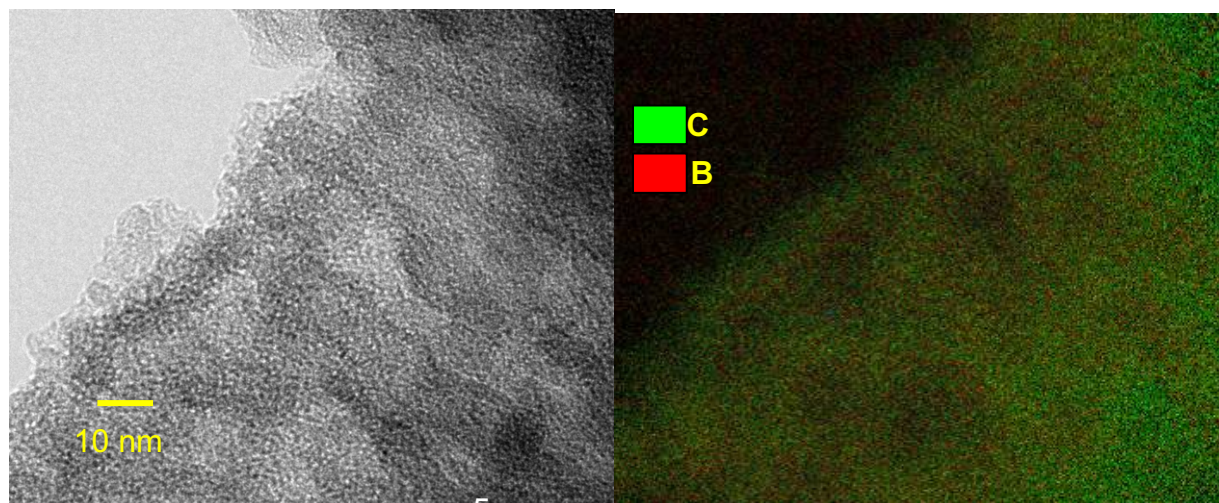
This figure shows the structure of the boron substituted graphene sheet. The boron concentration achieved so far is low than that indicate in the figure.



Raman spectrum of synthetic graphene with substituted boron. The sharp G peak shows good graphene sp<sup>2</sup> carbon, and the large D-peak indicates significant defects, perhaps due to strain from the introduced boron. The relatively weak 2D peak indicates significant stacking, probably several layers of graphene stacked together.

### 3b. Synthetic graphene with boron substitution



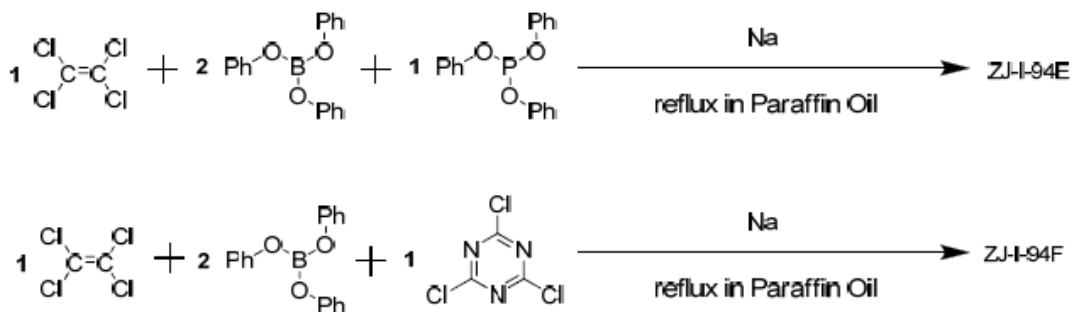


The figure on the left is a TEM image of the chemically synthesized graphene. The image on the right uses TEM with elemental sensitivity. The carbon atoms are false colored green, and the boron is red. As one can see, the boron is rather uniformly distributed in the graphene sheets. Sample JZ-I-85D

As with the graphene, these materials have been submitted for hydrogen uptake testing,

#### 4a. B/P-codoped and B/N-codoped carbon scaffolds.

This is achieved by supplying precursors containing carbon, boron and phosphorous in the first reaction, and by supplying precursors containing carbon, nitrogen and phosphorous in the second reaction

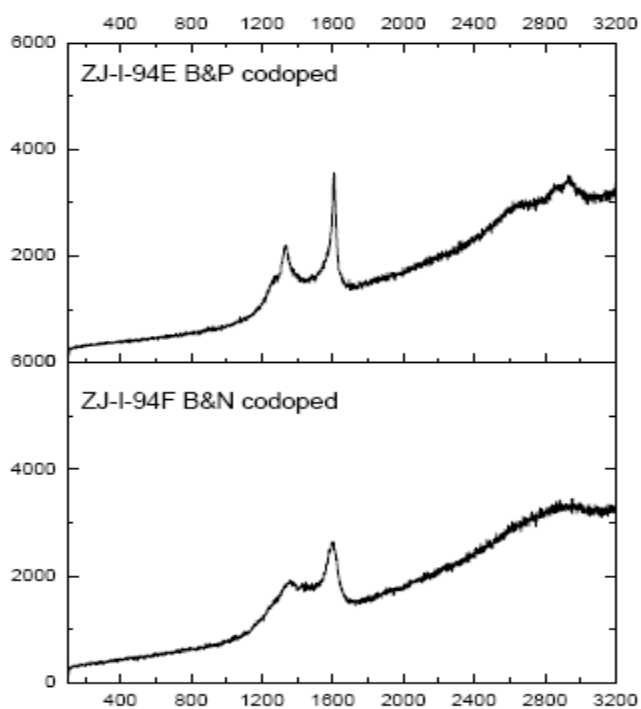


#### 4b. Atomic % measured by XPS.

sample	ZJ-I-94E	ZJ-I-94E	
carbon	C1s 87.9	C1s 83.6	
boron	B1s 5.9	B1s 5.7	
phosphorous	P2p 5.4		
nitrogen		bN1s 9.3	
chlorine	Cl2p 0.8	Cl2p 1.4	residual

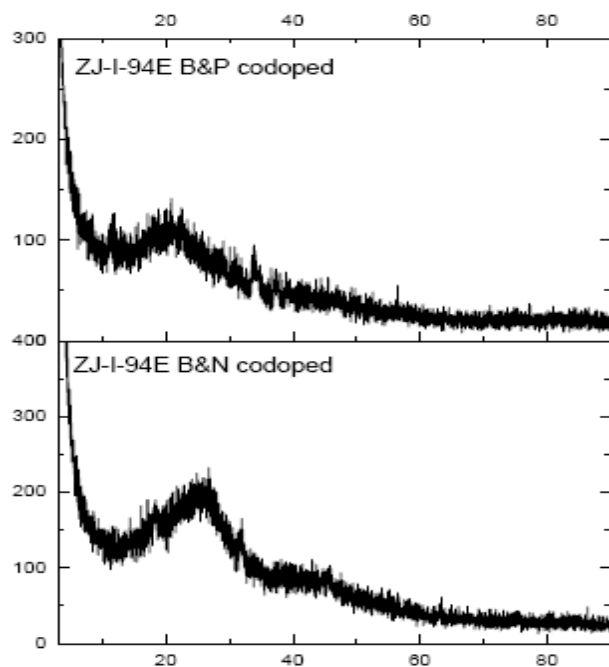
## 5. Raman diagnostics

Raman scattering shows a sharp G-peak indicating that the atom substitution still provides a good graphitic structure.



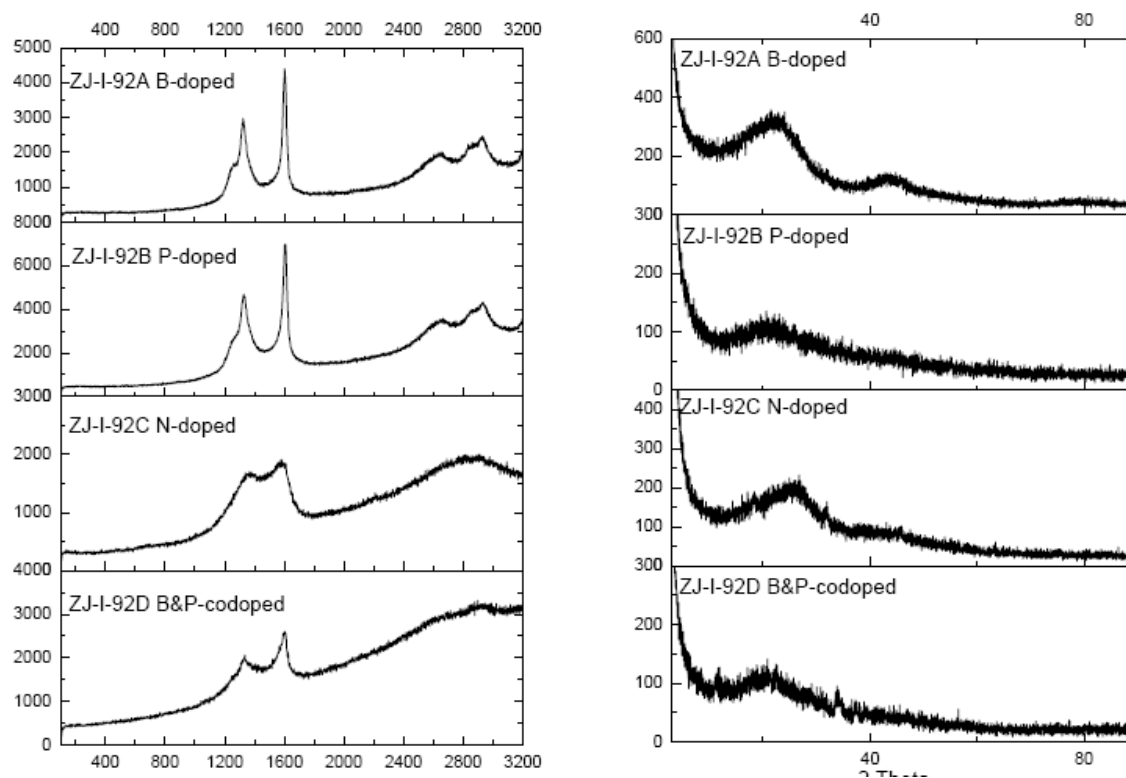
## 6. X-Ray diffraction diagnostics

XRD shows the characteristic graphitic peak at 26 degrees.



## 7a. Raman and XRD diagnostics for a series

Raman scattering shows a sharp G-peak indicating that the atom substitution still provides a good graphitic structure for four samples in the 92 series, although the G-peak becomes less distinct with high % atom substitution for nitrogen. The XRD still shows the 26 degree scattering.



## 7b. Atomic % measured by XPS.

Nitrogen was the highest with 13.5% in this series

Sample#	ZJ-I-92A	ZJ-I-92B	ZJ-I-92C	ZJ-I-92D
carbon	C1s 93.6	C1s 92.7	C1s 85.8	C1s 87.8
substitued atom	B1s 6.0	P2p 6.7	N1s 13.5	B1s 6.1
dual substitution				P2p 4.2
chlorine, residual	Cl2p 0.4	Cl2p 0.6	Cl2p 0.7	Cl2p 1.9

## 8. Table of samples: Atom substituted graphene

Chemically synthesized atom substituted graphene

Tables show samples made and BET surface area results at three temperatures.

More samples were made than shown; these had the best SA and were sent to NREL for testing.

Each sample has two sample numbers. The upper number corresponds to laboratory notebooks.

The lower number that always begins with 99X where X is an alphabet letter is used for the test numbers sent to NREL, and for later graphical representation.

Degassing Temperature	RT	200 °C	400 °C
ZJ-I-85A Pure ZJ-I-99A Pure	456.17	566.77	718.42
ZJ-I-85C Pure ZJ-I-99B Pure	483.70	525.11	598.88
ZJ-I-85D B-doped ZJ-I-99C B-doped	157.77	374.26	382.60
ZJ-I-87A P-doped ZJ-I-99H P-doped	361.03	391.56	431.10

Degassing Temperature	RT	200 °C	400 °C
ZJ-I-88B B-doped*	443.26	448.77	446.04

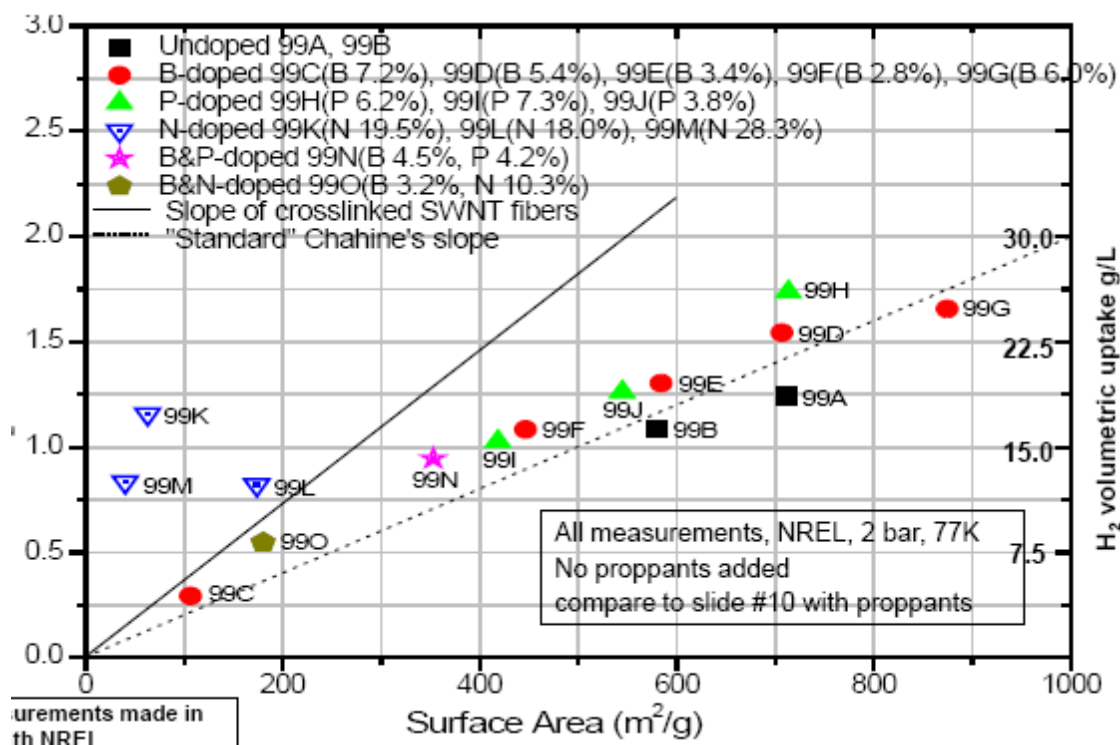
ZJ-I-99D B-doped			
ZJ-I-88C P-doped* ZJ-I-99I P-doped	238.77	241.67	407.56
ZJ-I-88E N-doped ZJ-I-99K N-doped	87.96	91.09	116.44

Temperature	RT	200 °C	400 °C
ZJ-I-97AB B-doped ZJ-I-99F B-doped	271.46	paraf	415.33
ZJ-I-97EF B-doped ZJ-I-99G B-doped	501.63	TG	594.57

Degassing Temperature	RT	400 °C
ZJ-I-92C N-doped* ZJ-I-99L N-doped	148.41	283.13
ZJ-I-94B B-doped ZJ-I-99E B-doped	389.17	551.45
ZJ-I-94C P-doped ZJ-I-99J P-doped	258.53	491.19
ZJ-I-94D N-doped ZJ-I-99M N-doped	96.49	137.26
ZJ-I-94E BP-doped ZJ-I-99N BP-doped	101.25	356.01
ZJ-I-94F BN-doped ZJ-I-99O BN-doped	163.51	276.11

## 1b. Atom substitution in synthetic graphene sheets tested for hydrogen uptake

A large variety of samples have been tested. These do not have proppants, and hence generally lie along the same slope typical for Chahine's rule.



The left axis is H<sub>2</sub> uptake in wt% and the right axis is volumetric uptake in g/L. The black squares are controls of synthetic graphene with no atom substitution. All data is from NREL.

1. High nitrogen substitution has been achieved, range of 18% to 28%.
2. Good success achieved with phosphorous, which enhanced binding energy and high 17at% achieved
3. These atom substituted materials have not been propped open and in almost all cases show no enhanced uptake.

## 2a. Atom substitution in synthetic graphene sheets tested for hydrogen binding energy, in collaboration with Channing Ahn and his graduate student, Nicholas Stadie

We are most indebted to them for their assistance in our research.

### Binding energy:

sample	Atom	at%	kJ/mol
99D	B	5.4	8.6
99I	P	7.5	8.3
99L	N	18	5.6 (no enhancement)

Binding energy extrapolated to zero coverage. P shows 5.5 kJ at 1wt%.

No enhanced binding energy observed for nitrogen substitution, as theoretically predicted.

Many thanks to Channing Ahn and his student Nicholas Stadie of Caltech for these measurements.

Phosphorous atom substitution into graphene behaves like boron in providing substantially increased H<sub>2</sub> binding energy, which will lead to higher temperature uptake

## Templated growth of substituted graphene on silicon dioxide particles.

We tried another approach to growing graphene, by using silicon dioxide as a template.

Sample # and type of atom substitution	BET Surface area Degas 400 °C
<b>ZJ-I-111A Boron</b>	<b>601.23 m<sup>2</sup>/g</b>
<b>ZJ-I-111B Boron</b>	<b>374.84</b>
<b>ZJ-I-111C Phosphor</b>	<b>377.08</b>
<b>ZJ-I-111D Phosphor</b>	<b>392.13</b>
<b>ZJ-I-111E Nitrogen</b>	<b>318.46</b>

X-Photoelectron spectroscopy analysis Atomic %

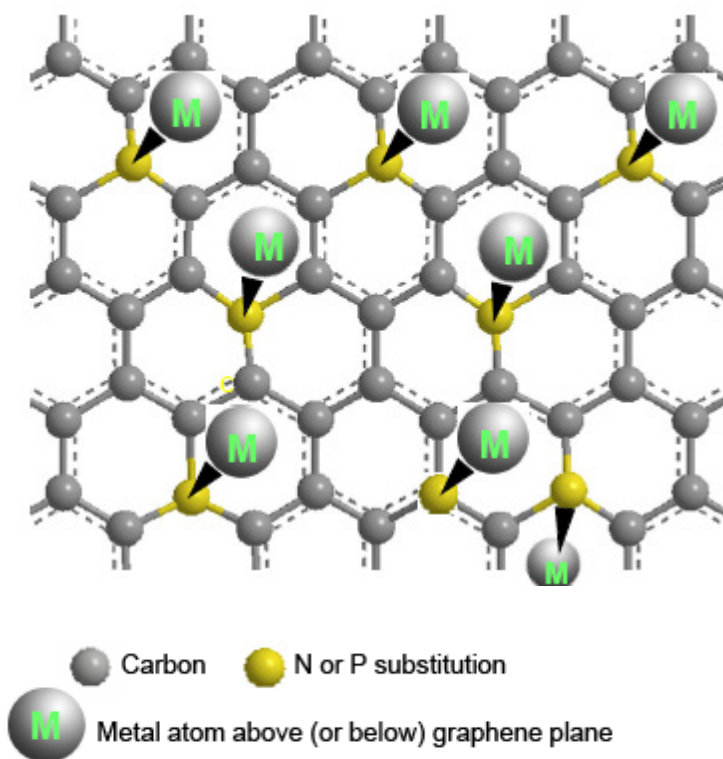
ZJ-I-111A	ZJ-I-111B	ZJ-I-111C	ZJ-I-111D	ZJ-I-111E
C1s 96.5	C1s 95.3	C1s 79.7	C1s 95.5	C1s 77.8
B1s 3.4	B1s 4.6	P2p 17.2	P2p 4.3	N1s 22.1
Cl2p 0.1	Cl2p 0.1	Cl2p 2.1	Cl2p 0.2	Cl2p 0.1

Top row is sample number

carbon is the majority species in all cases  
the substituted atom ranges from 3.4 at% for boron to 22.1 at% for nitrogen.  
Chlorine is a minor contaminant from the reaction chemistry.

## 5. Future direction: Graphene with metal functionalization on substituted nitrogen

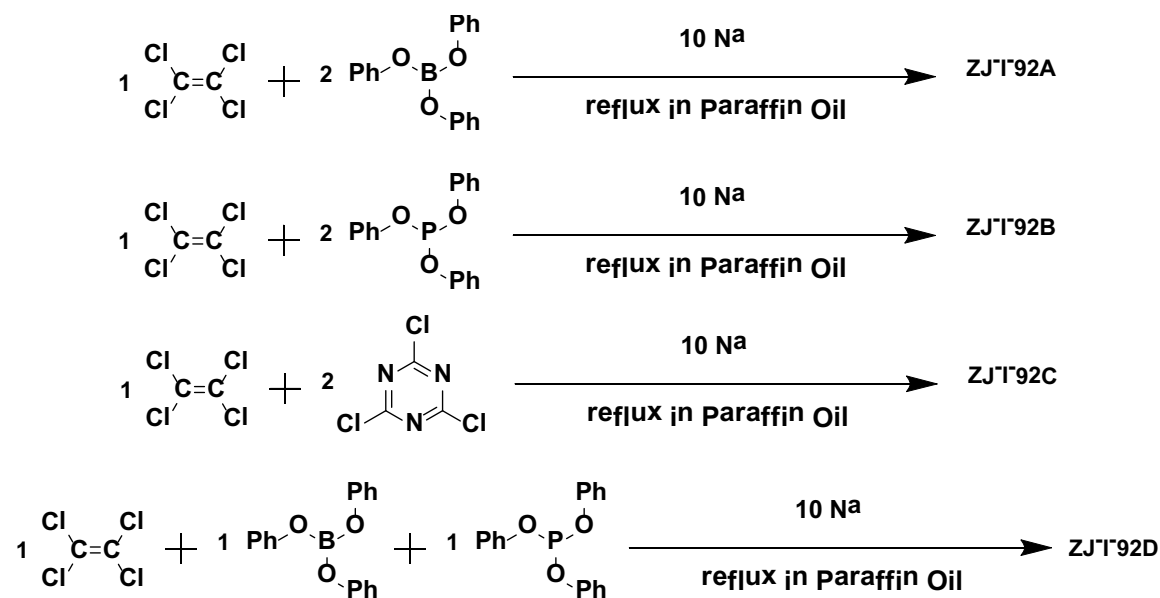
The generic illustration from 1a. shows how metal atoms can be added to the heteroatoms, which provide specific binding sites to secure the metal atoms without aggregation



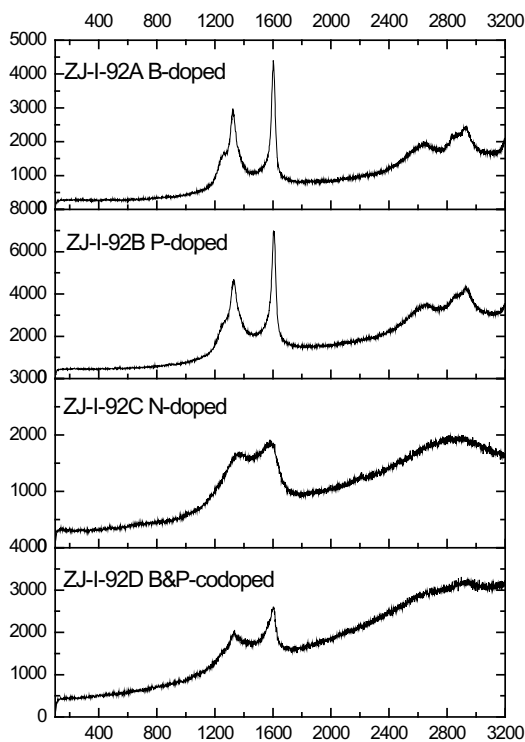
Our success with high % of atom substitution (up to 25%) indicates that we can bind individual metal atoms on the graphene scaffold & overcome previous problem of low density of “parking spots”.



Nitrogen readily forms a complexes with many metals. The density of atoms on the graphene surface will depend on the % atom substitution. We did not have time to test this but believe that it is a promising avenue for future work.



Reactions that produced the atom-substituted graphene



**XPS Atomic %**

**ZJ-I-92A**

**C1s 93.6**

**B1s 6.0**

**Cl2p 0.4**

**ZJ-I-92B**

**C1s 92.7**

**P2p 6.7**

**Cl2p 0.6**

**ZJ-I-92C**

**C1s 85.8**

**N1s 13.5**

**Cl2p 0.7**

**ZJ-I-92D**

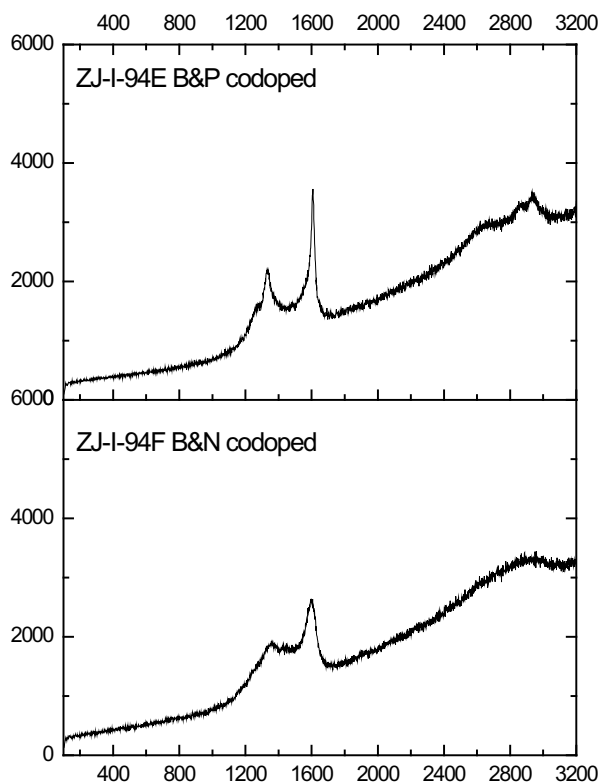
**C1s 87.8**

**B1s 6.1**

**P2p 4.2**

**Cl2p 1.9**

the Raman spectrum showed a sharp G-peak for the Boron and Phosphorous substituted graphene, but the nitrogen substituted showed a degraded G-peak, indicating that the graphene was of much lower quality for the N-substitution. filename = Zhong-Jin-2009-6-31-group-presentation



## XPS

### Atomic %

#### ZJ-I-94E

C1s	87.9
B1s	5.9
P2p	5.4
Cl2p	0.8

#### ZJ-I-94F

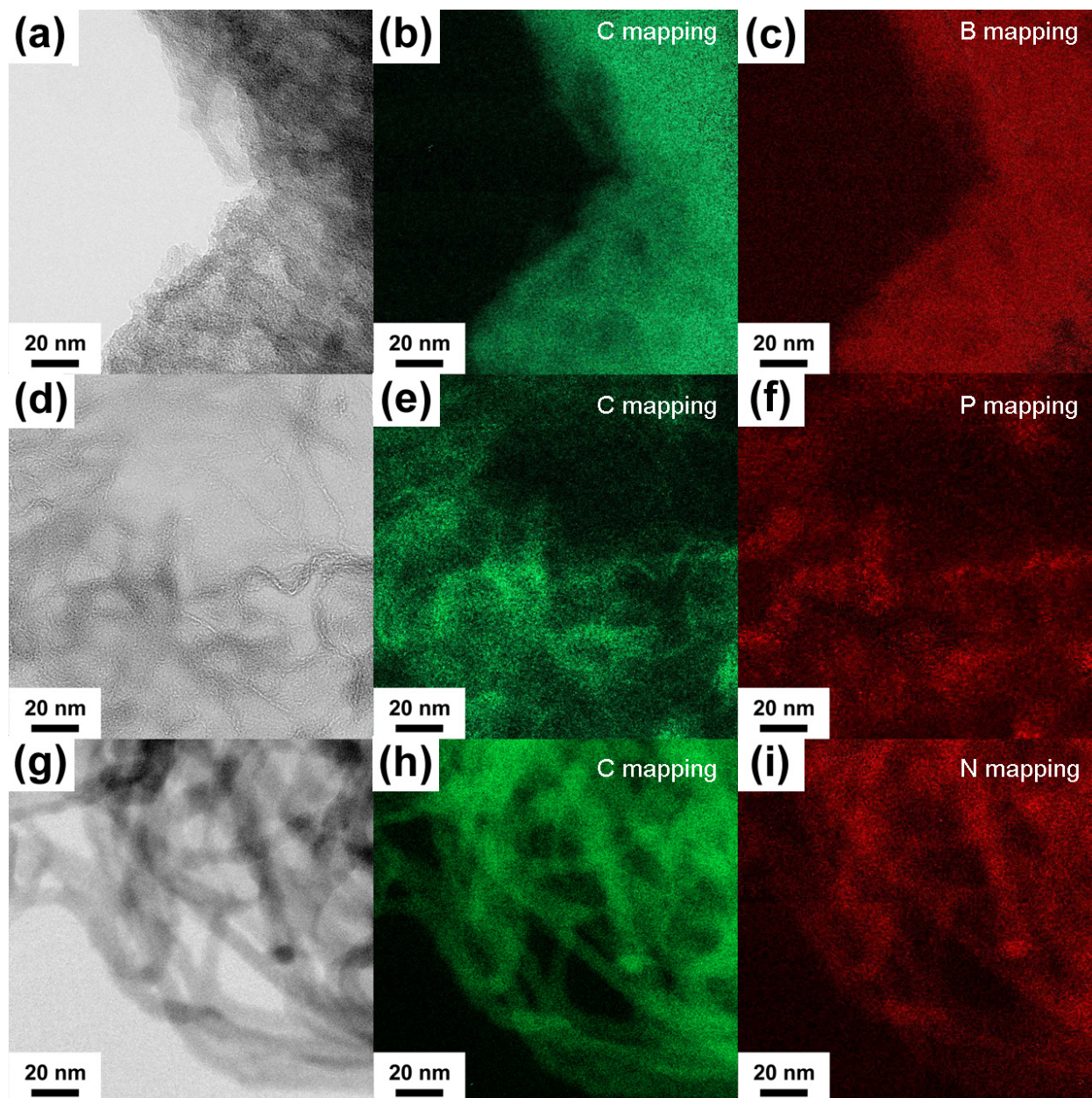
C1s	83.6
B1s	5.7
N1s	9.3
Cl2p	1.4

Co-substitution of two atoms is feasible, but as before, nitrogen leads to a degraded G-peak (slide 18)

## 2. Three different elements have been successfully incorporated into the graphene sheets as shown by elemental TEM

2. Boron, nitrogen and phosphorous substituted graphene has also been tested for hydrogen uptake. Elemental TEM shows the heteroatoms are uniformly distributed.

3. Raman spectroscopy shows that the material is graphitic, and XPS shows that the heteroatoms are bonded to carbon, not each other.
4. The unpropped media does not show enhancement, and data lies along the Chahine's rule slope. This is additional proof that propping open the graphene sheets enhances uptake.
5. Three samples have been measured in collaboration with Channing Ahn at Caltech for hydrogen isotherms, and two of them Boron and phosphorous have shown increased binding enthalpy, whereas nitrogen does not.



TEM images (left) and EFTEM elemental mapping of carbon (middle) and substituted elements (right) of heteroatom-substituted synthetic graphenes: boron (a, b, c), phosphorous (d, e, f) and nitrogen (g, h, i). The carbon atoms are represented by green dots while the substituted heteroatoms are represented by red dots.

1. High nitrogen substitution has been achieved, range of 18% to 28%.
2. Good success achieved with phosphorous, which enhanced binding energy and high 17at% achieved

### 3a. Raman spectroscopy demonstrates that the material is graphitic.

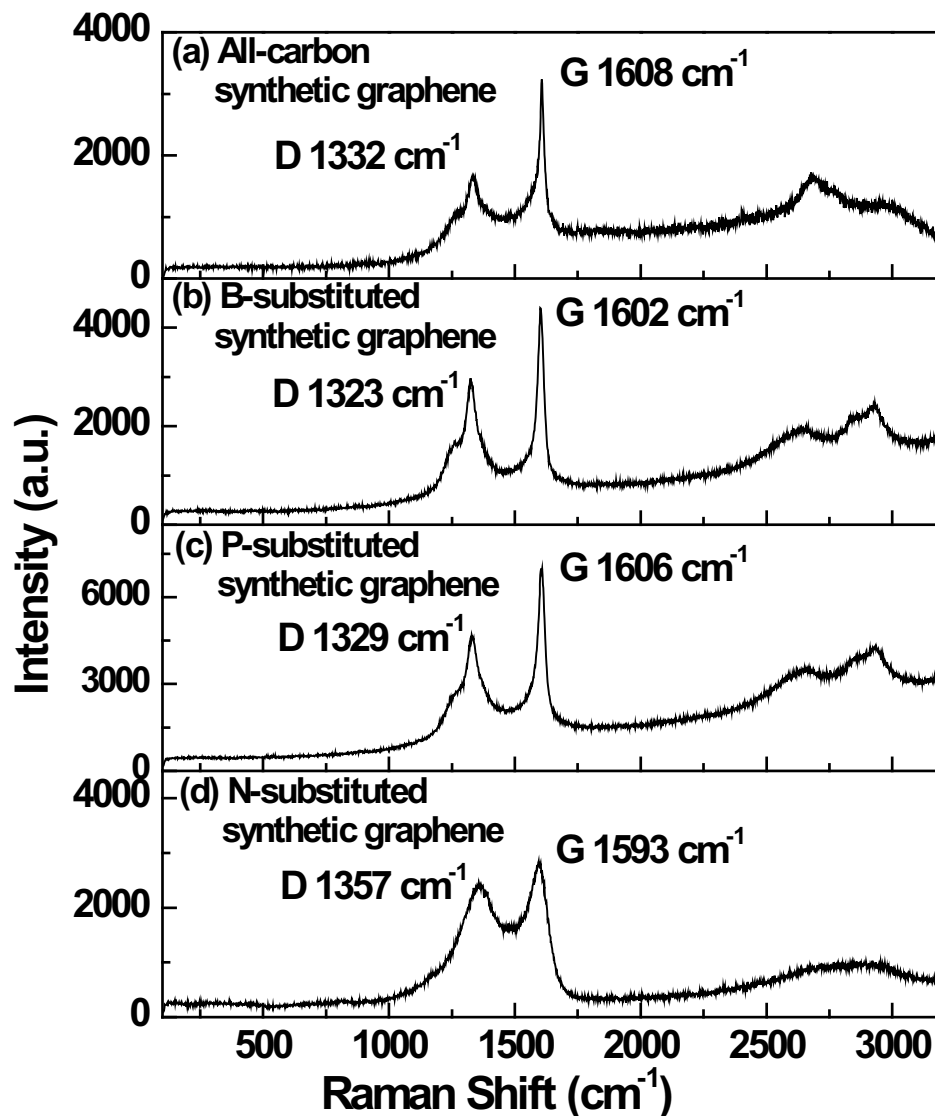


**Figure 4.** Raman spectra (514 nm) of (a) all-carbon synthetic graphene, (b) boron-, (c) phosphorous- and (d) nitrogen-substituted synthetic graphenes.

All spectra show the G-band near  $1600\text{ cm}^{-1}$  that is characteristic of graphene sheets. The D-band, also known as the "defect" band in the  $1320\text{-}1360\text{ cm}^{-1}$  region is characteristic of modified graphene. In this case, it is due to the reduced symmetry of the graphene with the heteroatom substitution; in all of the substituted graphene materials, it is substantially increased compared to the all carbon graphene.

### 3b. XPS demonstrates that the heteroatoms are bonded to carbon, and not clustered

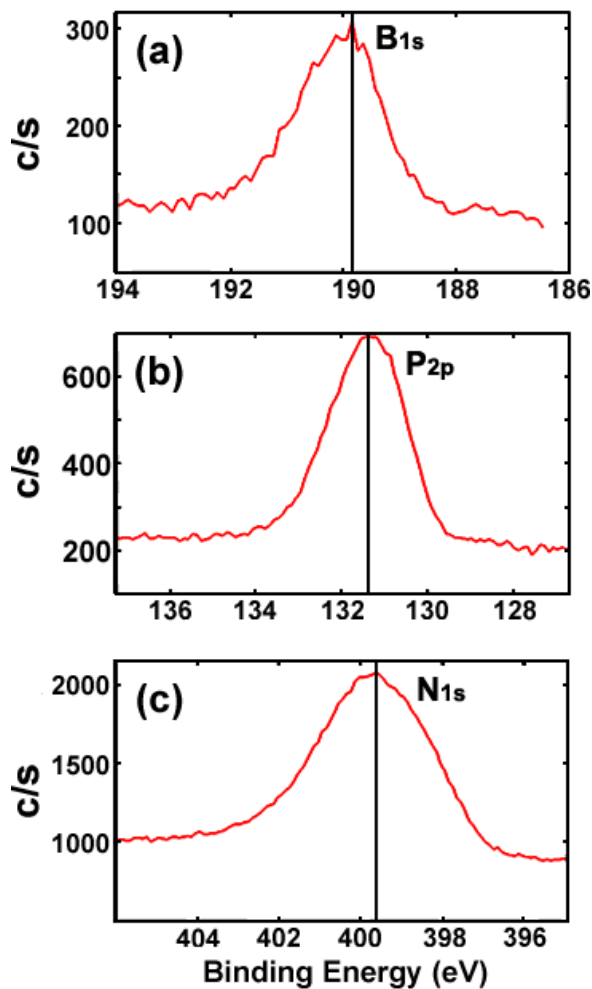


Figure 2. High-resolution XPS scans of the substituted elements in the synthetic graphenes; (a) boron, (b) phosphorous and (c) nitrogen. The single peaks indicate one type of bond between the heteroatom and the carbon, and not e.g., B-B bonds or P-P bonds.

#### 4. Plot of hydrogen uptake vs surface area.

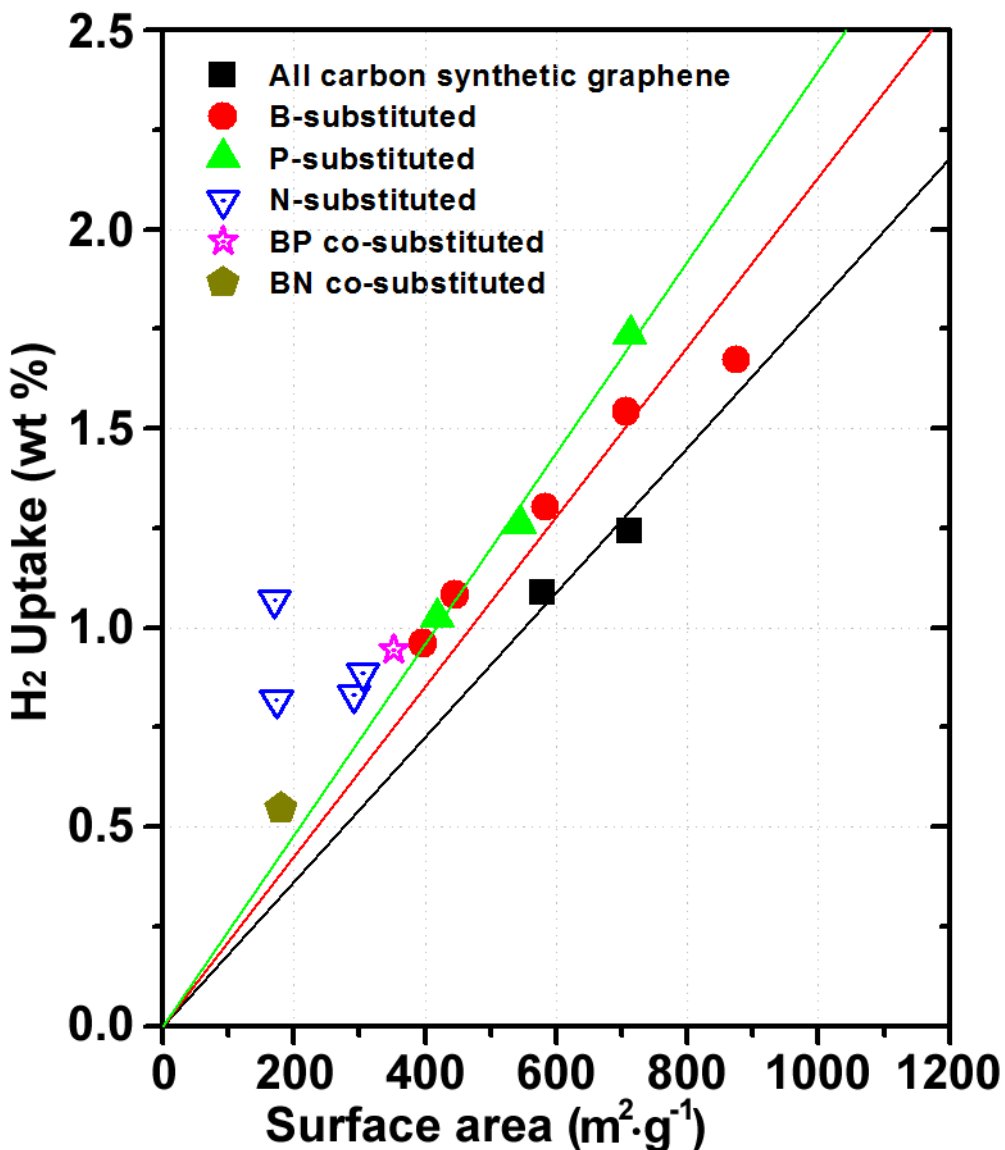
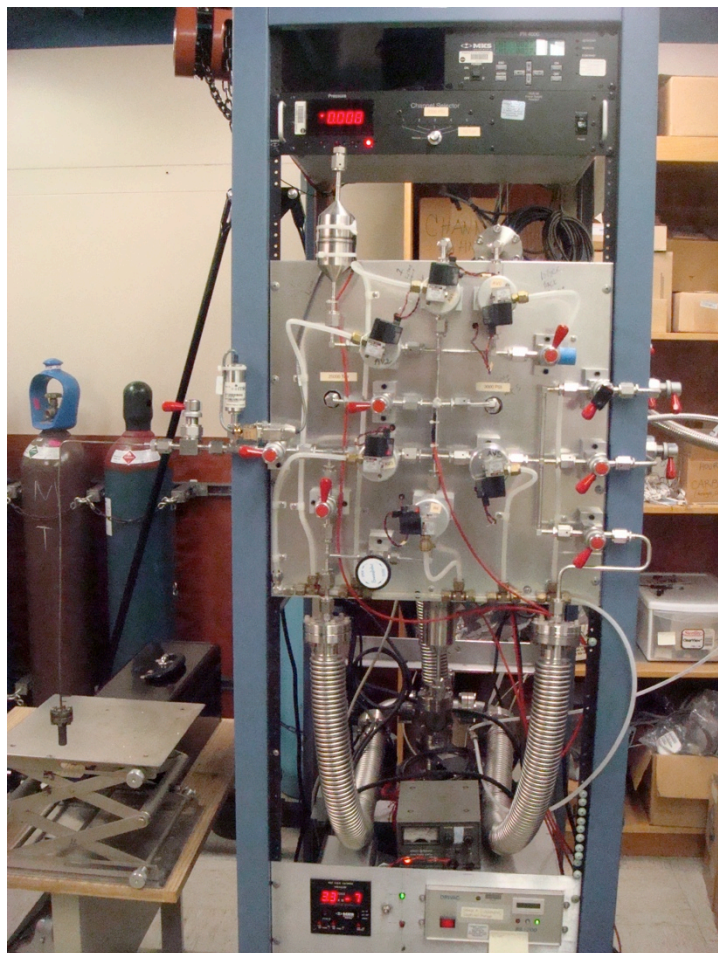


Figure 5. Specific surface area measurements from nitrogen BET at 77 K versus hydrogen uptake at 77 K and 2 bar. The data for all-carbon and substituted synthetic graphenes are indicated by the different colored symbols, as shown in the legend. The solid lines with the matching colors are the linear fits and extrapolations obtained from the sample data. These atom substituted materials have not been propped open and in almost all cases follow Chahine's rule for uptake at 77K, which is 2wt% per 1000 m<sup>2</sup>/g SA. show no enhanced uptake (i.e., increased compared to the propped graphene sheets).



**Isotherms of the uptake of hydrogen was measured in partner Channing Ahn's laboratory**



Sieverts apparatus in Channing Ahn's Lab -- permission to use? Yes.  
Gett-filename = Sieverts-1831a-Channing-H2-diagrams -- link to attachments

**(Nicholas Stadie of Caltech took the data)**

Channing data 30% increase. Check JACS paper, isotherms  
for boron, 2 atm = 0.44wt% & 12 atm = 0.56wt% = asymptotic for argon (1.27)  
for boron, 2 atm = 0.54wt% & 12 atm = 0.67wt% = asymptotic for nitrogen x1.24  
for Phosphorous, 2 atm = 0.87wt% & 12 atm = 1.15wt% = asymptotic 77K x1.32  
for Nitrogen, 2 atm = 0.475wt% & 16 atm = 0.67wt% = asymptotic 77K x 1.49  
(less weight, less binding) average of three = 1.35x

46

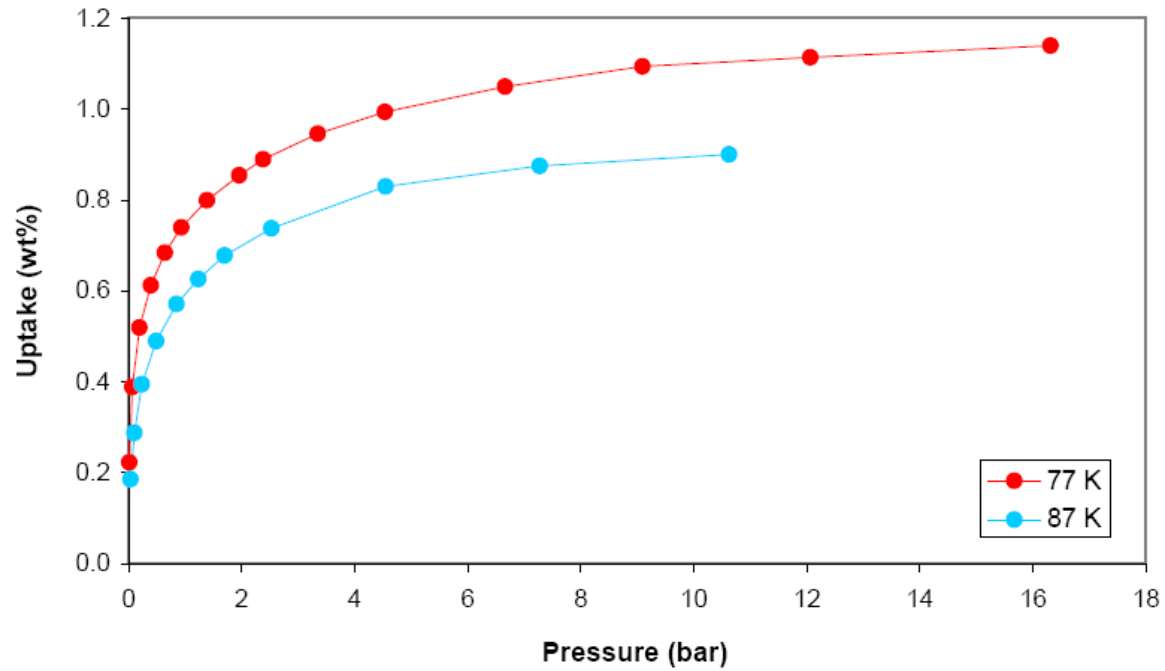
ZJ-I-88B boron	5.4% boron, 0.3% chlorine
99D	8.6 kJ, slopes to 7 kJ at 0.6 wt%
ZJ-I-88C Phosphorous	7.5% phosphorous, 0.1% chlorine

99I 8.3 kJ, slopes to 6 kJ at 1wt%

ZJ-I-92C nitrogen Report #44 490 SA, N-doped #41, 13.5% nitrogen, 0.7% Cl

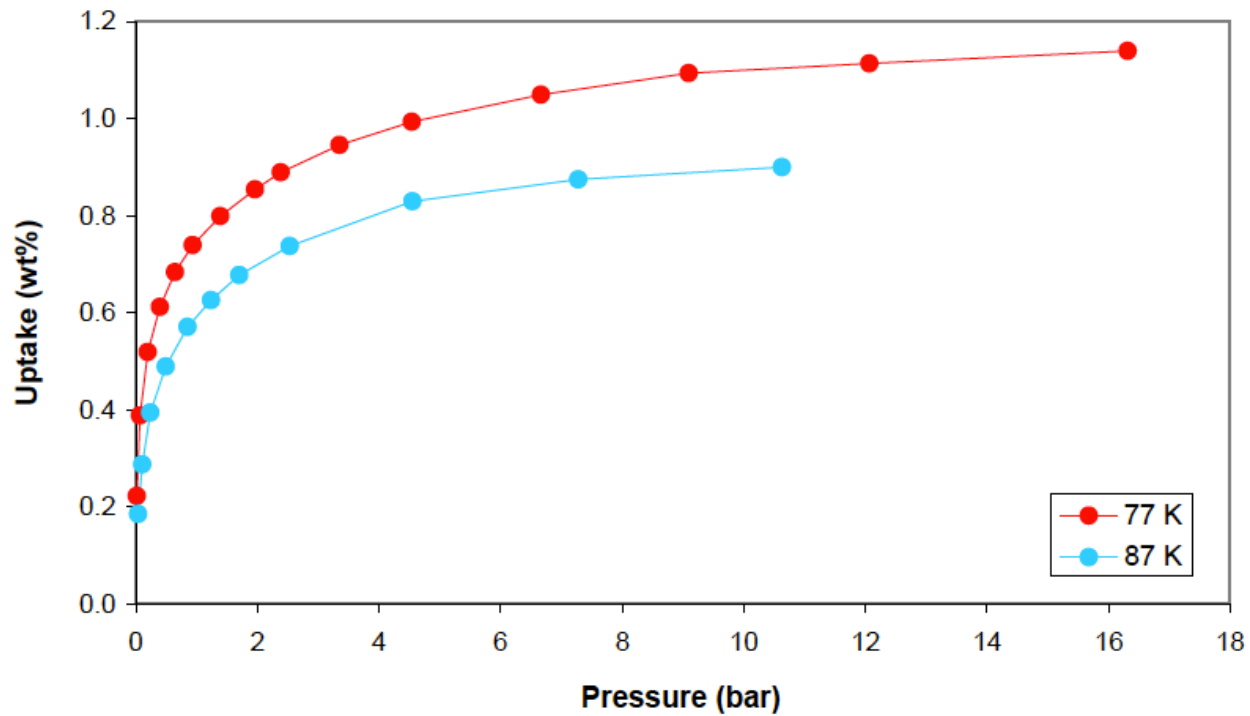
99L 5.6 kJ slopes to 4 kJ, 4.5 wt%, 0.4

From Ashley and 2009 AMR, prefunctionalized SWNT fibers, 2.5wt% and 2x Chahine's rule, 500 m<sup>2</sup>/g SA, with a density of about 1.2 specific gravity, this corresponds to 30 g/L

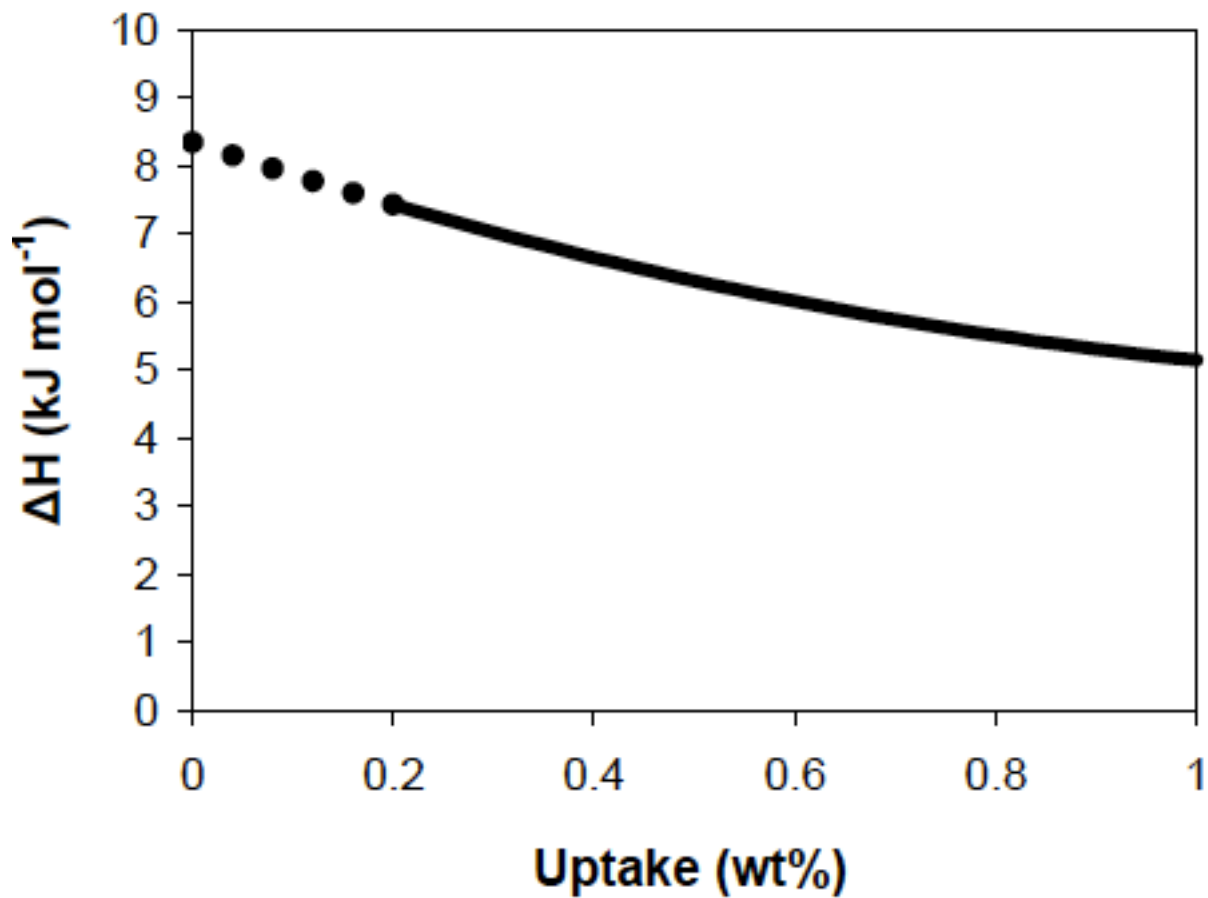


<b>Isotherm Data</b>			
<b>77 K</b>		<b>87 K</b>	
<b>Pressure (bar)</b>	<b>Uptake (wt%)</b>	<b>Pressure (bar)</b>	<b>Uptake (wt%)</b>
0.0	0.22	0.0	0.19
0.1	0.39	0.1	0.29
0.2	0.52	0.2	0.39
0.4	0.61	0.5	0.49
0.6	0.68	0.9	0.57
0.9	0.74	1.2	0.63
1.4	0.80	1.7	0.68
2.0	0.85	2.5	0.74
2.4	0.89	4.6	0.83
3.3	0.95	7.3	0.87
4.5	0.99	10.6	0.90
6.7	1.05	14.5	0.86
9.1	1.09		
12.1	1.11		
16.3	1.14		
22.9	1.13		

Channing-Phosphorous-substituted-Zj-I-88C-isotherm-table



Channing-Phosphorous-substituted-Zj-I-88C-isotherm-graph



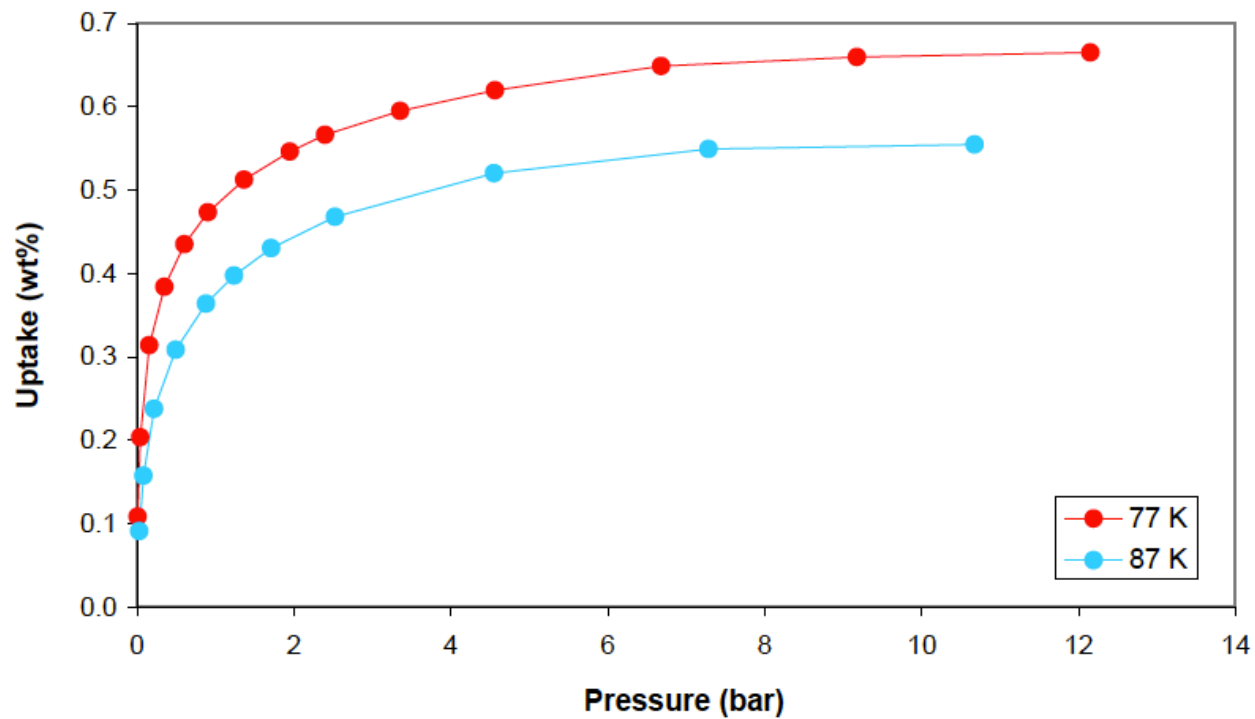
Channing-Phosphorous-substituted-Zj-I-88C-binding-enthalpy

Isosteric Heat Analysis	
Extrapolated Adsorption Enthalpy at Zero Coverage (kJ mol <sup>-1</sup> ):	8.3

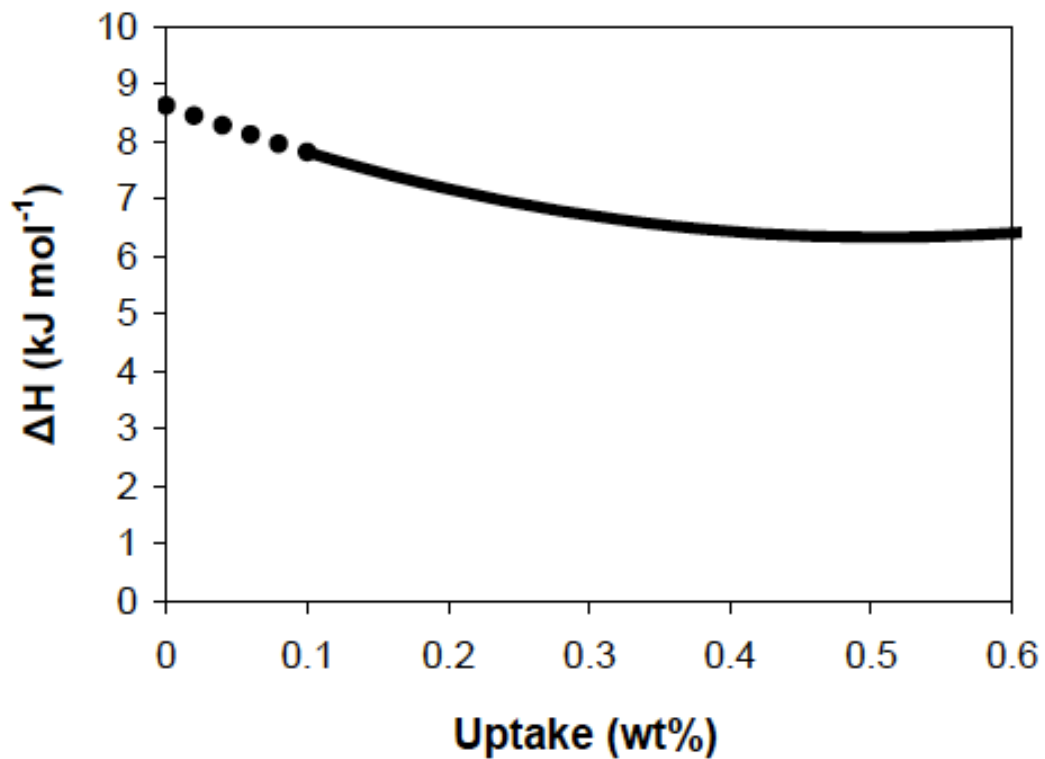
Channing-Phosphorous-substituted-Zj-I-88C-binding-enthalpy-zero

<b>Isotherm Data</b>			
<b>77 K</b>		<b>87 K</b>	
<b>Pressure (bar)</b>	<b>Uptake (wt%)</b>	<b>Pressure (bar)</b>	<b>Uptake (wt%)</b>
0.0	0.11	0.0	0.09
0.0	0.20	0.1	0.16
0.2	0.31	0.2	0.24
0.4	0.38	0.5	0.31
0.6	0.43	0.9	0.36
0.9	0.47	1.2	0.40
1.4	0.51	1.7	0.43
1.9	0.55	2.5	0.47
2.4	0.57	4.6	0.52
3.4	0.59	7.3	0.55
4.6	0.62	10.7	0.55
6.7	0.65	14.6	0.55
9.2	0.66	19.7	0.51
12.1	0.66	25.7	0.41
16.3	0.66	31.8	0.31
22.7	0.64		

Channing-Boron-substituted-Zj-I-88B-isotherm-table



Channing-Boron-substituted-Zj-I-88B-isotherm-graph



Channing-Boron-substituted-Zj-I-88B-binding-enthalpy

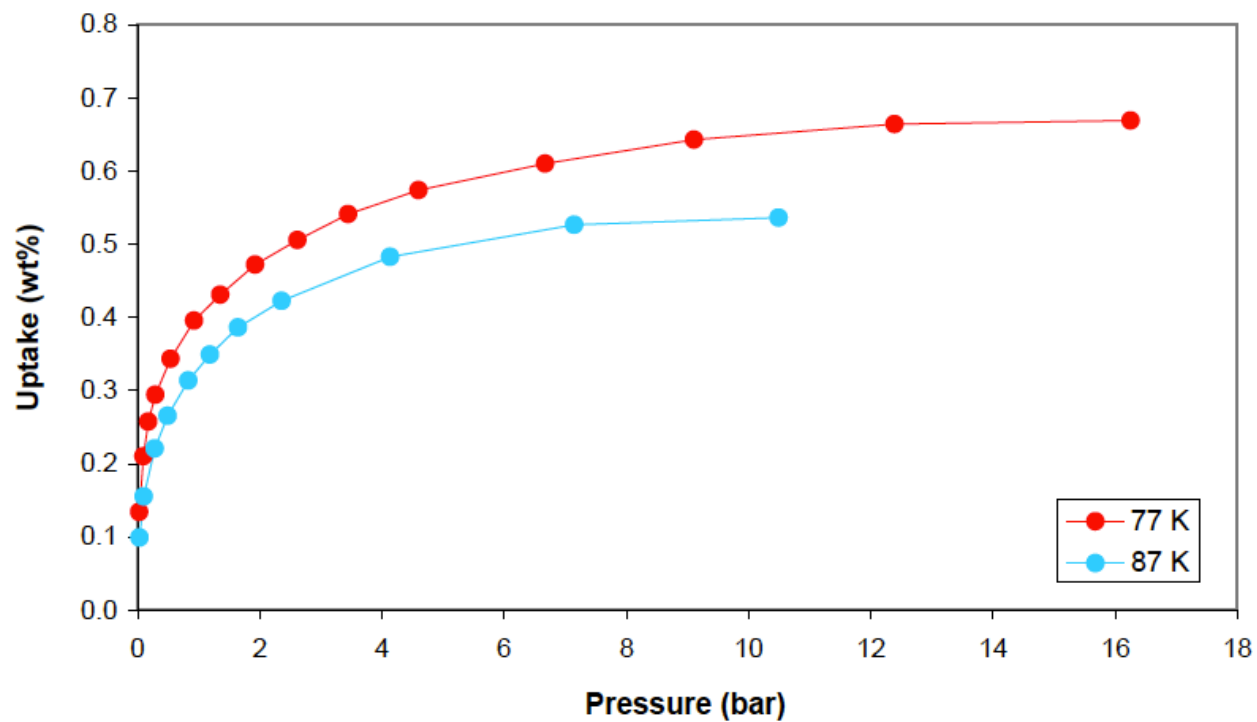
Isosteric Heat Analysis	
Extrapolated Adsorption Enthalpy at Zero Coverage ( $\text{kJ mol}^{-1}$ ):	8.6

Channing-Boron-substituted-Zj-I-88B-isotherm-zero

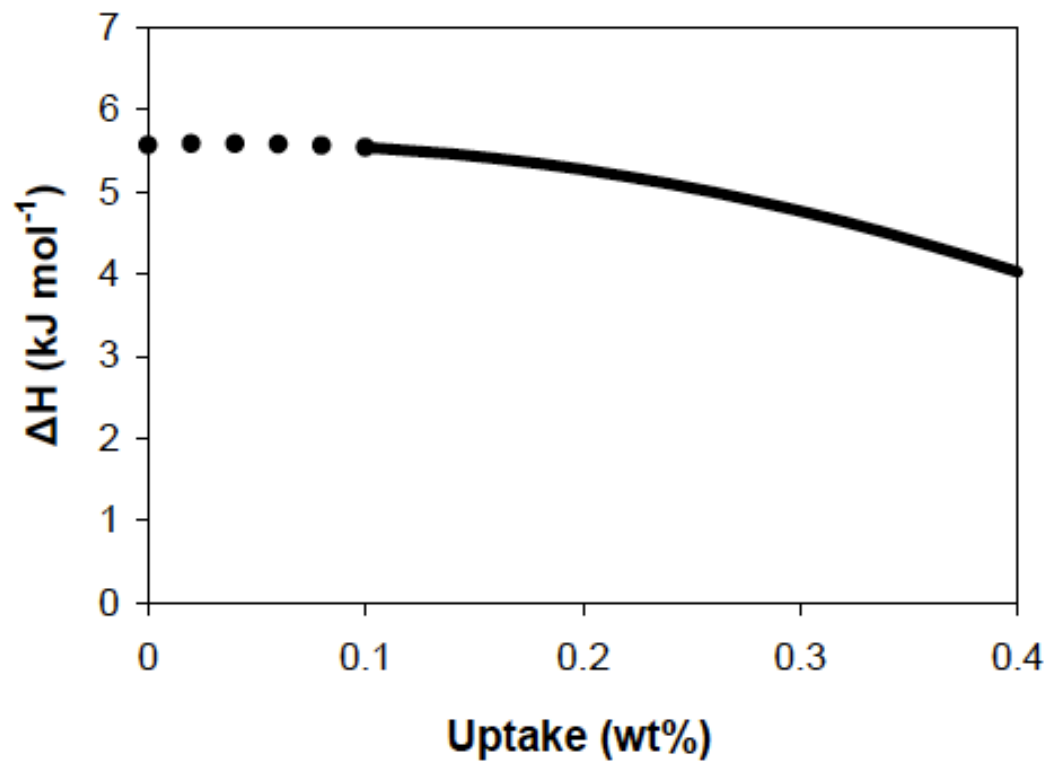


<b>Isotherm Data</b>			
<b>77 K</b>		<b>87 K</b>	
<b>Pressure (bar)</b>	<b>Uptake (wt%)</b>	<b>Pressure (bar)</b>	<b>Uptake (wt%)</b>
0.0	0.13	0.0	0.10
0.1	0.21	0.1	0.16
0.2	0.26	0.3	0.22
0.3	0.29	0.5	0.27
0.5	0.34	0.8	0.31
0.9	0.40	1.2	0.35
1.4	0.43	1.6	0.39
1.9	0.47	2.4	0.42
2.6	0.51	4.1	0.48
3.4	0.54	7.1	0.53
4.6	0.57	10.5	0.54
6.7	0.61	14.4	0.50
9.1	0.64		
12.4	0.66		
16.2	0.67		
22.6	0.65		

Channing-Nitrogen-substituted-Zj-I-92C-isotherm-table



Channing-Nitrogen-substituted-Zj-I-92C-isotherm-graph



Channing-Nitrogen-substituted-Zj-I-92C-binding-enthalpy

<b>Isosteric Heat Analysis</b>	
<b>Extrapolated Adsorption Enthalpy at Zero Coverage (kJ mol<sup>-1</sup>):</b>	<b>5.6</b>

Channing-Nitrogen-substituted-Zj-I-92C-binding-enthalpy-zero

phosphorous from DoE-1850a, slide 43 Channing Ahn data, Phosphorous 7/5%  
Gett -- Go to Channing Isotherm data PDF for his data.

Enhanced binding energy

-----  
7.5% atom phosphorous content determined by XPS  
BET surface area: 320 m<sup>2</sup>/g  
Zhong-Jen sample ZJ-I-88C  
Feb 1, 2010

We used solution-based chemistry to synthetically form substituted graphene materials. The general goal was to chemically form stable substituted graphene sheets with high substituted content and then to use the graphene scaffolding processes Rice has developed for their optimized nanostructures work to form high specific surface area materials with high substituted concentrations. Initial efforts resulted in isosteric heats of adsorption of 8.6 kJ/mol for B-graphene with 5.4 atomic% boron substitution; 8.3 kJ for P-Graphene with 7.5 atomic% phosphorous substitution, and 5.6kJ for N-Graphene with 13.5 atomic% nitrogen doping. While the goal is to find routes to much higher substitution concentrations for boron and perhaps phosphorous, these initial results demonstrate that high (i.e. 25 atomic%) sp<sup>2</sup> coordinated substitutions can be achieved (e.g. with nitrogen) and the result confirm the original calculations that predicted that nitrogen substituted in carbon would not significantly increase hydrogen binding. However, as predicted, B substitution did increase hydrogen binding, and it appears that P does as well. These results also demonstrate the intrinsic issue of limited substitution for elements that appear to increase binding. While the specific surface areas are still low, the hydrogen storage capacities of these materials were significantly higher than expected for typical activated carbon with similar specific surface areas.

We are able to successfully expand and crosslink CNT fibers into a rigid and stable frame with chosen pore size, and subsequently applied similar methods to graphene. Uptake of hydrogen exceeds the slope provided by “Chahine’s rule” by a factor of 2 or more indicating that properly engineered pores that are surrounded entirely by a pi cloud structure and have the

correct pore size may have the capability of exceptionally large uptake per unit area. Theoretical research from other groups supports this concept and other reports showed high local concentrations of H<sub>2</sub> were observed where they could find a “just right” nm sized pore with TEM.

(Both theory and experiment, including our own work, point to unusually strong binding and high density packing in the sp<sup>2</sup> pore. )

### **Downselect metal atoms on the surface**

Transition metal atoms are not stable on sp<sup>2</sup> carbon as isolated atoms in the presence of hydrogen, as we presented in AMR 2008. (AKA Kubas-type binding) While we had some encouraging results with lithium intercalation, also AMR2008, the highly reactive nature of the metal, such as the irreversible conversion to the hydroxide with any trace of moisture, and reports from other groups on the formation of lithium hydride favored downselection of this approach also. Instead, we chose atom substitution into the carbon lattice as a means of enhancing binding energy but these are neither unstable nor reactive. The ingredients of boron and phosphorous are low cost, and the expense of handling a highly air-sensitive media when fabricating the storage tank is also mitigated.

### **Increased uptake with higher pressures (earlier report 2219a messed up at this point)**

Although most of our H<sub>2</sub> uptake was performed at 2 bar, as we wished to obtain comparative results on the highly accurate 2 bar Sieverts apparatus at NREL, we have three tests at higher pressures provided by our collaborator Channing Ahn at Caltech, on three different atom substitution graphene materials. Although the higher pressures were 12 atm for B and P substituted materials, and 16 atm for N-substituted, we will use the higher uptake at 77K as the asymptotic limit. B, P, and N showed increases of 1.24x, 1.32x, and 1.49x. The nitrogen substituted graphene is most like carbon as it has the same H<sub>2</sub> binding energy as all-carbon graphene, whereas B, and P have enhanced binding energies about 50% higher. The average increase in uptake is 1.35 times, even though the pressures are not more than 16 atm. We also report [Leonard, JACS 2008, reference 22] an expected increase of 23% to 33% uptake to achieve surface saturation at increased pressures. For the purposes here, we will use 1.3x as the projected enhancement for increasing the pressure from 2 bar to the asymptotic pressure limit for excess H<sub>2</sub> uptake. (need all of Channing’s data here)

As reported in the Amr2009 and AMR2010 meeting, our volumetric uptake using a CNT scaffold met DoE 2010 volumetric goals at 30 g/L as measured at 2 bar, compare to 28g/L DoE. our gravimetric uptake was 2.4wt% and utilizing the factor of 1.3x for 40 bar, this is 3.1wt% less than 4.5wt% of the DoE goal. 2008-2009 was a transition period from CNT to graphene, and 2009 we obtained 18g/L for graphene, increasing to 27g/L at 2 bar and projected 1.3x to 35 g/L in 2010, well above the 28g/L for DoE 2010 goals (materials only)

### **Enhanced uptake not explained by increased binding enthalpy (Section added March 29)**

One might argue that the ~2x enhancement is due to the greater binding enthalpy of H<sub>2</sub> in the slit pore, which has been both calculated and measured by other researchers ca. 8 to 9 kJ/mol.

However, our non-scaffold B-substituted and P-substituted graphene has similar increase to  $\sim 8.5$  kJ/mol, but shows only a 1.2x enhancement rather than a 2x enhancement, a minimally significant increase, which is strong evidence that enhanced binding enthalpy does not a “nano-compressor” make, and does not explain the large enhanced uptake. From a theoretical viewpoint, increased attraction to the surface does not increase  $H_2$ - $H_2$  attraction, and will not squeeze the  $H_2$  closer to each other on the surface. It is the  $sp^2$  carbon slit pore that is essential in order to make a nano-compressor.

## Graphene as low cost media

The cost of SWCNT is a concern; hence we then switched to graphene, which is also  $sp^2$  carbon, upon recommendation from our HSCoE team leader at the NREL. While it is not yet manufactured in bulk, all the major raw ingredients are among the least expensive industrial chemicals. With graphite  $\sim \$500$ /tonne, sulfuric acid  $\sim \$100$ /tonne, etc., and using standard commercial solvent fiber spinning techniques, we estimated  $\$25$  to  $\$45$  media only cost for 1 kg  $H_2$  capacity in our 2010 AMR presentation for large-scale production. Since  $H_2$  has an energy capacity of 33.5 kWh/kg, this can be calculated to be in the range of  $\$0.75$  to  $\$1.35$  per kWh (materials only). This is less than the DOE 2015 system target is  $\$2$ /kWh which provides some leeway for other system costs. We also determined graphene could be spun into a fiber using the same commercial type spinning techniques developed for SWCNT fibers.

### Transition from SWCNT to Graphene, with the same enhanced uptake

In the last two years of the 5-year project, we transferred our extensive knowledge of nano-engineered materials from SWCNT to graphene, a monolayer of carbon atom sheet, and the “new kid on the block” at that time. We found that the same enhanced uptake per unit SA applied to graphene that had been propped open. However, unpropped graphene closely follows Chahine’s rule, once again proving that correctly spaced slit nanopores have considerably enhanced uptake. And in lieu of Kubas-type binding or alkali metal surface atoms, we chose atom substitution using boron, phosphorous and nitrogen. Since these are incorporated into the graphene lattice, there are no issues of migration, air sensitivity, or chemical reaction with water vapor; hence no special handling techniques would be needed for the media beyond that of the carbon. With 5.6 atom% B we obtained an increase from 5.5 kJ/mol  $H_2$  binding to 8.6 kJ/mol, and with 7.5 atom% P, the increase was to 8.3 kJ/mol, both showing substantial binding enhancement even though the atom% substitutions were rather low. Nitrogen provided no such enhancement, as other researchers have also reported, and that material was quite disordered. We also experimentally verified the increased  $H_2$  uptake in increasing pressure from 2 bar to 16 bar, with an experimental average of 1.35 $\times$  increase. For simplicity, we use a more conservative value of 1.3 $\times$  for uptake at higher pressures. Our highest volumetric uptake was 27 g/L at 2 bar, or 35 g/L at 16 bar (materials only). This substantially exceeds the DOE 2010 system goals of 28 g/L. We did not achieve the gravimetric uptake goal for either SWCNT or graphene. As the program came to a close, we decided that enhanced binding energy was a more important and challenging goal for the remaining time, as this is another proof of principle for the nano-structured material. (We are most grateful to HSCoE partner Channing Ahn of Caltech for the isotherms up to 16 bar and binding energy determinations for N, B, and P substituted graphene; these were the only  $H_2$  uptake measurements not done at NREL.)

### Why this is important for vehicular hydrogen storage

Since our research was primarily focused on proof of concept that a nanoengineered  $sp^2$  carbon framework is a new direction for  $H_2$  adsorption media has special and superior  $H_2$  uptake properties, we think the best way to demonstrate the importance of our rather unique approach is to project the outcome of a fully nano-structured graphene media based on extrapolating our quantitative measurements. Can this approach of “packing the pores” conceivably reach the ultimate goals for physisorbed  $H_2$  storage, and in particular, address the difficult problem of high volumetric storage? In addition, the exceptionally high

thermal conductivity of  $sp^2$  carbon fibrous media can reduce or eliminate the need for internal coolant tubes saving system weight and volume.

**A high-density media that is projected to help reach the ultimate DoE goals** (*added section on residual hydrogen, March 29*)

The full SA of graphene is  $2650 \text{ m}^2/\text{g}$ , hence is inherently less than carbon aerogel or metal organic framework (MOF) - type structures. But this is compensated for by our emphasis on doubling of the uptake per unit SA. Assume 5% SA is consumed by the proppants, with 0.8 nm graphene spacing from both theory and our experiments, then the nano-scaffold density is  $\sim 1 \text{ kg/L}$  including the  $\text{H}_2$ . The average for our six measurements on propped graphene is 1.8 wt% per  $500 \text{ m}^2/\text{g}$  at 2 bar and 77K. Hence 1.8 wt% becomes 9 wt% at 2 bar and  $2500 \text{ m}^2/\text{g}$ . Then using the factor of  $1.3\times$  increasing pressure to 40 bar, and combining both factors, this can be projected to 11.7 wt% (media +  $\text{H}_2$ ). Although our spacing of 0.8 nm for the slit pores in graphene provides a density of  $1 \text{ kg/L}$  with  $\text{H}_2$ , but allowing a volumetric increase from 0.8 nm to a 1.0 nm pore spacing, with no change of  $\text{H}_2$  stored in the slit pore, this still provides a good projection for volumetric capacity of  $95 \text{ kg/L}$ . With the ultimate DOE system goals of 7.5 wt%, and  $70 \text{ g/L}$  this projection provides leeway for significant additional weight and volume for the rest of the system. Nearly all of the  $\text{H}_2$  capacity can be utilized. Much of the  $\text{H}_2$  can be drawn off at the initial temperature of 77K to 120K and the “nano-compressor” will equilibrate with the bulk gas, or the temperature can be allowed to increase gradually to maintain ca. 40 bar in the  $\text{H}_2$  bulk. If one allows that 10% to 15% of the  $\text{H}_2$  is kept as a “reserve” then the temperature cycling need not be more than about 75K while retaining 3 bar delivery pressure. If it is necessary to utilize the “reserve”, then the tank is allowed to warm to ambient temperatures (such as with FC coolant), then the “nano-compressor” effect essentially ceases and the residual  $\text{H}_2$  gas at 3 bar will be similar to any common carbon sorbent, 0.05wt% to 0.15wt%. In addition, enhanced binding with atom substitution is projected to increase the storage temperature to 120K and possibly to 150K, reducing insulation requirements. We conclude that our new nano-structured media can pack enough  $\text{H}_2$  into the pores to make a media that is projected to help reach the “ultimate” DOE goals for  $\text{H}_2$  storage.

## Glossary

AIBN 2,2-azobis(2-methylpropionitrile) a free radical initiator

AFM atomic force microscopy

BES Basic Energy Sciences

BWF Brett-Wigner-Fano = phonon-electronic state resonance condition, occurs for “metallic” character

CNT carbon nanotube

CT charge transfer

DAC donor-acceptor-complex

DMLA dynamic multi-layer adsorption

D-band carbon Raman “disorder” mode characteristic of sp<sup>3</sup> sites or “defects” on sp<sup>2</sup> graphene

G-band cm-1 shift Raman tangential mode characteristic of sp<sup>2</sup> graphene-type carbon, typically 1590

G graphene

GNR graphene nano-ribbons

GO graphene oxide

MWCNT multi-wall carbon nanotubes

ORNL Oak Ridge National Laboratory

Pd palladium

Pt platinum

RT room temperature

SEM scanning electron microscopy

SWNT single wall carbon nanotube

TEM transmission electron microscopy

TTF tetrathiofulvalene – electron donor and the

TTNQ tetracyano-p-quinodimethane -- electron acceptor

XPS X-ray photoelectron spectroscopy

## Publications and presentations

The list is **all publications relevant** to the hydrogen storage project.

.

### 2010-2011

Jin, Z.; Yao, J.; Kittrell, C.; Tour, J. M. “Large-Scale Growth and Characterizations of Nitrogen-Doped Monolayer Graphene Sheets,” *ACS Nano* **2011**, 5, 4112-4117. (DOE acknowledged)

Jin, Z.; Lu, W.; O'Neill, K. J.; Parilla, P. A.; Simpson, L. J.; Kittrell, C.; Tour, J. M. "Nano-Engineered Spacing in Graphene Sheets for Hydrogen Storage," *Chem. Mater.* **2011**, *23*, 923-925. (DOE acknowledged)

Jin, Z.; Sun, Z.; Simpson, L. J.; O'Neill, K. J.; Parilla, P. A.; Li, Y.; Stadie, N. P.; Ahn, C. C.; Kittrell, C.; Tour, J. M. "Solution-Phase Synthesis of Heteroatom-Substituted Carbon Scaffolds for Hydrogen Storage," *J. Am. Chem. Soc.* **2010**, *132*, 15246-15251. (DOE acknowledged)

Jin, Z.; Nackashi, D.; Lu, W.; Kittrell, C.; Tour, J. M. "Decoration, Migration, and Aggregation of Palladium Nanoparticles on Graphene Sheets," *Chem. Mater.* **2010**, *22*, 5695-5699. (DOE acknowledged)

Sun, Z.; Kohama, S.; Zhang, Z.; Lomeda, J. R.; Tour, J. M. "Soluble Graphene Through Edge-Selective Functionalization," *Nano Res.* **2010**, *3*, 117-125. (DOE acknowledged)

Higginbotham, A. L.; Kosynkin, D. V.; Sinitskii, A.; Sun, Z.; Tour, J. M. "Low-Defect Graphene Oxide Nanoribbons from Multiwalled Carbon Nanotubes," *ACS Nano* **2010**, *4*, 2059-2069. (DOE acknowledged)

## 2009

Jin, Z.; Lomeda, J. R.; Price, B. P.; Lu, W.; Zhu, Y.; Tour, J. M. "Mechanically Assisted Exfoliation and Functionalization of Thermally Converted Graphene Sheets" *Chem. Mater.* **2009**, *21*, 3045-3047. (DOE acknowledged)

Dmitry V. Kosynkin, Amanda L. Higginbotham, Alexander Sinitskii<sup>1</sup>, Jay R. Lomeda<sup>1</sup>, Ayrat Dimiev, B., Katherine Price & James M. Tour, "Longitudinal unzipping of carbon nanotubes to form graphene nanoribbons", *Nature*, **2009**, *452*, 872-876.

Ashley D. Leonard, Jared L. Hudson, Hua Fan, Richard Booker, Lin J. Simpson, Kevin J. O'Neill, Philip A. Parilla, Michael J. Heben, Matteo Pasquali, Carter Kittrell, and James M. Tour, "Nanoengineered Carbon Scaffolds for Hydrogen Storage", *Journal of the American Chemical Society*, *131* (2), 723-728 (2009)

Zhang, Z.; Sun, Z.; Yao, J.; Kosynkin, D. V.; Tour, J. M. "Transforming Carbon Nanotube Devices into Nanoribbon Devices," *Journal of the American Chemical Society*, *131*, 13460-13463. (2009),

## 2008

6. Jay R. Lomeda, Condell D. Doyle, Dmitry V. Kosynkin, Wen-Fang Hwang, and James M. Tour; "Diazonium Functionalization of Surfactant-Wrapped Chemically Converted Graphene Sheets"; *Journal of the American Chemical Society*, *130*, 16201 (2008)

James Tour: presentation "Nanotechnology: The Passive, Hybrid and Active Sides" M. V. Lomonosov State University, Moscow, Russia. (12 to 14 October 2008)



James Tour, Keynote Speaker Presentation by James Tour; Nanotechnology: The Passive, Hybrid and Active Sides" SERMACS Cope Scholar Symposium, Nashville, TN. (13-14 November 2008)

James Tour, Keynote Speaker Presentation; Wageningen Symposium on Organic Chemistry; "Nanotechnology: The Passive, Hybrid and Active Sides"; Wageningen, The Netherlands. (April 2 and 4, 2008)

## 2007

C. Kittrell, A. D. Leonard, S. Chakraborty, H. Fan, E. Billups, R. H. Hauge, H. K. Schmidt, M. Pasquali, J. M. Tour; "Hydrogen Storage in Nanoengineered Scaffolds of Carbon Nanotubes" Presentation at the International Symposium on Materials Issues in a Hydrogen Economy, Jena Puru, Chairman, Richmond, VA, Nov. 12-15, 2007.

Ogrin, D.; Anderson, R. E.; Colorado, R., Jr.; Maruyama, B.; Pender, M. J.; Moore, V. C.; Pheasant, S. T.; McJilton, L.; Schmidt, H. K.; Hauge, R. H.; Billups, W. E.; Tour, J. M.; Smalley, R. E.; Barron, A. R. "Amplification of Single-Walled Carbon Nanotubes from Designed Seeds: Separation of Nucleation and Growth," **J. Phys. Chem. B.** **2007**, 111, 17804-17806.

**Stephenson**, J. J.; Hudson, J. L.; Leonard, A. D.; Price, B. P.; Tour, J. M. "Repetitive Functionalization of Water-Soluble Single-Walled Carbon Nanotubes. Addition of Acid-Sensitive Addends," **Chem. Mater.** **2007**, 19, 3491-3498

## 2006

Chen, Z. Y.; Ziegler, K. J.; Shaver, J.; Hauge, R. H.; Smalley, R. E., Cutting of single-walled carbon nanotubes by ozonolysis. **Journal of Physical Chemistry B** **2006**, 110, (24), 11624-11627

Price, B. K.; Tour, J. M. "Functionalization of Single-Walled Carbon Nanotubes 'On Water'," **2006**, *128*, 12899-12904.

Smalley, R. E.; Li, Y.; Moore, V. C.; Price, B. K.; Colorado, R., Jr., Schmidt, H. K.; Hauge, R. H.; Barron, A. R.; Tour, J. M. "Single Wall Carbon Nanotube Amplification: En Route to a Type-Specific Growth Mechanism," **J** **2006**, *128*, 15824-15829.

**Stephenson**, J. J.; Sadana, A. K.; Higginbotham, A. L.; Tour, J. M. "Highly Functionalized and Soluble Multi-Walled Carbon Nanotubes by Reductive Alkylation and Arylation: the Billups Reaction," **2006**, *18*, 4658-4661.

Stephenson, J. J.; Hudson, J. L.; Azad, S.; Tour, J. M. "Individualized SWNTs from Bulk Material Using 96% Sulfuric Acid as Solvent," **2006**, *18*, 374-377.

Xu, Y. Q.; Flor, E.; Kim, M. J.; Hamadani, B.; Schmidt, H.; Smalley, R. E.; Hauge, R. H., Vertical array growth of small diameter single-walled carbon nanotubes. **Journal of the American Chemical Society** **2006**, 128, (20), 6560-6561.

Ya-Qiong Xu, Erica Flor, Howard Schmidt, Richard E. Smalley, and Robert H. Hauge, "Effect of Atomic Hydrogen and Active Carbon Species in the 1mm Vertically Aligned Single-Walled Carbon Nanotubes Growth", **Appl. Phys. Lett.** **2006**, 89, 123116.

Yaqiong Xu "Study of Purification and Growth of Single Wall Carbon Nanotubes", Ph D Thesis, Rice University, 2006

## 2005

Dyke, C. A.; Stewart, M. P.; Tour, J. M. "Separation Of Single-walled Carbon Nanotubes On Silica Gel. Materials Morphology And Raman Excitation Wavelength Affect Data Interpretation," *J. Am. Chem. Soc.* **2005**, 127, 4497-4509.

Wang, Y. H.; Kim, M. J.; Shan, H. W.; Kittrell, C.; Fan, H.; Ericson, L. M.; Hwang, W. F.; Arepalli, S.; Hauge, R. H.; Smalley, R. E., Continued growth of single-walled carbon nanotubes. **2005**, 5, (6), 997-1002.

Ziegler, K. J.; Gu, Z. N.; Peng, H. Q.; Flor, E. L.; Hauge, R. H.; Smalley, R. E., Controlled oxidative cutting of single-walled carbon nanotubes. **2005**, 127, (5), 1541-1547.

Ziegler, K. J.; Gu, Z. N.; Shaver, J.; Chen, Z. Y.; Flor, E. L.; Schmidt, D. J.; Chan, C.; Hauge, R. H.; Smalley, R. E., Cutting single-walled carbon nanotubes. **2005**, 16, (7), S539-S544.

Ziegler, K. J.; Schmidt, D. J.; Rauwald, U.; Shah, K. N.; Flor, E. L.; Hauge, R. H.; Smalley, R. E., Length-dependent extraction of single-walled carbon nanotubes. **2005**, 5, (12), 2355-2359.

Price, B. K.; Hudson, J. L.; Tour, J. M. "Green Chemical Functionalization of Single Walled Carbon Nanotubes in Ionic Liquids," **2005**, 127, 14867-14870.

Dyke, C. A.; Stewart, M. P.; Tour, J. M. "Separation Of Single-walled Carbon Nanotubes On Silica Gel. Materials Morphology And Raman Excitation Wavelength Affect Data Interpretation," *J. Am. Chem. Soc.* **2005**, 127, 4497-4509.

## 2004

Dyke, C. A.; Tour, J. M. "Overcoming the Insolubility of Carbon Nanotubes through High Degrees of Sidewall Functionalization," *2004, 10*, 812-817.

Ericson, Lars M., et.al., "Macroscopic, Neat, Single-walled Carbon Nanotube Fibers", *2004, 305*, 1447-1450

General--

7. Invited departmental colloquia at other universities including DOE H2 storage: approx. one per month, 2008-2009

## References

[BES 2003] "Multilayer adsorption is therefore necessary, and researchers do not yet know how to perform this process." [Basic Research Needs for the Hydrogen Economy, BES Workshop, May, 2003, page 99.]

[Brown-2007] (NIST) Mircea Dinca, Won Seok Han, Yun Liu, Anne Dailly, Craig M. Brown, and Jeffrey R. Long "Observation of Cu<sup>2+</sup>-H<sub>2</sub> Interactions in a Fully Desolvated Sodalite-Type Metal-Organic Framework"; *Angew. Chem. Int. Ed.*, 46, 1419–1422 (2007)

[Cheng 2005] (Air Products) Cheng, H. S.; Cooper, A. C.; Pez, G. P.; Kostov, M. K.; Piotrowski, P.; Stuart, S. J., "Molecular Dynamics Simulations on the Effects of Diameter and Chirality on Hydrogen", *Adsorption in Single Walled Carbon Nanotubes* J. Phys. Chem. B 2005, 109, 3780.

•[Doorn2004] Michael J. O'Connell, Saujan Sivaram, and Stephen K. Doorn\* "Near-infrared resonance Raman excitation profile studies of single-walled carbon nanotube intertube interactions: A direct comparison of bundled and individually dispersed HiPco nanotubes", *Phys. Rev. B* 69, 235415 (2004)

[Chahine 2001] Pierre Benard and R. Chahine, "Modeling of adsorption storage of hydrogen on activated carbons", *Int. J. Hydrogen Energy* 26 (2001) 849–855

[Do 2003] D.D. Do, H.D. Do, "Adsorption of supercritical fluids in non-porous and porous carbons: analysis of adsorbed phase volume and density", *Carbon* 41 (2003) 1777–1791

[Eklund 2002] (Penn State) Bhabendra K. Pradhan, Gamini U. Sumanasekera, Kofi W. Adu, Hugo E. Romero, Keith A. Williams, Peter C. Eklund, "Experimental probes of the molecular hydrogen-carbon nanotube interaction" *Physica B* 323 (2002) 115–121

[Iijima 2002] K. Murata, K. Kaneko, H. Kanoh, D. Kasuya, K. Takahashi, F. Kokai, M. Yudasaka, and S. Iijima, "Adsorption Mechanism of Supercritical Hydrogen in Internal and Interstitial Nanospaces of Single-Wall Carbon Nanohorn Assembly", *J. Phys. Chem. B*, 106, 11132-1 (2002)

[Kowalczyk 2005] Piotr Kowalczyk, Hideki Tanaka, Robert Hołyst, Katsumi Kaneko, Takumi Ohmori, and Junichi Miyamoto, "Storage of Hydrogen at 303 K in Graphite Slitlike Pores from Grand Canonical Monte Carlo Simulation", *J. Phys. Chem. B*, 109, 17174-17183 (2005) (collision diameter = 0.2958 nm; rounded to 0.15 nm)

- [Kubas 2001] Gregory J. Kubas, “Metal–dihydrogen and  $\sigma$ -bond coordination: the consummate extension of the Dewar–Chatt–Duncanson model for metal–olefin bonding”, *Journal of Organometallic Chemistry* 635 (2001) 37–68
- [Kuc 2007] Agnieszka Kuc, Lyuben Zhechkov, Serguei Patchkovskii, Gotthard Seifert, and Thomas Heine, “Hydrogen Sieving and Storage in Fullerene Intercalated Graphite”, *Nano Letters*, 7, 1, (2007)
- [Mills 1977] R. L. Mills, D. H. Liebenberg, J. C. Bronson, and C. Schmidt, “Equation of state of fluid n-H<sub>2</sub> from PVT and sound velocity measurements to 20 kbar”, *J. Chem. Phys.*, 66, 3078, (1977)
- [Namilae 2007] (ORNL); S. Namilae M. Fuentes-Cabrera, B. Radhakrishnan, G.B. Sarma, D.M. Nicholson; “Energetics of hydrogen storage in organolithium nanostructures” *Chem Phys Lett.*, 436 (2007) 150–154
- [Morpurgo 2008] Helena Alves, Anna S. Molinari, Hangxing Xie And Alberto F. Morpurgo, “Metallic conduction at organic charge-transfer interfaces”; *Nature Materials*, Vol 7, 674 (2008)
- [Nature 2006] *Nature News* “Moving towards a graphene world” Vol 442 page 228 (July 20 2006)
- [Noorden 2006] Rickard Noorden, “Moving towards a graphene world”, *Nature News*, Vol 442 page 228 (July 20 2006)
- [Patchkovskii 2005] “Graphene nanostructures as tunable storage media for molecular hydrogen” Serguei Patchkovskii, John S. Tse, Sergei N. Yurchenko, Lyuben Zhechkov, Thomas Heine, and Gotthard Seifert, *PNAS* 2005;102;10439-10444 (2005)
- [Shaw 1964] Herbert R. Shaw And David R. Wones, “Fugacity Coefficients For Hydrogen Gas Between 0° And 1000°C, For Pressures To 3000 Atm” *Am J. Science*, 262, 918, (1964)
- [Sidorov 2007] Anton N Sidorov, Mehdi M Yazdanpanah, Romaneh Jalilian, P J Ouseph, R W Cohn and G U Sumanasekera, “Electrostatic deposition of graphene” *Nanotechnology* 18 (2007) 135301
- [Tour 2009a] (Rice) Dmitry V. Kosynkin, Amanda L. Higginbotham, Alexander Sinitskii, Jay R. Lomeda, Ayrat Dimiev, B. Katherine Price & James M. Tour “Longitudinal unzipping of carbon nanotubes to form graphene nanoribbons” *Nature*, 2009, on-line
- [Tour 2009b] (Rice) Ashley D. Leonard, Jared L. Hudson, Hua Fan, Richard Booker, Lin J. Simpson, Kevin J.O’Neill, Philip A. Parilla, Michael J. Heben, Matteo Pasquali, Carter Kittrell, and James M. Tour, “Nanoengineered Carbon Scaffolds for Hydrogen Storage”, *Journal of the American Chemical Society*, 131 (2), 723-728 (2009)
- [Tour 2008] (Rice) Jay R. Lomeda, Condell D. Doyle, Dmitry V. Kosynkin, Wen-Fang Hwang, and James M. Tour; “Diazonium Functionalization of Surfactant-Wrapped Chemically Converted Graphene Sheets”; *J. Am. Chem Soc.*, 130, 16201 (2008)
- [Tour 1990] (Rice) James M. Tour,\*J Shekhar L. Pendalwar, and, Joel P. Cooper, “Homogeneous Deposition of Palladium(0) into Sol-Gel-Derived Materials”, *Chem. Mater.* 2, 647, (1990)
- [Yakobson2008] (Rice) L. Ci, Zhiping Xu, L. Wang<sup>2</sup>, W. Gao, F. Ding, K. F. Kelly, B. I. Yakobson, and P. M. Ajayan; “Controlled Nanocutting of Graphene”, *Nano Res*) 1: 116 122 (2008)
- [Yakobson 2007a] (Rice) Pulickel M. Ajayan and Boris I. Yakobson. “Oxygen breaks into carbon world” *Nature* Vol 441, 15 June 2006[Yildirim 2007] (NIST) W. Zhou, T. Yildirim, E. Durgun, and S. Ciraci, Hydrogen absorption properties of metal-ethylene complexes

[Yakobson 2007b] (Rice) Pavel O. Krasnov, Feng Ding, Abhishek K. Singh, and Boris I. Yakobson, "Clustering of Sc on SWNT and Reduction of Hydrogen Uptake: Ab-Initio All-Electron Calculations", J. Phys. Chem. C, 111, 17977-17980 (2007),  
[[Yakobson 2007c] (Rice) Pulickel M. Ajayan and Boris I. Yakobson. "Oxygen breaks into carbon world" Nature Vol 441, 15 June 2006  
[Yildirim 2005] (NIST) T. Yildirim and M. R. Hartman Direct Observation of Hydrogen Adsorption Sites and Nanocage Formation in Metal-Organic Frameworks, Phys Rev. Lett. 95, 215504 (2005) H<sub>2</sub> uptake 11wt% observed at 30K.  
[Yoon 2008] (ORNL) Mina Yoon\*, Shenyuan Yang, Christian Hicke, Enge Wang, David Geohegan, and Zhenyu Zhang, "Calcium as the Superior Coating Metal in Functionalization of Carbon Fullerenes" Phys. Rev. Lett., 100, 206806, (2008)  
[Yoon 2007] (ORNL) Mina Yoon\*, Shenyuan Yang, Enge Wang, and Zhenyu Zhang, "Charged Fullerenes as High-Capacity Hydrogen Storage Media" Nano Lett Vol 7, 15 (2007)  
Presentation prepared by Carter Kittrell 03-27-09

## Materials properties

Due to the great variety of materials made and tested in our search for sp<sup>2</sup> carbon materials, we did not do systematic tests of material properties. Most samples were made in mg amounts, just enough for hydrogen uptake measurements, and were not scaled for bulk property characterization. However, there are generic properties of the multitude of carbon materials that have found to be rather consistent when we occasionally made larger quantities and did spot checks.

The SWCNTs were spun into fibers with a typical range of diameters of 50 to 100 micrometers, and strength ca. 100 MPa, similar to a cotton fiber. The graphene materials, with a few exceptions were produced as fine powders. These particles were sufficiently large to not be easily airborne, but almost always less than 1 mm maximum dimension. The density of the SWCNT spun fibers was typically in the range of 1.3 g/mL, and that of graphene 1.2 g/mL. This is the density of the individual particle or fibril, obtained by immersing in mixtures of solvents that do not solvate the particles. Hence this is the density of the particle (which separate in the solvent), or the individual fibrils in the spun fiber, as the solvent will penetrate into the gaps between the fibrils that constitute the fiber. We did not measure bulk density, as we did not attempt to compress the material into larger pellets.

The surface area and H<sub>2</sub> uptake is optimized by baking in vacuum to 400-600C. the materials are stable below 600C, and generally lose SA and uptake capacity >700C. samples were tested to 1000C, which brought about irreversible degradation. No significant permeability problems were reported by NREL who did the hydrogen uptake tests, and we don't expect any problems with diffusion due to the slit-like pores that does not restrict gas flow.

## **Deliverables: Project Management and Reporting**

- Attend the HSCoE face-to-face and other Center technical exchange workshops/meetings

-----  
We attended and presented our research results at all HSCoE workshops and meetings, including hosting one meeting at Rice.

- Material samples resulting from the R&D effort will be sent for independent, standardized testing at a facility specified by DOE, as appropriate.

-----  
We had all H<sub>2</sub> uptake measurements performed at NREL on the same apparatus for consistent and comparable results; and we had isotherm measurements done in collaboration with Channing Ahn at Caltech

- The Recipient is required to submit input to the DOE Hydrogen Program Annual Progress Report. Such input should include technical progress, accomplishments, and results.

-----  
We submitted quarterly and annual progress reports as required.

- Participation in the FreedomCAR and Fuel Hydrogen Storage Technical Team Meetings as requested by DOE, usually in Detroit, Michigan.

-----  
We participated in all meetings with the Tech Team as part of our HSCoE program

- Yearly participation at the DOE Hydrogen Program Merit Review and Peer Evaluation meeting, usually in Washington, D.C.

-----  
We participated in all AMR meetings in Washington which occurred in May or June each year and alternately provided oral or poster presentations as determined by the H<sub>2</sub> storage program.

---